Extensive Riparian Vegetation Monitoring – Remote Sensing Pilot Study
Agreement No. IAA 16-205

L. Monika Moskal[1,2], Andrew Cooke[3], Travis Axe[4] & Jeffrey M. Comnick[3]
[1]Associate Professor & Associate Director – School of Environmental and Forest Sciences (SEFS), University of Washington (UW)
[2]Director -- Precision Forestry Cooperative (PFC), UW
lmmoskal@uw.edu
[3]Research Scientist/Associate -- Natural Resource Spatial Informatics Group, PFC, UW
[4]Research Assistant, Remote Sensing and Geospatial Analysis Laboratory, PFC, UW

Table of Contents

List of Figures and Tables

Summary
This pilot project is focused on monitoring riparian stand conditions on private lands in Washington State using remote sensing data.

Time Period: November 1-2015 – June 30, 2017

Goals and objectives
The main goal of this pilot project is to provide background information to serve as a basis for potentially developing a Washington State riparian forests status and trends monitoring protocol based on remote sensing methods.

Specific objectives of the pilot project included:

1. Develop a protocol for field plot sample design and collect the necessary field data to perform analysis in the riparian forests of the Mashel watershed.

2. Use direct and modeled methods for assessing13 riparian metrics using remote sensing methods that were identified in the previous literature review and assessed as appropriate for the Mashel watershed.

3. Provide a focused synthesis, per indicator, summarizing the analysis, methods and feasibilities as well as costs and recommendations for state level analysis, we focused on comparing passive optical imagery based approaches to active LiDAR based approaches.

Deliverables
Monthly updates consisting of 30 minute presentations were provided during the RSAG monthly meetings and feedback from the committee was used to progress on the project. This included decisions involving field sampling protocol process and review, and the elimination of analysis due to time and cost constraints. For example, delineating streams in the field was not performed because collection was deemed too expensive due to the time involved and the processing of the survey grade GPS data.

The final deliverables include:

1. Protocol for field data collection and field database.
    - Moskal, L. M., A. Cooke and T. Axe, 2016. The Riparian Assessment Field Guide 2016. Extensive Riparian Vegetation Monitoring – Remote Sensing Pilot Study, Agreement No. IAA 16-205 (Revised 6/8/2016); Prepared for Washington Department of Natural Resources.

2. Geodatabases of all modeled riparian metrics.

3. Project final report.

Recommendations

The following recommendation are being made based on this research, more in-depth explanations of the recommendations are in the individual sections section:

- LiDAR technology is the most efficient tool for hydrological mapping; albeit the field validation and hydrological flow rectification (such as the proper catchment of culverts) of such maps can be challenging. Optical technologies, such as satellite and aerial imagery, even when collected in stereo are not suitable for this task due to poor quality of ground models generated by such data when compared to LiDAR capabilities.

- Remote sensing approaches that capture structural characteristics of the riparian forest, and the complex terrain of the landscape, specifically, LiDAR, are most suitable for mapping height, basal area and DBH of riparian forest. These characteristics also play a role in vegetation class determination. This is due to the LiDAR's ability to capture ground characteristics as well as above and within canopy structure characteristics.
    - However, no wall-to-wall LiDAR data is yet available for Washington State. Moreover, future repeat collection of LiDAR data for the same sites, as needed to track changes over time, is also unknown. We recommend that baseline conditions capturing these characteristic for riparian forests are established from LiDAR data, with the understanding that the models developed are temporally, location and data sensitive. Other technologies, such as stereo satellite or aerial imaging and the developments in analyzing these data sources should continue to be followed as a potential alternative for long-term monitoring in place of multi-date LiDAR data. These data could be used to compare and monitor the trends in the riparian forests when utilizing the LiDAR-based baseline.

- Additional research to address the number of models and the spatiotemporal reusability of models will need to be undertaken to extrapolate these models to other forest types in Washington State, which will also need to take into consideration permanent plot establishment and remeasurement on a five-year (or more) basis in those additional forests.
    - The pilot developed models at a cell level, as the project scales up, investigations of how to best aggregate these cells to forest stand types should be addressed.

- We identified three further research areas to focus research in:
    - Hydrological mapping and validation,
    - Vegetation class and how these classes specifically translate to the riparian function, and;
    - Fusion of LiDAR and NAIP imagery for conifer/deciduous classification.

- Finally, new technologies, currently, Structure from Motion (SfM), either from satellite (example: World View) or aerial imagery (example: NAIP), should be kept up with and eventually assessed for its ability to provide monitoring capabilities.

1. Study Design

The study is based on a literature review conducted by UW Precision Forestry Cooperative (PFC) for RSAG in 2015 to identify and compare the suitability of remote sensing techniques for mapping riparian forest structural characteristics and composition (i.e., riparian forest metrics):

- Moskal, L. M. and A. Cooke, 2015. Feasibility of applying remote sensing to a riparian stand conditions assessment, Agreement No. IAA 15-118 (Revised 1/1/2015); Prepared for Washington Department of Natural Resources.

The review findings were used in refining the focus on types of remote sensing data and their suitability for assessing riparian metrics and lead to the decision of which metric analysis would be feasible to undertake as a pilot to explore the feasibility and relative benefits of using optical and LiDAR remote sensing in the state of Washington.

1.1 Remotely Sensed Data

We chose to work within the Mashel watershed since both LiDAR and imagery data was available. This is a hydrologically complex landscape, with an extensive drainage network and thus, a range of riparian forest types. The hydrological complexity of this landscape and the hydrological flow modeling associated with it are described in Appendix A. The forests in the watershed capture a range of management and age structures, which allowed provided a complex landscape to be applied in the remote sensing based-modeling. A more detailed description of the Mashel watershed study area including land ownership as well as forest structure is provided in Appendix B.

1.1.1 LIDAR

The LIDAR data for this project was collected by Watershed Sciences Inc. (now called Quantum Spatial) for Pierce County, Washington. The dataset was made publicly available through the Puget Sound LIDAR Consortium (PSLC). Data was acquired between October 2010 and September 2011, and was processed and provided to Pierce County in 21 separate deliveries. The total acquisition covered 933,000 acres. The data was collected using Leica ALS50 Phase II and Leica ALS60 lasers collecting at rates between 83,000 kHz and 105,900 kHz and flying heights between 900 and 1300 meters. The contract specified a native pulse density of 8 or more pulses per square meter. Watershed Sciences (now Quantum Spatial) provided processed point data files in LAS 1.2 format, and digital elevation model (DEM) ground surface files in ERDAS Imagine IMG format. Data and full documentation are available on the PSLC website: http://pugetsoundLiDAR.ess.washington.edu/

1.1.2 NAIP

The National Agriculture Imagery Program (NAIP) imagery used for this project was collected in 2015 by the USDA Farm Services Agency. It is four band natural color (red, green, blue) and near infrared, at a one-meter resolution. It was delivered in the GeoTIFF format as individual Quarter Quad tiles. The focus of the program is to capture leaf-on imagery during the agricultural growing season. More information is available at the program website: https://www.fsa.usda.gov/programs-and-services/aerial-photography/imagery-programs/naip-imagery/.

1.1.3 World View 3 Imagery

The World View 3 scene for this project was provided by the US Geological Survey (USGS). The satellite acquired the image October 11, 2016. World View 3 is a Digital Globe satellite with a 0.31m

panchromatic band and eight 1.24m visible/NIR bands. It also has two lower resolution instruments providing an additional 8, 3.7m bands and 12, 30m bands.

1.2 Validation

To best asses the validity of the techniques a field protocol and field data were also developed and collected as part of this project. These, including the number of plots, plot locations selection are described in depth Appendix B, the plot size, field data collected and measurements are given in Appendix C, moreover the Field Protocol has been delivered and can be downloaded here (Moskal L. M., 2016). Time and cost limited the field data collection, which in turn limited the analysis chosen. For example, canopy present cover, which is captured quite well with LiDAR is difficult to capture quickly in the field. Some field methods such as the densitometer, although commonly used with image analysis have been shown to be less useful with LiDAR data. Other methods such as hemispherical photography require time consuming post-field processing. Similarly, although we have survey grade GPS equipment and the skillsets for collecting and processing this type of field data, the time and costs to collect hydrological data in the field was deemed to take away from the more consuming questions of remote sensing applications. The question of collecting such data at a State scale should be considered.

Other data deemed too time and cost prohibitive to collect included individual stem maps and crown closure/density measurement suitable for evaluating LiDAR canopy percent cover data. This limited our ability to do any individual tree modeling or mapping from the remote sensing data. Vegetation class was also not collected in the field, because such data can be very subjective. All can be acquired, but at a cost. Moreover, canopy percent cover from LiDAR has already been established as a metric that is strongly related with LiDAR data in the literature, as documented in our previous pilot literature review (Moskal & Cooke 2015).

1.3 Model External Validity

It is critical to understand that all models developed in this project are geared towards the specific datasets and vegetation characteristics captured in the Mashel watershed. The models will likely perform in similar forest stand types (e.g, Western Cascades), but performance is questionable in coastal forests of Washington state. Therefore, we do not recommend extrapolating these models beyond the Mashel watershed as the errors and uncertainties associated with such extrapolations cannot be accounted for.

1.4 Results Synthesis

The table below (Table 1) summarizes the results of the pilot project. The Root Means Square Error (RMSE) estimates the deviation of the actual y-values from the regression line. Red squares indicate metrics which were not undertaken due to poor evidence of remote sensing methods capable of such modeling (in case of species) and the prohibitive costs of collecting age field data needed to develop the models (tree coring). Yellow cells indicate that the accuracy assessments for the models was not feasible due to lack of field data. Figure 1 shows a general graphic of the LiDAR models derived for the Mashel study area.

Table 1. Quick Reference Table of Results.

Metric	Status	LiDAR			Imagery		
		Model Type	R2	RMSE	Model Type	R2	RMSE
Species	not modeled	N/A	N/A	N/A	N/A	N/A	N/A
Age	not modeled	N/A	N/A	N/A	N/A	N/A	N/A
Hydrology	completed; describe method; no accuracy assessment	DEM processing, flow accumulation, initiation point definition	N/A	N/A	N/A	N/A	N/A
Canopy % Cover	completed; describe method; no accuracy assessment	direct LIDAR measurement	N/A	N/A	linear regression	0.56*	0.34
Vegetation Class	completed; describe method; no accuracy assessment	probability based classification	N/A	N/A	NA	N/A	N/A
Height (ft)	completed	linear regression	0.86, 0.89	9.74, 11.12	N/A	N/A	N/A
Crown Diameter (ft)	completed	linear regression	0.54	4.03	linear regression	0.5	8.19
Stand Density	completed	linear regression	0.49	67.12	linear regression	0.45	105.14
Basal Area (sq. ft)	completed	linear regression	0.73	62.11	linear regression	0.27	116.15
DBH	completed	linear regression	0.7	2.77	N/A	N/A	N/A
Snag Detection	completed	combined logistic regression / linear regression	0.47	2.53	N/A	N/A	NA
Conifer/Deciduous Classification	completed	combined logistic regression / linear regression	0.67	2.8	linear regression	0.78	2.6
Large Woody Debris	completed	combined logistic regression / linear regression	0.19	6223.04	NA	NA	NA

* field data only suitable for imagery methods

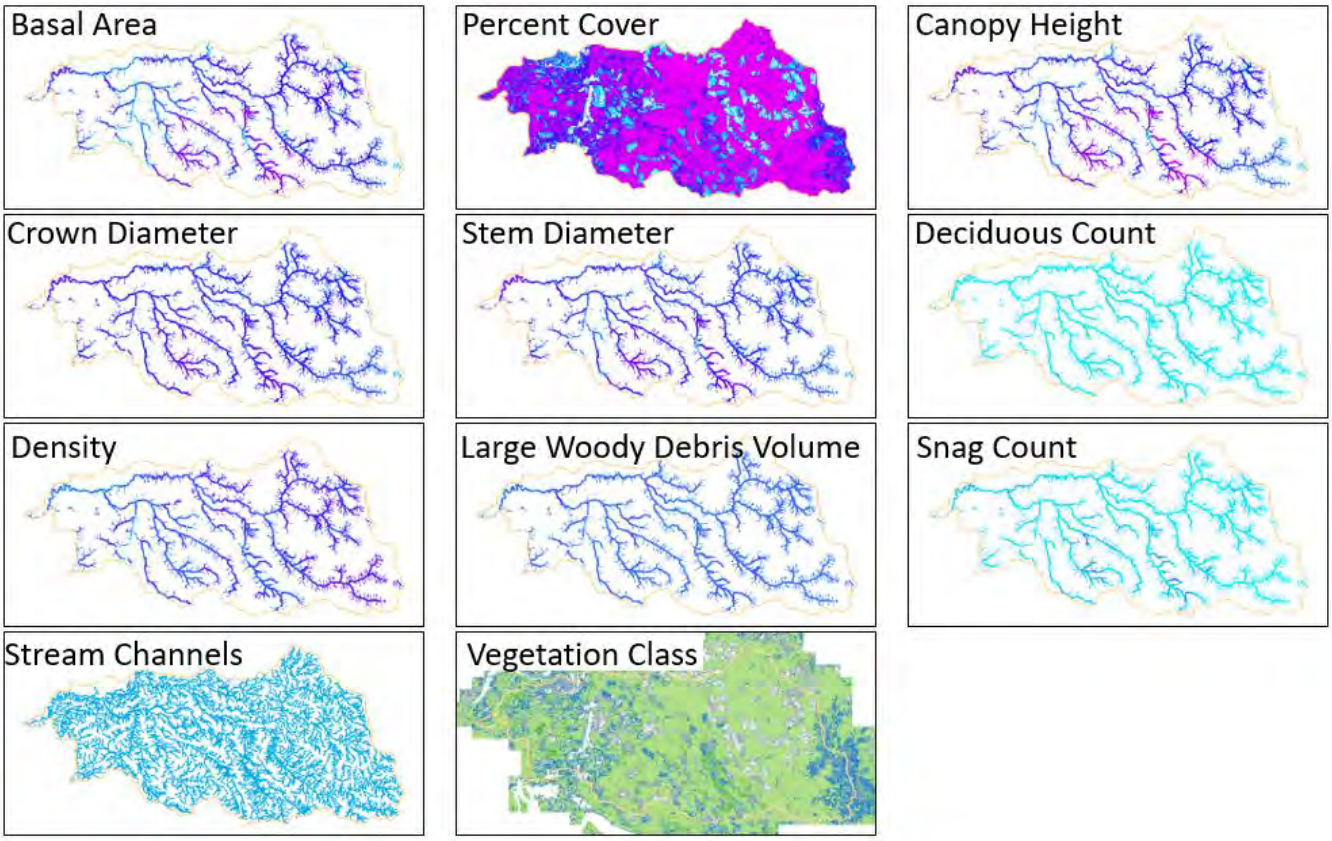

Figure 1. LiDAR-based models for Mashel study area.

2. Hydrology (Channel Locations)

2.1 LIDAR Method

The development of channel locations from LIDAR is a standardized process, but involves making choices, all of which impact the final outcome.

The general approach involves the following steps: develop a digital elevation model (DEM), perform a flow accumulation on the DEM, set a flow accumulation threshold to determine the perennial initiation point, and convert the result to a vector GIS dataset. Details of the specific processing performed for this project are available in Appendix A.

2.1.1 Digital Elevation Model Resolution

The DEM for this project was provided by the LIDAR vendor, Watershed Sciences Inc. (now Quantum Spatial), at a three-foot resolution. The process for creating a DEM from LIDAR data can be complicated, and it is commonly assumed that a DEM provided by the vendor will have a higher accuracy.

The first significant decision to be made when developing stream channel locations is the resolution of the DEM. The maximum resolution of most DEMs is around one meter, and is limited by the density of returns in the LIDAR acquisition. Higher return density allows for higher DEM resolution. A common return density for many acquisitions is eight returns per square meter. Producing a DEM with a

resolution higher than one meter at this return density would result in many areas having few or no returns, resulting in greater inaccuracy due to cells in the model being interpolated.

It is often assumed that higher resolution for a DEM is better, but very high resolution ground models introduce complications. It is not possible to know if the texture in a high resolution DEM is actually the ground, or if it is low vegetation, stumps and logs, or data processing artifacts, etc. Additionally, where streams cross roads in high resolution ground models, the roads often block the streams and redirect flow down the roads. It is possible, but again unknowable from the LIDAR alone, that culverts or cross drains are present, which would allow streams to flow under the road. These problems seem to occur less frequently in lower resolution DEMs, which may argue for their use (Figure 2).

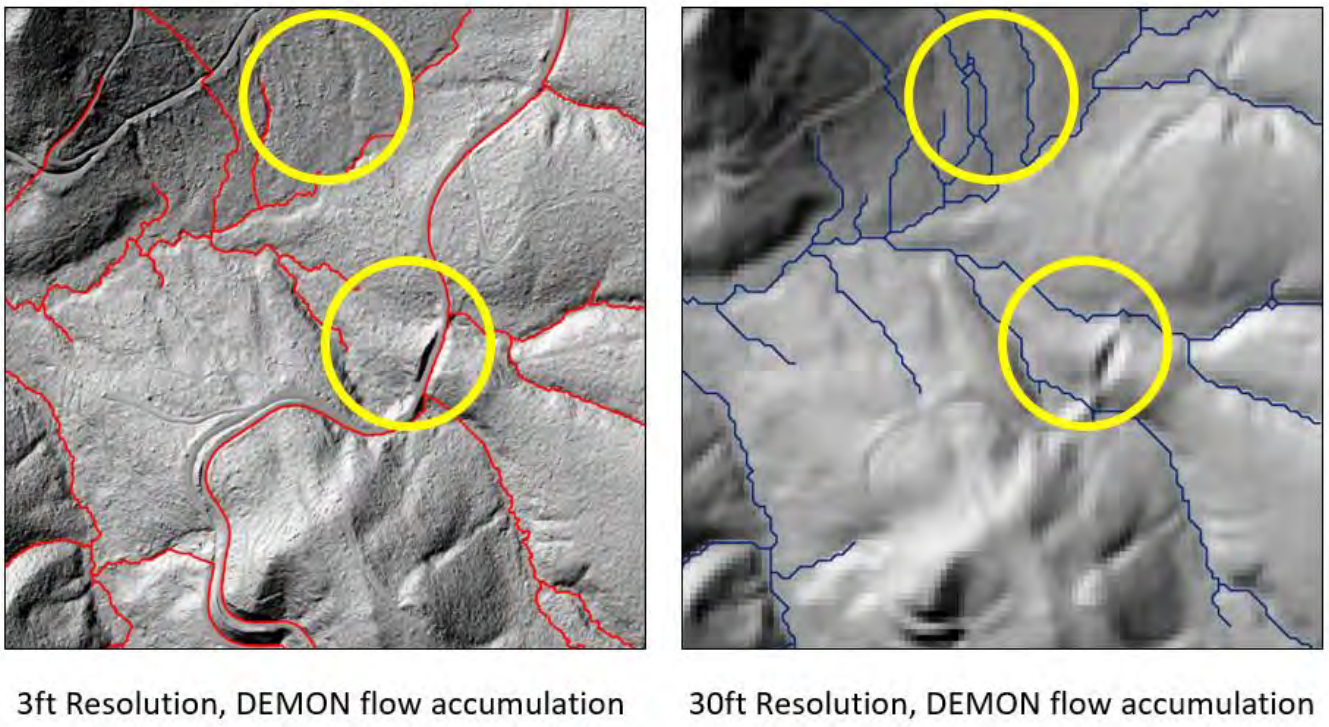

Figure 2. Comparison of DEMON flow accumulation results using 3 ft. high resolution (left) and 30 ft. low resolution (right) DEMs for the same location. The yellow circles highlight differences in flow accumulation behavior.

For the purposes of testing, the vendor provided DEM was down-sampled to four lower resolutions: six, nine, fifteen, and thirty feet. All resolutions produced different stream channel locations when all other processing was the same.

Final processing was performed at the three-foot resolution as that was deemed the most visually accurate model.

2.1.2 Flow Accumulation Algorithm

The second important decision to make is the flow accumulation algorithm. In the software used for this project, SagaGIS, there are eleven algorithms available. The most common algorithm, Deterministic-8, or D8, is widely available in many different software packages, is commonly used, and is fast, but is

known to have limitations. All flow entering a cell can only leave the cell in one direction, which is problematic in flatter areas where flow would disperse. This often results in channel braiding.

More complex flow accumulation algorithms exist, allowing for flow in multiple directions from each cell, and that handle both accumulation and dispersion of flow across a DEM, but these are often less widely available, and have large increases in processing time. The most sophisticated of these would require processing on high-end computing hardware or require a large amount of processing time in order to model flow accumulation statewide or over large areas. One of the most common of this type of algorithm is called Digital Elevation Model Networks or DEMON (Costa-Cabral & Burges, 1994).

Final processing was performed using the DEMON algorithm. The processing for this single watershed took several days on a very high power desktop computer.

2.1.3 Flow Accumulation Threshold

There is no basis for choosing a particular flow accumulation threshold to identify perennial initiation points for streams. Weather, slope, geology, and vegetation, among other things, all impact how water flows and accumulates across a surface. Each stream will have a unique combination of factors such that, no one threshold number will be appropriate for all streams.

In previous work done by the DNR to classify streams for fish presence (Conrad, Fransen, Duke, Liermann, & Needham, 2003), (Fransen, Duke, McWethy, Walter, & Bilby, 2006), a threshold of 3.7 acres, or 1.5 hectares, was used. The 1.5-hectare number was also used for this project. The exact number is not important, so long as the size of the contributing area is sufficiently small. This may result in pushing initiation points slightly further upstream, but this is more appropriate than having them too low.

2.1.4 Digital Culvert

Stream-road intersections are problematic for identifying stream channel locations from LIDAR. True road, culvert, and cross-drain locations are often not known with high accuracy or across ownership boundaries. In a LIDAR DEM, roads are often higher than the stream channels they cross, blocking flow, and diverting streams in non-natural directions, often down the road (Figure 3).

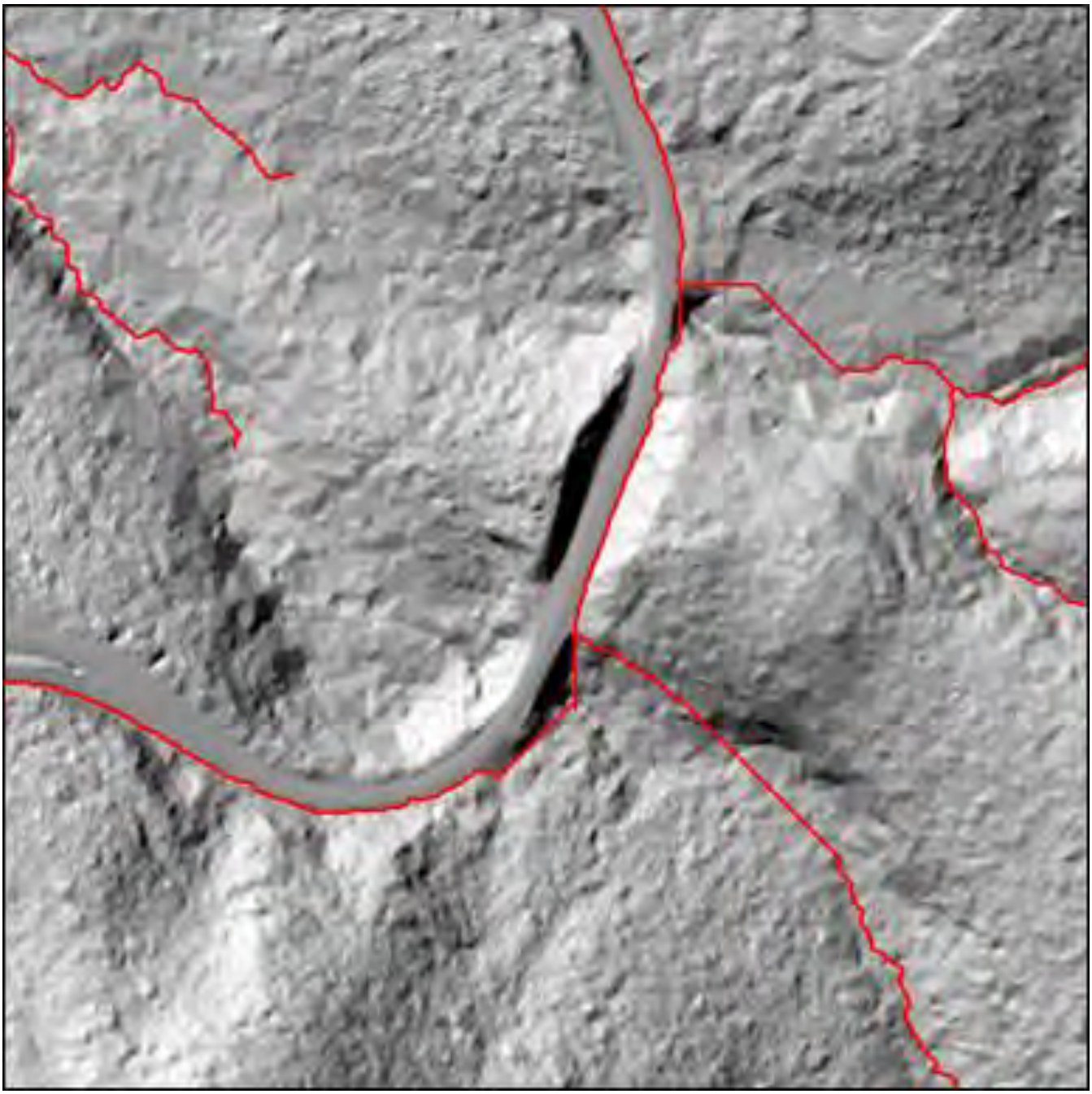

Figure 3. Flow accumulation streams (red) intersecting roads, and having flow diverted.

Areas where streams are blocked often have a sink, an area into which water flows, but with no way for it to flow out. An approach to automatically identify these sinks, and create flow paths out of them was described by the USGS in a Scientific Investigations Report (Poppenga, Worstell, Stoker, & Greenlee, 2010).

This method was implemented in ArcGIS, and was used to modify the original 3 ft. DEM so that flow accumulation algorithms would continue to route flow through stream channels at stream-road intersections (Figure 4). This method is completely automated and does not require knowing where

roads, culverts, or cross-drains are located. This is not a 100% effective means of modeling culvert locations. It is possible that real culverts may be missed, and that digital culverts may be placed where real culverts do not exist. Visual validation and manual cleanup could solve this, but implementation at statewide level would require a substantial investment of time in this part of the post-processing and would be a significant cost to the project. Anecdotally, an examination of stream/road intersections in the Mashel watershed indicate that digital culverts are helpful, and their usefulness may outweigh the errors in modeling their locations. If this limitation is acceptable, it may be possible to skip validation and cleanup.

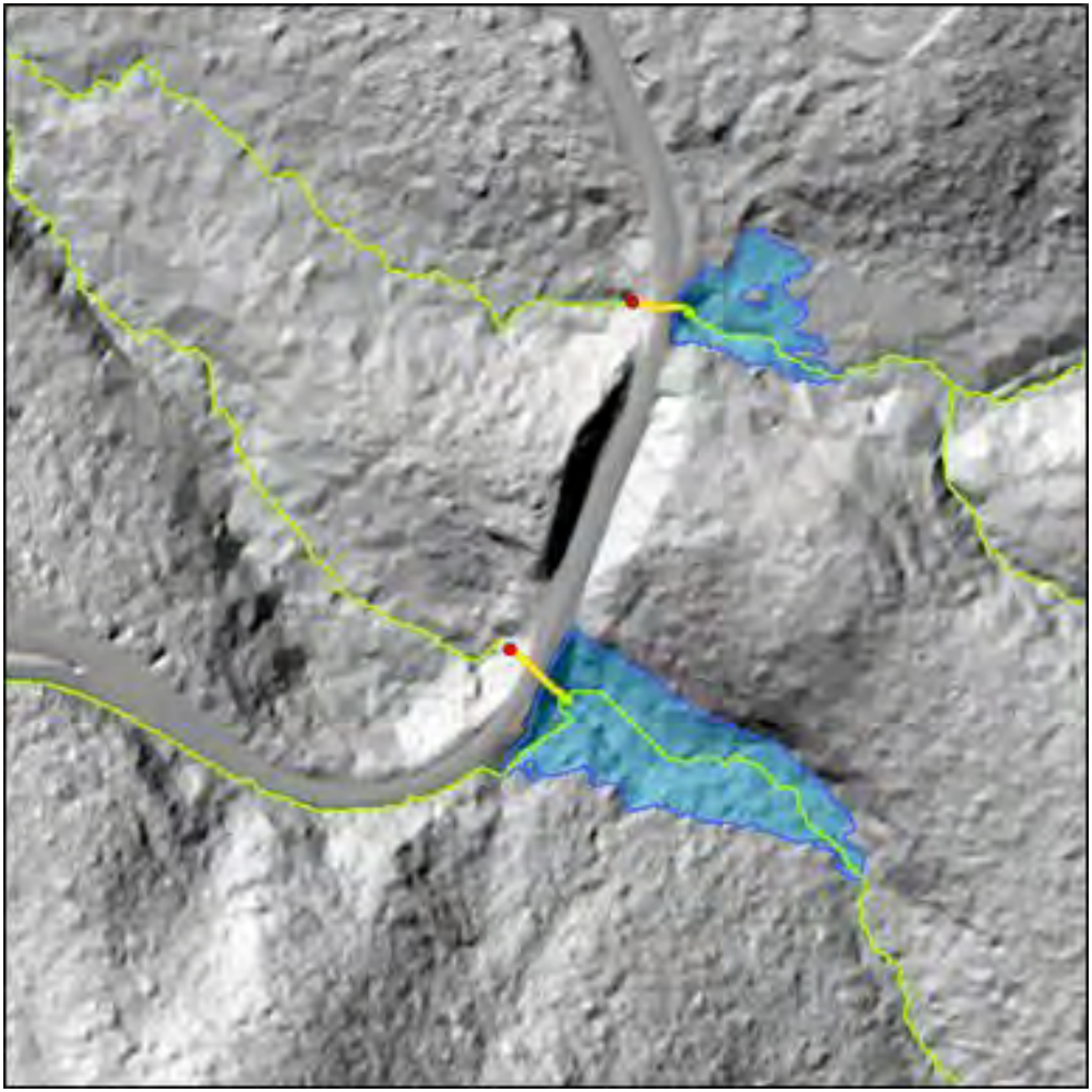

Figure 4. Stream channels (green), entering sinks (blue), and flowing out through digital culverts (yellow) under the road.

2.1.5 Limiting Factors

At this time, it is not known which DEM resolution, flow accumulation algorithm, or flow accumulation threshold produce the most accurate stream channel locations. Flow accumulation algorithms and digital culvert development can take a large amount of processing time, especially for large areas.

2.2 Accuracy Assessment

We did not collect data on where the true channel locations were, so there was no way to test the accuracy of any specific stream channel model or the set of processing choices used to create it, however, as the above figures show, LiDAR is very effective at capturing hydrological features on the landscape due to the detail ground models, this is beyond and above the abilities of other remote sensing technologies.

2.3 Other Techniques

No appropriate data are available for the Mashel watershed study area to attempt an NAIP Stereo or aerial IfSAR assessment approaches. Due to the high stand density and poor ground visibility in the riparian areas the manual stream digitization from aerial orthophotography by a technician were not attempted. Moreover, the accuracy of such manually approaches is also unknown and not believed to exceed accuracies feasible form LiDAR, with similar field data needs required to test the accuracies. Unfortunately, because of the issue of shadows in optical imagery, the utility of such data to manually clean up or improve on the features such as culvert locations in LiDAR data is unfeasible.

2.4 Recommendations

- We recommend LiDAR based methods, over imagery, based on expected accuracy. The higher resolution DEM available from LiDAR facilitates more accurate delineation of channel location, which is essential for identifying riparian forests. Although data availability makes this option not currently feasible for the whole state of Washington.

- As stated in the limitations, the resolution, algorithms and thresholds of these models should be further explored in an additional pilot project. Ideally, a project should be established to compare the accuracies of using different DEM resolutions and flow accumulation algorithms, as well as ways to better predict perennial initiation points.

- To do so adequately a robust field-derived hydrology dataset would be needed for model validation and testing. Ideally hydrology derived from LiDAR would be validated with survey grade GPS field observation or other comprehensive culvert data, however, to acquire such data under conditions of high variability in topography and canopy cover the GPS occupation times might have to vary from a few minutes to a few hours making the costs of such data collections extremely expensive at a watershed level. These costs would be amplified at a state level.

3. Canopy Height

3.1 LIDAR Method: Comprehensive Model Selection

The methods described here for evaluating the performance of the canopy height metric were also used for Stand Density, Basal Area, and Diameter.

Two standard forestry height metrics for plots are the mean plot height, and Lorey's height, a basal area weighted height that allows larger trees to affect the height more than smaller trees. Mean height and Lorey's height were calculated for each plot from the field data for live, large (diameter >= 5"), hardwoods and softwoods. Linear regression models for both height metrics were developed for this project.

3.1.1 Dependent Variable Transformation

The field-measured tree heights, are the dependent variables the models are trying to predict. They were examined using the Shapiro-Wilk test for normality to determine if the data needed to be transformed. The original data, and three transformations of the data (log, square root, and squared) were all tested using the Shapiro-Wilk test.

Table 2. Shapiro-Wilk Normality Test p-values.

Variable	y	log(y)	sqrt(y)	(y)^2
Lorey's Height	0.012	0.001	0.031	0.000
Mean Height	0.075	0.030	0.393	0.000

For the Shapiro-Wilk test, p-values should be 0.05 or higher, for the distribution to be considered normal. If multiple distributions had p-values of 0.05 or higher, the one with the highest p-value was chosen. For these metrics, this test indicates that Lorey's height could be, but does not need to be transformed, while mean height should be square root transformed.

Quantile-Quantile Plots (QQ Plot) were also created to identify unusual residual behavior in the transformed data, shown in Figure 5 and Figure 6.

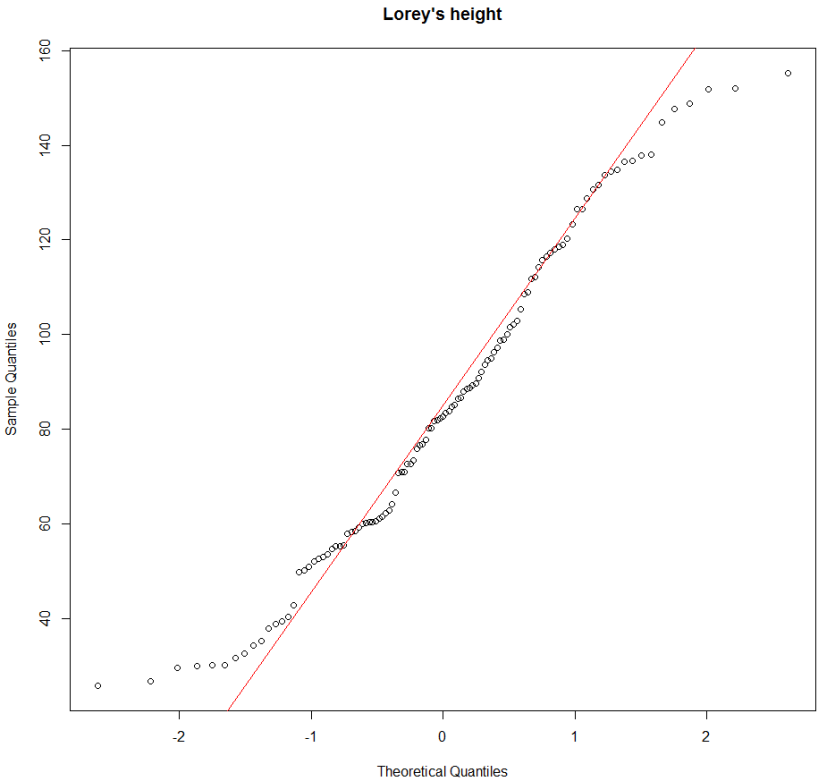

Figure 5. QQ Plot of Lorey's height.

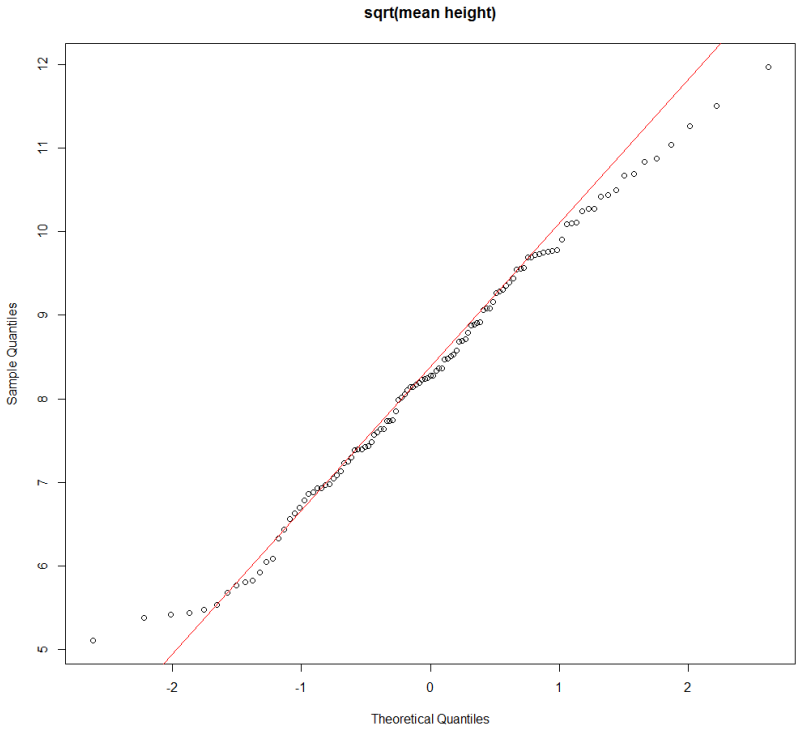

Figure 6. QQ Plot of square root transformed mean height.

3.1.2 Dependent Variable Selection

The Fusion LIDAR processing program CloudMetrics, (McGaughey, 2016), was used to calculate 100 different metrics for each of the 113 plots from the LIDAR data. The models that most successfully predict heights needed to be identified. These models will use some of these LIDAR metrics and not others. Additionally, some LIDAR metrics are highly collinear, and models should avoid using multiple collinear metrics.

Our experience has shown that Intensity, L Moment, and Count metrics could be removed from consideration for modeling heights, because they have not been useful in previous height modeling work. The remaining metrics tend to form three categories: height, cover, and distribution of heights. To avoid collinearity issues, models were limited to using only one metric from each category. To this end, only models with three or fewer predictor variables were considered.

An automated process was developed in the statistical software R to compare all possible models with one, two, or three predictor variables. This process considered all distinct metric combinations, with and without interaction between predictor variables, and tested each predictor variable without transformation and with log and square root transformations. Each model was ranked by its R^2 value (these were back-transformed if the dependent variable was transformed). This allowed for a relatively simple, straight forward and repeatable, but effective method of model selection.

3.1.3 Model Verification

The best performing models from the comprehensive modeling process (those with the highest R^2 values) were selected and investigated further. Models with collinearity among the predictor variables were removed from consideration.

Often, multiple models have similar performance, so the logic for choosing one comes down to factors such as explainability and implementability. A simpler model, one with fewer predictor variables or fewer interaction terms, is often easier to understand and explain, and easier to use. It might be better to choose a model because it is easier to explain and use even if it performs slightly less well (i.e. no practical difference). Models that tend to tie to tree physiology and simple parameters are easy to characterize and interpret.

The remaining model with the highest R^2 value was then examined looking for non-significant coefficients. If interaction terms were non-significant, they were removed. The model was plotted, again looking for undesirable behavior, for example, significant trending captured by sloping in the residuals.

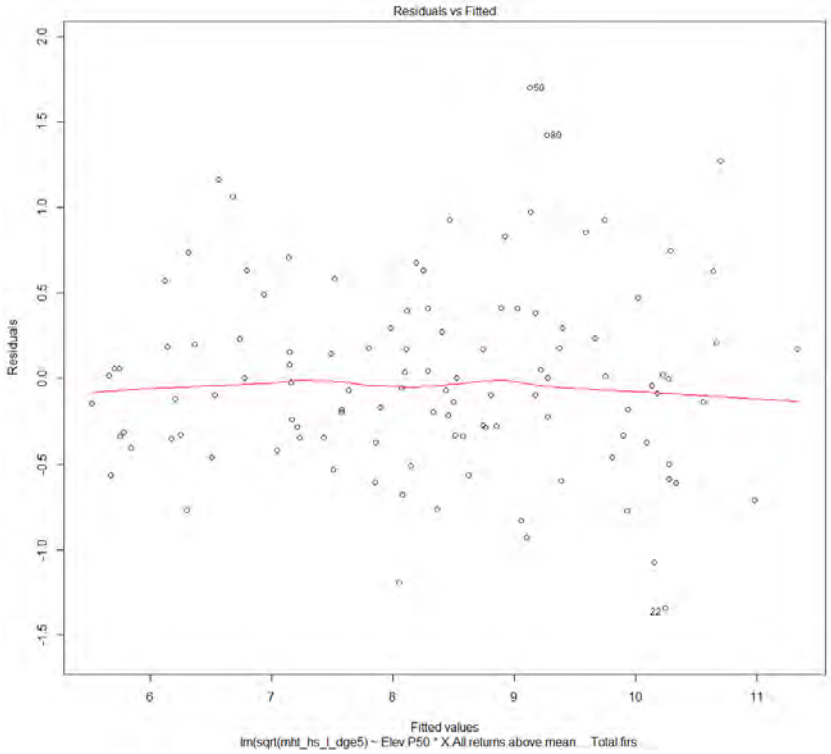

Figure 7. Lorey's height model behavior, Fitted Values vs. Residuals plot.

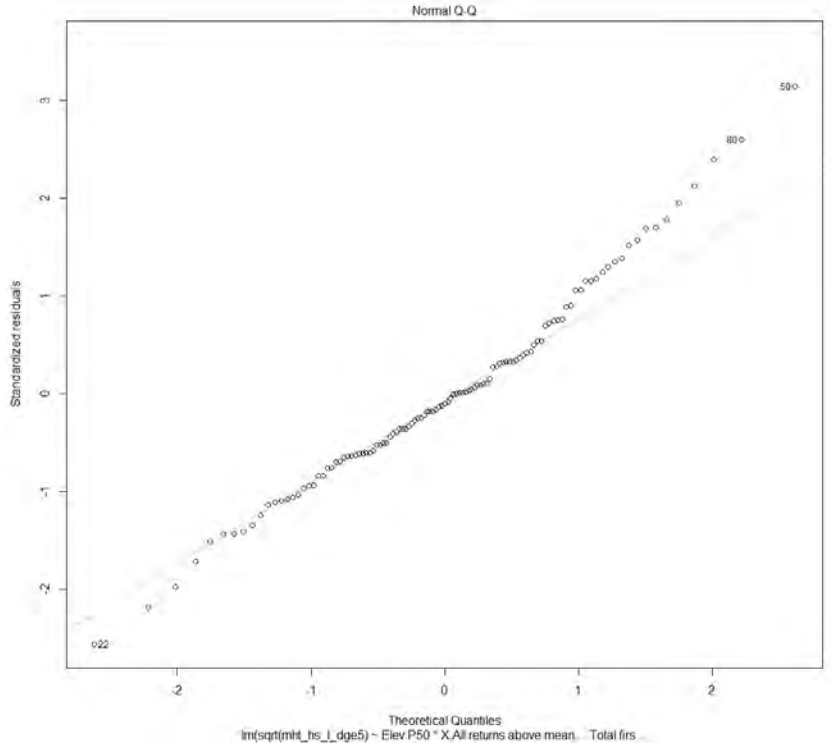

Figure 8. Lorey's height model behavior, Normal Quantile-Quantile plot.

Once the final models were selected, they were further reviewed using Box-Cox power transformations to verify the original dependent variable transformation.

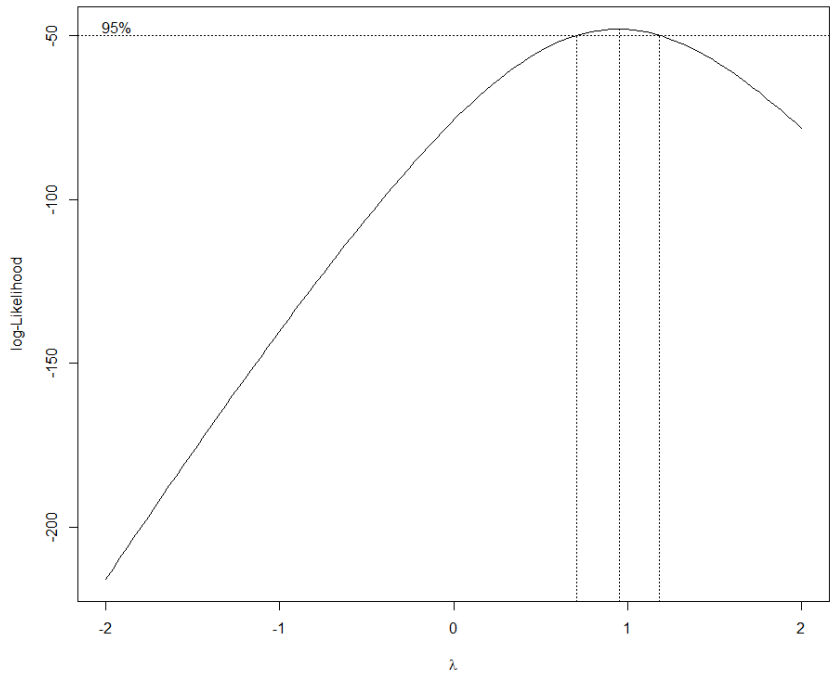

Figure 9. Box-Cox Test for Lorey's Height.

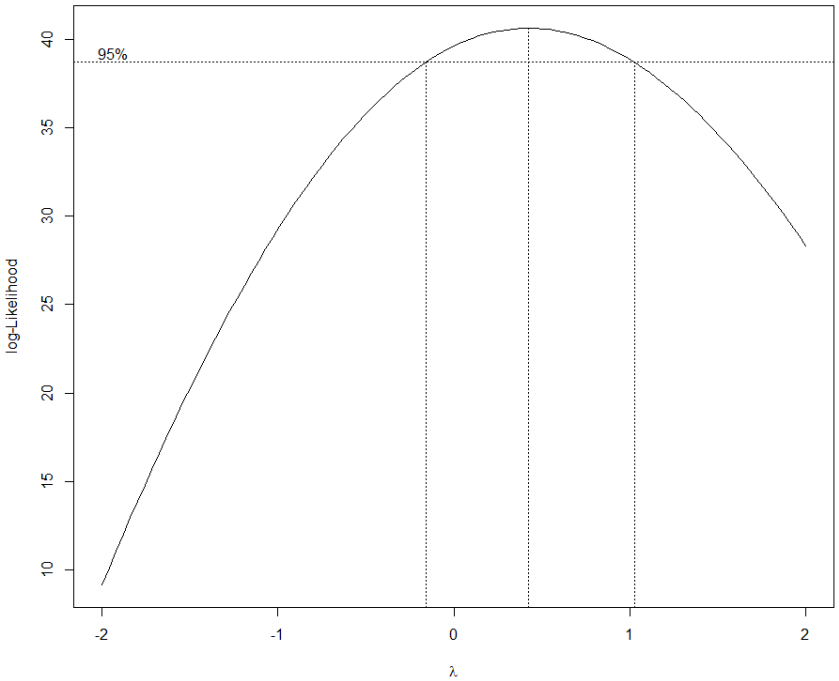

Figure 10. Box-Cox Test for Mean Height.

3.1.4 Final Selected Models

The results reported here are for Lorey's height (see Glossary Section for equation and further details) and mean height. Lorey's height weights the contribution of trees to the stand height by their basal area. Lorey's height is more stable than an unweighted mean height because it is less affected by mortality and harvesting of the smaller trees.

R^2 and RMSE values for models with transformed dependent variables have been back-transformed where necessary.

The comprehensive modeling approach described here may not identify the absolute 'best' model. However, the final selected models should be close to the 'best', and are similar in performance to other work in the literature. The applicability of landscape level analysis with these types of dynamic models is shown in Figure 13.

Table 3. Height models.*

**all models presented in this report are location and LiDAR data specific, thus, these models should not be used with other LiDAR acquisitions or at other geographic locations (even in Washington state).*

Metric	Model	R^2	RMSE
Lorey's Height	LoreysHeight = 20.62292 + (0.98899 *A)	0.89	11.12
Mean Height	sqrt(MeanHeight) = 4.942 + (0.05989*B) + (0.02393*C) + (-0.0003889*B*C)	0.86	9.74

Table 4. Height model variables.

Model Variable	Fusion CloudMetrics Variable	Variable Explanation
A	Elev.CURT.mean.CUBE	cube root of the mean cube height, all returns
B	Elev.P50	50th percentile of the heights, all returns
C	(All returns above mean) / (Total first returns) * 100	percent cover; number of all returns above mean height / total number of first returns

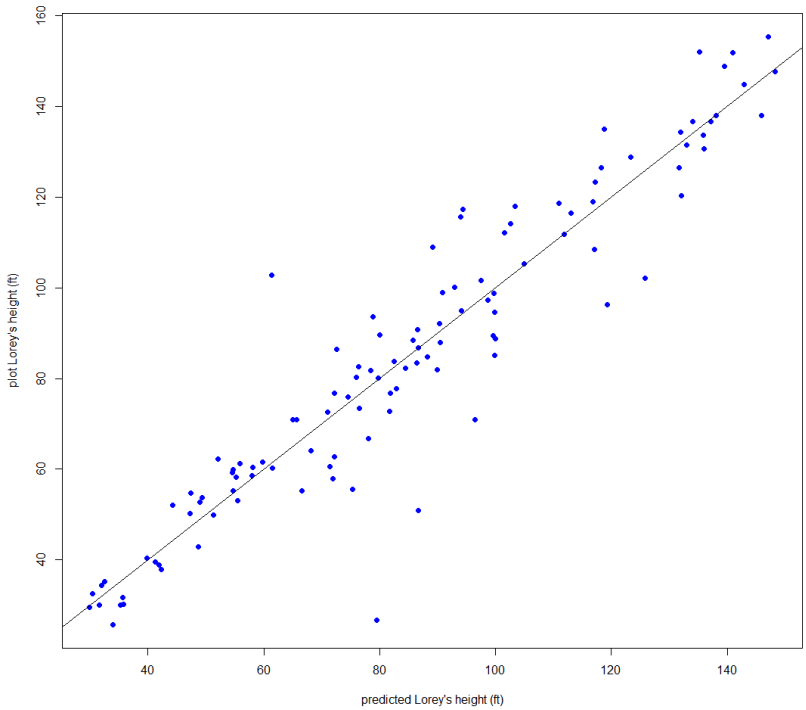

Figure 11. Predicted vs. plot Lorey's height with the line of equality.

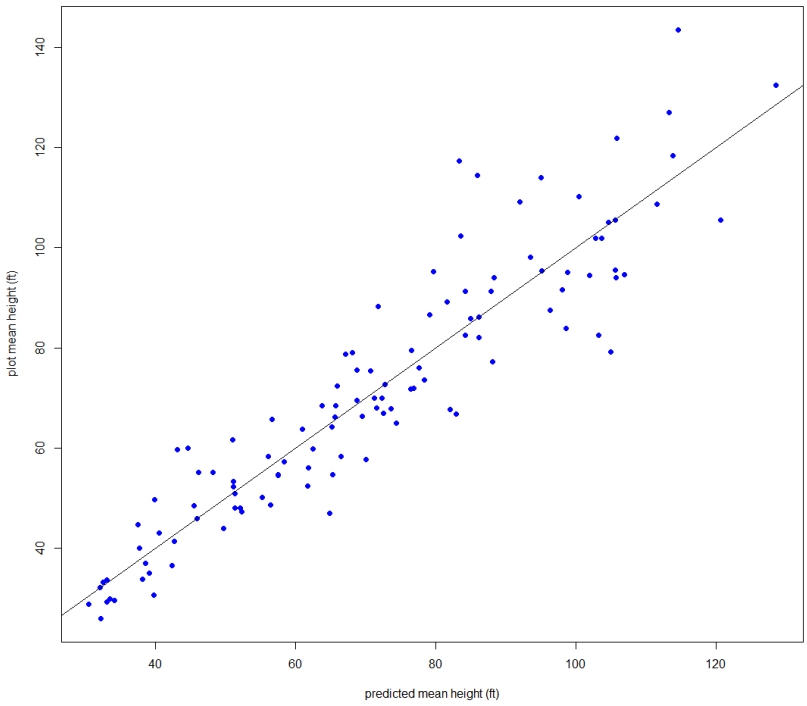

Figure 12. Predicted vs. plot mean height with the line of equality.

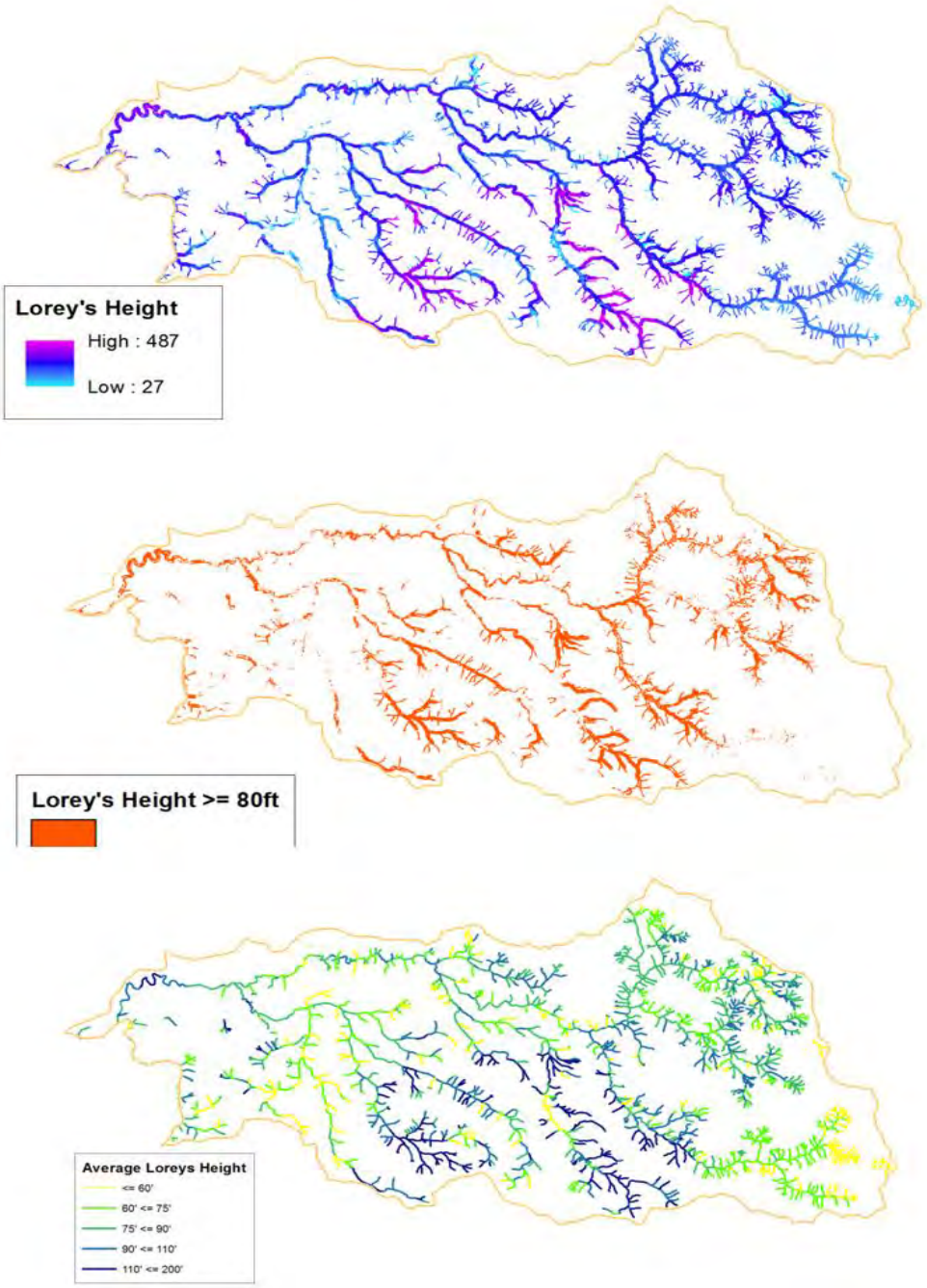

Figure 13. Mashel riparian buffer forest height analysis, top map Lorey's height, middle height above 50ft, bottom averages height classes per stream reach, all from derived LiDAR based height models.

3.1.5 Limiting Factors

LIDAR is expensive per unit area. LIDAR data is not available statewide; it is only available in relatively small spatial extents where acquisitions have taken place. LIDAR point data requires a large amount of storage space and processing capability.

All models presented in this report are specific to the LiDAR data and geographic location, thus the models cannot be and should not be extrapolated to other landscapes and watersheds without understanding that the errors and uncertainties will change and cannot be evaluated.

3.2 Accuracy Assessment

3.2.1 Field Data

A primary goal of the field data collection, was to locate the 130 field plots across the full range of riparian forest types in the Mashel watershed. These plots were then measured for the various riparian forest metrics under investigation and either used to build the models, assess the accuracy of the models or both.

The watershed was pre-stratified into bins, and eight to 14 plot locations were randomly chosen for each bin from potential areas of the watershed in that bin, this binning process is described more in-depth in Appendix B. Certain bins made up a higher proportion of the watershed, so these bins were assigned more plots. Thus, very large trees, which are rare on the landscape, had fewer bins and thus fewer plots. There are also fewer of these trees in our models and the residuals associated with these heights of these trees are larger, thus the errors in height estimates for these taller trees will also be slightly greater. This is a common issue with LiDAR data, especially since we don't expect the LIDAR pulse to hit the or even register a return off the most top leader of the tree.

For more detailed information, see Appendix B - Plot Location Selection. The field data collection is described briefly in Appendix C and a full field data collection Protocol is provided as a separate publication (Moskal L. M., 2016).

1. Moskal, L. M., A. Cooke and T. Axe, 2016. The Riparian Assessment Field Guide 2016. Extensive Riparian Vegetation Monitoring – Remote Sensing Pilot Study, Agreement No. IAA 16-205 (Revised 6/8/2016); Prepared for Washington Department of Natural Resources.

3.3 InSAR and Other Technologies

No Interferometric Synthetic Aperture Radar (InSAR) data was currently available for study area, nor elsewhere in the state. InSAR data will eventually be available nationwide, however, this future technology was not readily available for assessment during the time scope of this project.

Future technologies such as those utilizing, satellite stereo imagery and/or Structure from Motion (SfM) might be able to provide state wide estimates of canopy height. One such project is being proposed as a collaboration between the USDA Forest Service Pacific Northwest Research Station and the Environmental Protection Agency. The approach would use already collected 2016 Washington State near-infrared NAIP imagery to produce a canopy surface model. Although the error of optical imagery-based surface height models, can be up to 5m for canopy heights, this error would be reduced in areas with LiDAR data (potentially to as low as 20cm) (Shean, 2016). These errors have not been specifically investigated for height models of forest canopies.

We have performed a very preliminary test of stereo based satellite imagery canopy height modeling in the Mashel watershed, and report on these preliminary results in Section 15. Future Technologies.

3.4 Recommendations

It is critical to understand that all models, including the height models, developed in this project are geared towards this specific LiDAR acquisitions (the point spacing of the data) and to the characteristics of the vegetation captured in the Mashel watershed. We do not recommend extrapolating these models beyond the Mashel watershed as the errors and uncertainties associated with such extrapolations cannot be accounted for.

- We recommend LiDAR based canopy height models. In general height modeling with LiDAR has been well accepted and can even outperform field data collection. However, LiDAR data availability makes this option not currently feasible for the whole state of Washington.

4. Crown Diameter

4.1 LIDAR Method

The method used to build these linear regression models is described in further detail in Section 3, the LIDAR Method for Canopy Height.

Two models were developed to estimate crown diameter from LIDAR. The first used only metrics derived directly from the LIDAR data itself. The second could include radius or diameter values calculated from the individual tree objects (ITOs) created during the segmentation of the 6 ft. resolution canopy height model (CHM). The process of segmenting the canopy model into individual tree objects (i.e. portions of LiDAR point cloud assumed to represent individual trees) is described further in Appendix D.

Two models were developed because it was believed that ITOs provide additional information about the trees on the plot, and could potentially improve the accuracy of the crown diameter model. However, segmenting a canopy height model and measuring diameters and radii of the resulting ITOs, is time consuming. The additional processing time, may outweigh the value of any additional accuracy.

In Table 5 below, we describe the different crown size metrics that were calculated for each tree object. These were averaged for the trees objects on each plot. The plot averages were included as possible metrics in the regression models.

The center of the tree, the high point, is the center of the cell with the highest height in the tree object, and can be considered the stem location. Each tree object has 16 vertices in the cardinal directions, at the cell centers nearest the edges of the crown. Distances from the high point to each vertex were calculated and used for the crown size metrics.

Table 5. Diameter and radius metrics calculated for each tree object.

Maximum Radius	The longest radius from the high point (the furthest vertex).
Minimum Radius	The shortest radius from the high point (the closest vertex).
Longest and Perpendicular Diameter	The diameter based on averaging the longest transect with the transect perpendicular to the longest transect.
NS/EW Average Diameter	The diameter based on averaging the North/South transect and the East/West transect lengths; these may not be the longest transects.
Average Radii Diameter	The diameter based on averaging the lengths of all the radii from the high point to each vertex, and doubling the average.
Crown Area Diameter	The diameter based on treating the polygon as a circle and back-calculating the diameter from the circle's area.

Table 6. Crown Diameter Model without Canopy Height.

Metric	Model	R^2	RMSE
Crown Diameter	log(Crown Diameter) = 3.087 + (0.0005992 * A) + (-0.0001125 * B^2) + (0.000000974 * A * B^2)	0.46	4.35

Table 7: Model variables.

Model Variable	Fusion CloudMetrics Variable	Variable Explanation
A	Elev.P99	99th percentile of the heights, all returns
B	Int.mean	mean intensity, all returns

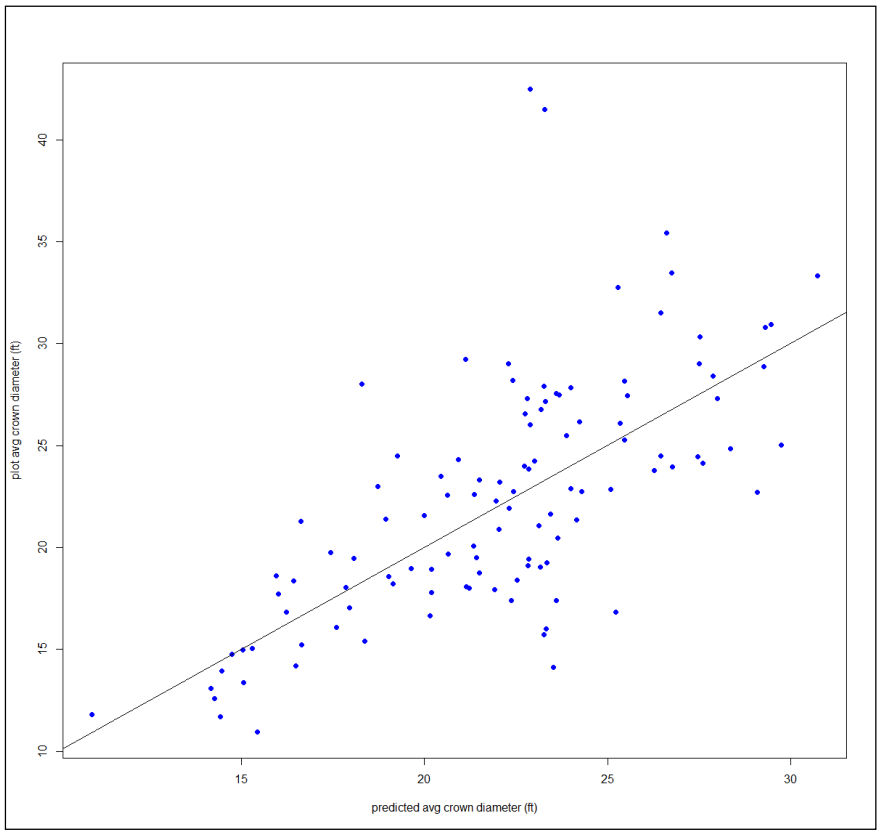

Figure 14. Predicted vs. plot crown diameter with the line of equality; model without CHM metric.

Table 8. Model with the Canopy Height Model.

Metric	Model	R^2	RMSE
Crown Diameter	log(Crown Diameter) = 7.269 + (-0.6733 * sqrt(A)) + (-0.001303 * B^2) + (-2.112 * log(C)) + (0.0001857 * sqrt(A) * B^2) + (0.3434 * sqrt(A) * log(C)) + (0.0006011 * B^2 * log(C)) + (-0.0000873 * sqrt(A) * B^2 * log(C))	0.54	4.03

Table 9. Model Variables.

Model Variable	Fusion CloudMetrics Variable	Variable Explanation
A	Elev.P50	50th percentile of the heights, all returns
B	Int.mean	mean intensity, all returns
C	Average minimum radius of the individual tree objects in each plot	see Appendix D

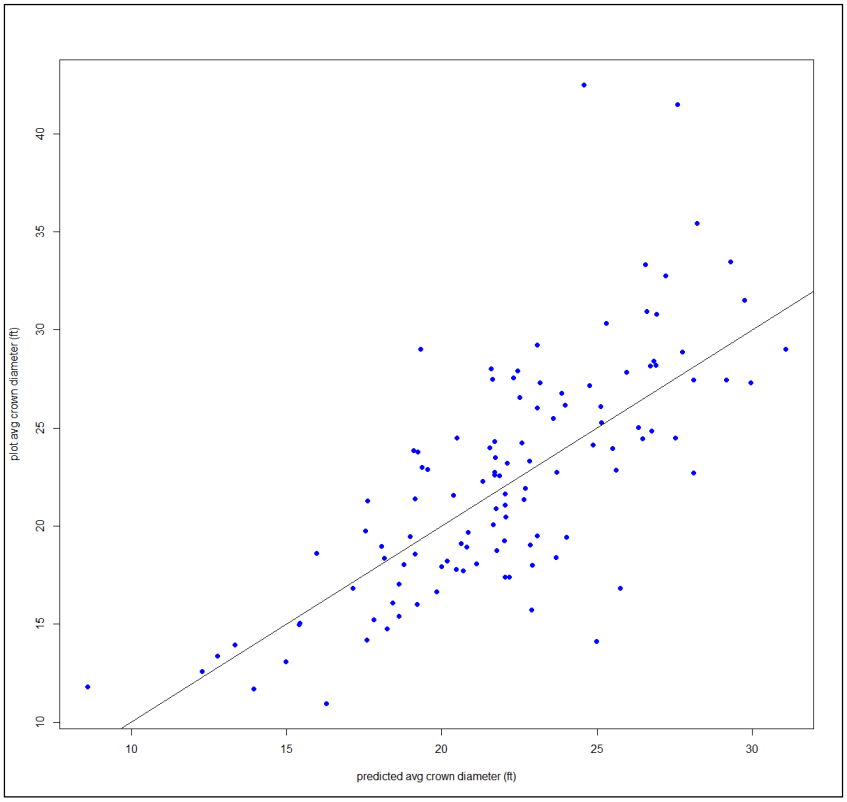

Figure 15. Predicted vs. plot crown diameter with the line of equality; model with CHM metric.

4.1.1 Limiting Factors

Development of the canopy height model, and measuring the diameters of the individual tree objects is very time consuming. This processing took several weeks for the Mashel watershed. The inclusion of the Canopy Height Model (CHM) radius and diameter information as possible metrics for the model did increase the accuracy, but not by a substantial amount. The additional processing time may not be worth the accuracy improvement. This will need to be determined based on available project budget and goals.

4.2 Imagery Analysis Method

Imagery analysis consisted of two phases. The first was the identification and spatial-delineation of individual tree crowns. The second was the interpretation of the respective geometric and spectral signatures associated with these estimated tree crowns. Supplemental information regarding the exact data, time, and resources that were used can be found in Appendix E. The general approach and methodology of individual tree identification is discussed below.

Before any crown measurements can be accurately summarized, individual trees need to be delineated into distinct objects. These will serve as the base for analysis and are referred to as Individual Tree Objects [ITOs]. This is essential for most of the model estimations derived from imagery. An algorithm was created that masks out unwanted features on the ground, identifies bright points that represent the tops of trees, and then grows the crown out until one of several evaluation thresholds is met. Once ITOs are located, they can be manipulated further in order accommodate for varying scenarios on the landscape. This report does not offer specific approaches to the unique problems, but it does serve to identify major areas where refinement can be made.

4.2.1 Tree Delineation Algorithm Overview

The primary segmentation and classification algorithm used in the project area will hereby be referred to as the TDA [Tree Delineation Algorithm]. The TDA identifies and delineates individual tree crowns that are visually evident within the imagery. From this, information pertaining to each identified tree can be exported for further analyses. It is important to note that only a single algorithm was used for the entire project area, and the accuracy results for many of the project metrics reflect this singular approach. This will be discussed more in the 4.2.3 Limiting Factors section at the end of this section.

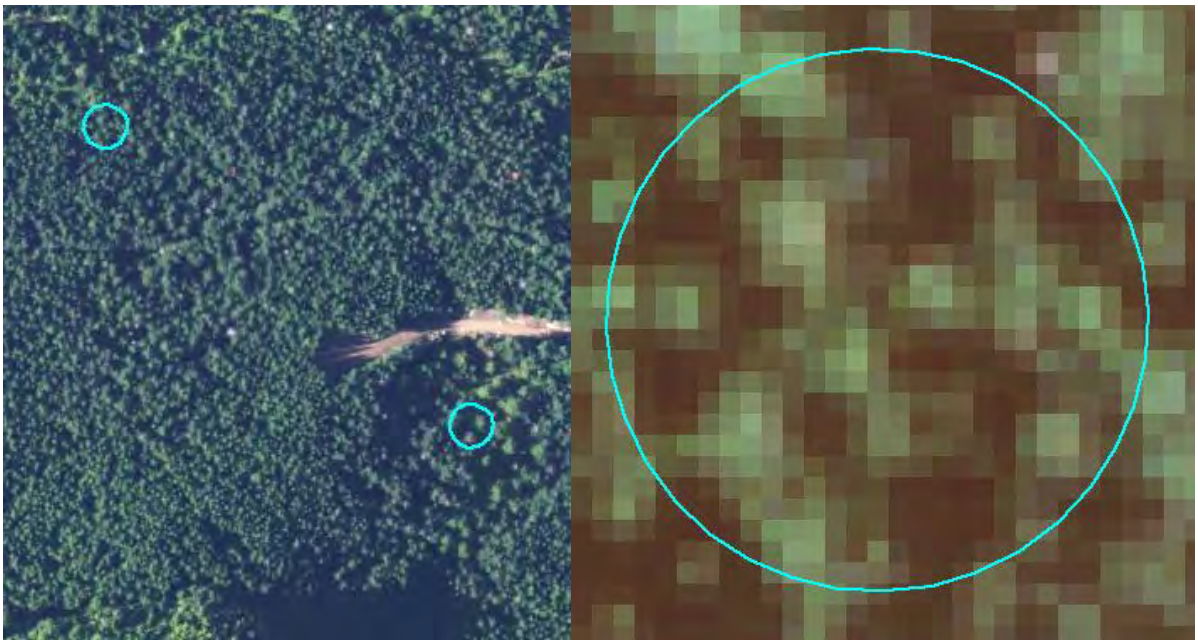

Figure 16.Left: Sample Plots 4113 & 2102 Zoomed out. Right: Sample Plot 4113: Zoomed in

Step 1: Find, classify, and mask non-tree objects.

To achieve this, a valley-following technique was used. This approach utilizes the "valleys" of shade that typically exist between the crowns of dense forest stands, which can be defined by thresholding a

local minima of pixel brightness values. This same approach is also applied to non-forest objects, like bare ground, roads, and other man-made structures, by evaluating levels of brightness and several pixel thresholds that help discriminate vegetation from non-vegetation. First the landscape is segmented, drawing borders around our perception of these objects. Then conditional evaluations are used to assign classes to each.

The segmentation used for identifying roads, bare ground, and man-made structures used a balanced approach of object size, the emphasis placed on color, and how continuous the object may be across large areas. From here, thresholds for brightness and NDVI were evaluated to identify these objects non-vegetative objects, so they could be immediately masked out or saved for future work.

$$NDVI = \frac{NIR - Red}{NIR + Red} \mid \text{Thresholds: Brightness >= 100 and NDVI <0.1}$$

Next, the "basins" existing between trees are located and masked as well. The segmentation for this process focuses much more on the compactness, continuousness, variability in size, and emphasis on color in order to draw borders around the basins. Because of the emphasis on color in this classification, all the remaining bands are used. The dark gaps between trees were identified by band thresholds, found in Table 9.

It is important to have positive thresholds for NIR and NDVI, unlike the rest. This helps identify areas that are too dark to analyze but still most likely vegetation. This could serve as some use in troubleshooting or assumption-building, but masking these areas is important for further crown identification.

The two figures below show the change when the masking function is applied. The first figure is the same original snapshot from above. The black area in Figure 17 represents all landscapes falling outside plot boundaries. The grey represents the basins or canopy gaps between the trees. The final variations of green is the remaining area of interest and analysis: visible tree canopy. All remaining algorithm functions will be applied only to this green area. The advantages of applying the mask serve to simplify the complexity of both the remaining algorithm and total processing time.

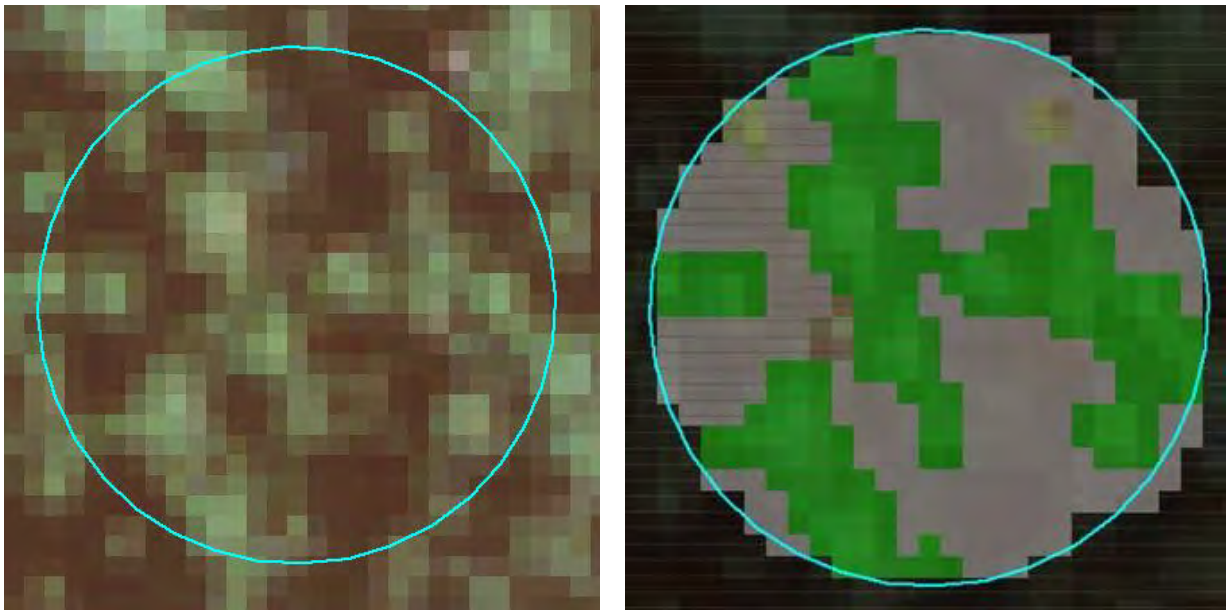

Figure 17. Sample Plot 4113 before any processing show in in true color imagery (left) and after masking of background vegetation with the crowns colored in green (right).

Step 2: Find the "Seeds" of individual tree crowns

The processing from here forward is dealing only with pixels representing trees, as most other land features have been masked. First, a watershed segmentation is used to delineate visually evident tree crowns, using NDVI and Green as the band inputs. Any segmentations containing only 1 pixel were combined using a nearest neighbor approach. This serves to either eliminate false tree tops or smooth potential trees that lack the resolution necessary to be evaluated with the remainder of the algorithm. Using these newly formed tree objects, the algorithm evaluates NIR values to locate local maxima. Because this step evaluates potential tree objects against one another, it does not necessarily mean every current object will have a corresponding tree top.

Step 3: Grow Seeds and remove false Seeds

Once potential individual trees are located a re-structuring of image object borders is performed. It starts first by making the "seed" its own object and then grows it outward based neighboring pixel's ratio of NIR value. It evaluates if this value is in an acceptable range by comparing it to the NDVI and Red standard deviation values of all existing seeds. This ensures whether or not a neighboring pixel is likely to be part of the same tree. As this process loops the new tree line grows and terminates if the comparison in band values breaches a threshold, reverses in direction or an existing boundary is met.

Step 4: Clean up and Export

Remaining unclassified regions are merged together so only ITOs are the most visually distinguishable. After this, the ITOs are exported as either a vector or a raster layer, with important attributes saved for each object, including but not limited to: The sample plot of location, statistical band values, size and geometry, shape and skewness, and specific coordinates.

The snapshot in Figure 18 shows the classification of plot 4113, with an individual tree selected. Information pertaining to this tree is located in the dialogue box next to it. This data is then used to estimate respective forestry metrics included in this study.

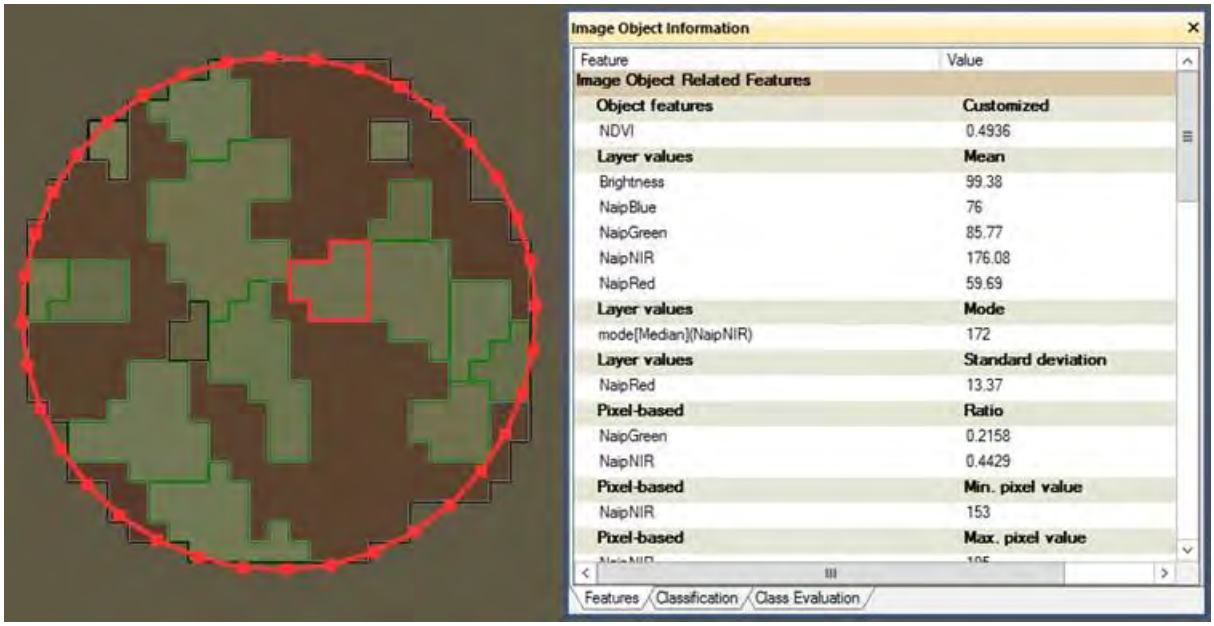

Figure 18.Classification results of plot 4113.

4.2.2 Accuracy Assessment

Average crown diameter estimates are within plus or minus five feet of the actual mean crown diameter for over 60% of the sample plots – represented by the histogram in Figure 19. This result is the first major reflection of only using a single algorithm for tree identification; it may perform relatively well for many of the stand structures in the area, but outliers do exist and may introduce extraneous error if they are not specifically accounted for.

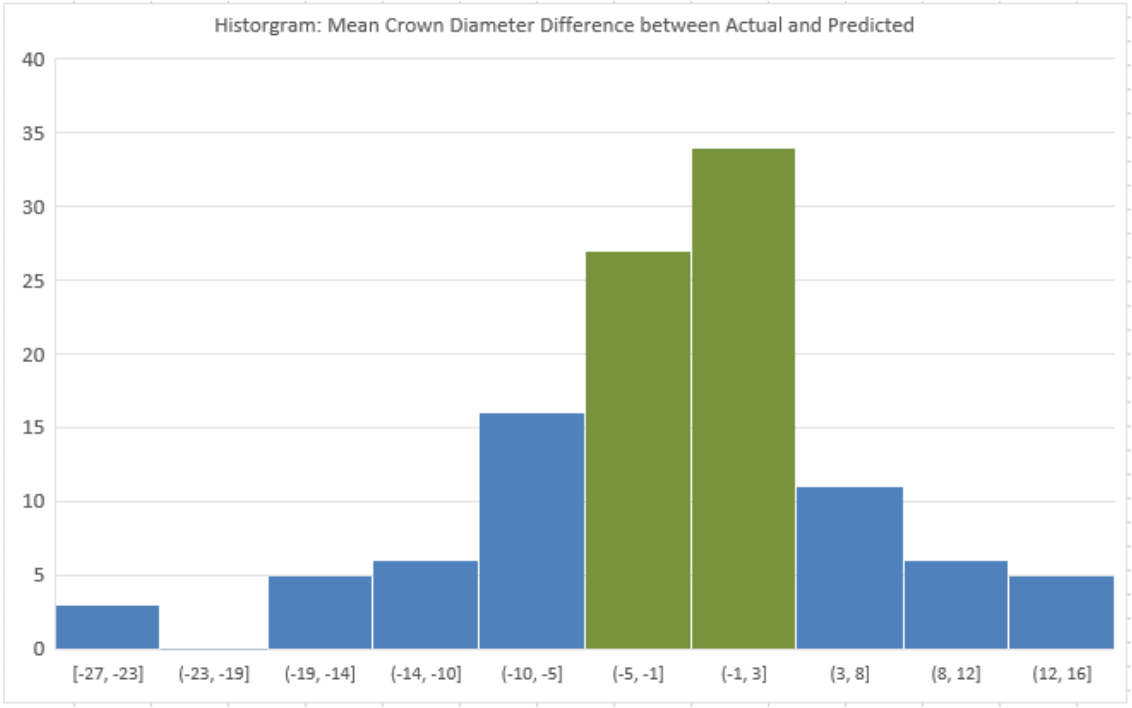

Figure 19. Histogram of mean crown diameter.

Error in estimating crown diameter also depends on the relative crown sizes within a plot. If tree crowns for a plot have an average diameter ranging between 10 and 20 ft. the algorithm shows a tendency to overestimate crown diameters. Conversely, if a sample plot's tree crowns are much larger, averaging beyond 25 feet, then the algorithm tends to underestimate crown diameter. This variation of inaccuracy is captured in Figure 20.

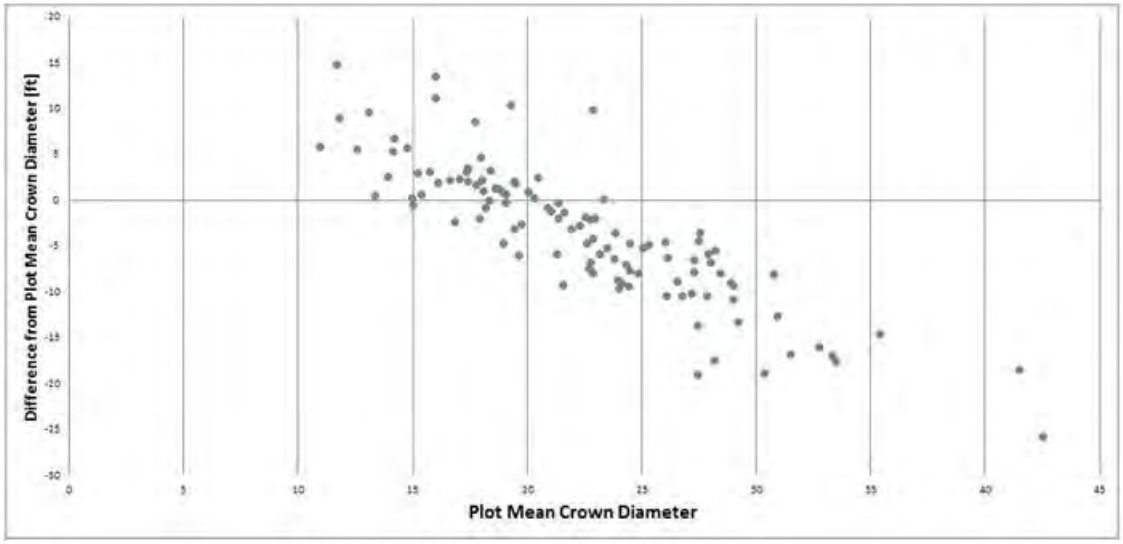

Figure 20. Error in estimating crown diameter.

Accuracy results for crown diameter increases generally when only attempting to estimate large, living trees [as the alluded algorithm is designed to find]. For small trees, or standing dead trees, accuracy results diminish because they are not detectable via the pixel composition of the image, this can be observed in Figure 18. Furthermore, the technique appears to do better when plots are located in older,

more established tree stands. The variance in crown diameters is much wider in field measurements than in model predictions, which generally exhibit much smaller ranges crown diameter predictions. This is most likely because segmentations are predisposed to making somewhat uniform shapes and growth patterns from tree "seeds". Moreover, crown diameters are estimated using the perimeter and area of the estimated crown, not necessarily from taking the largest linear estimation from within any vector representation of the tree.

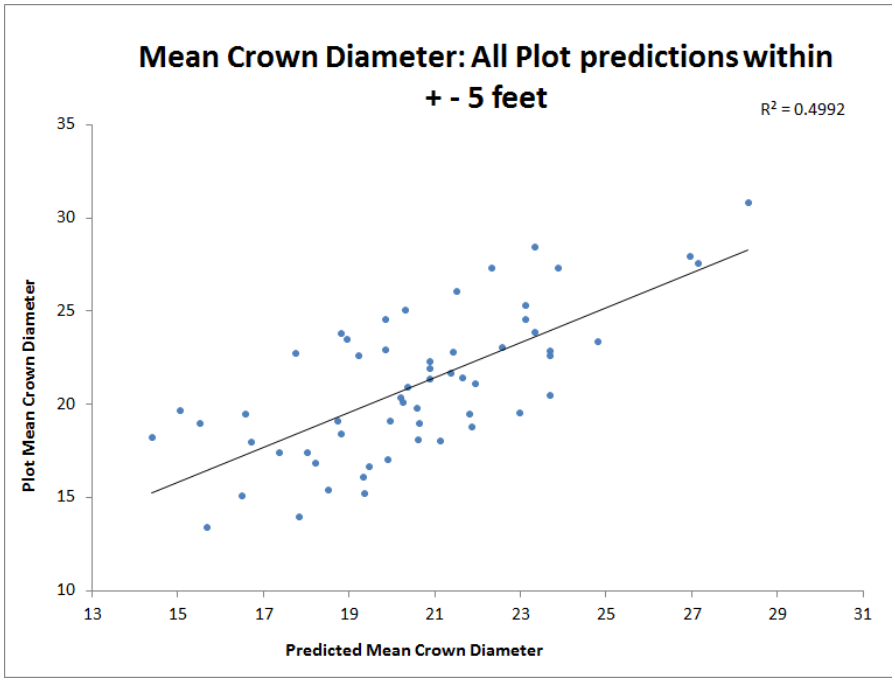

Figure 21. Scatterplot of predicted vs. observed crown diameter +-5 feet.

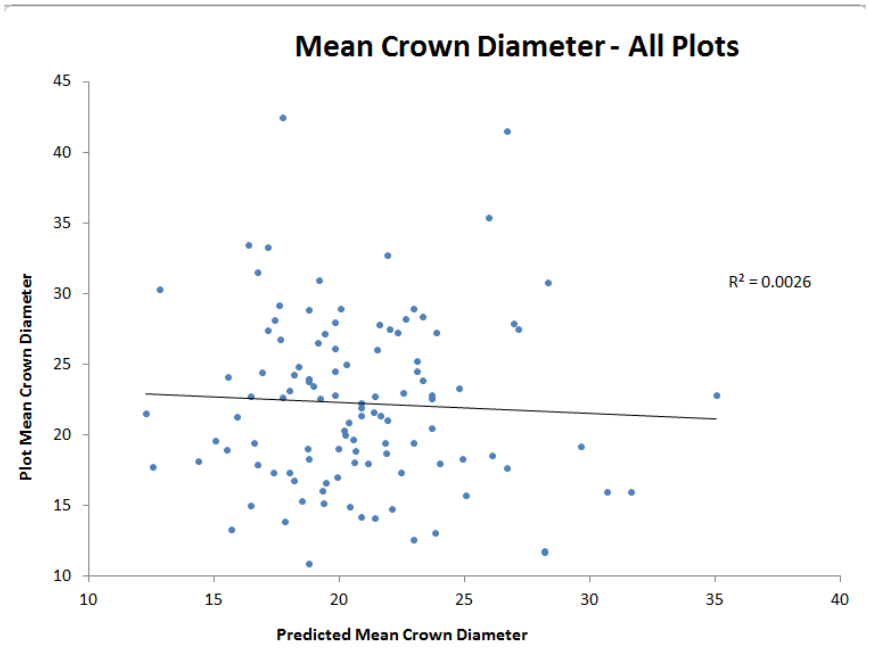

Figure 22. Scatterplot of predicted vs. observed crown diameter - all plots.

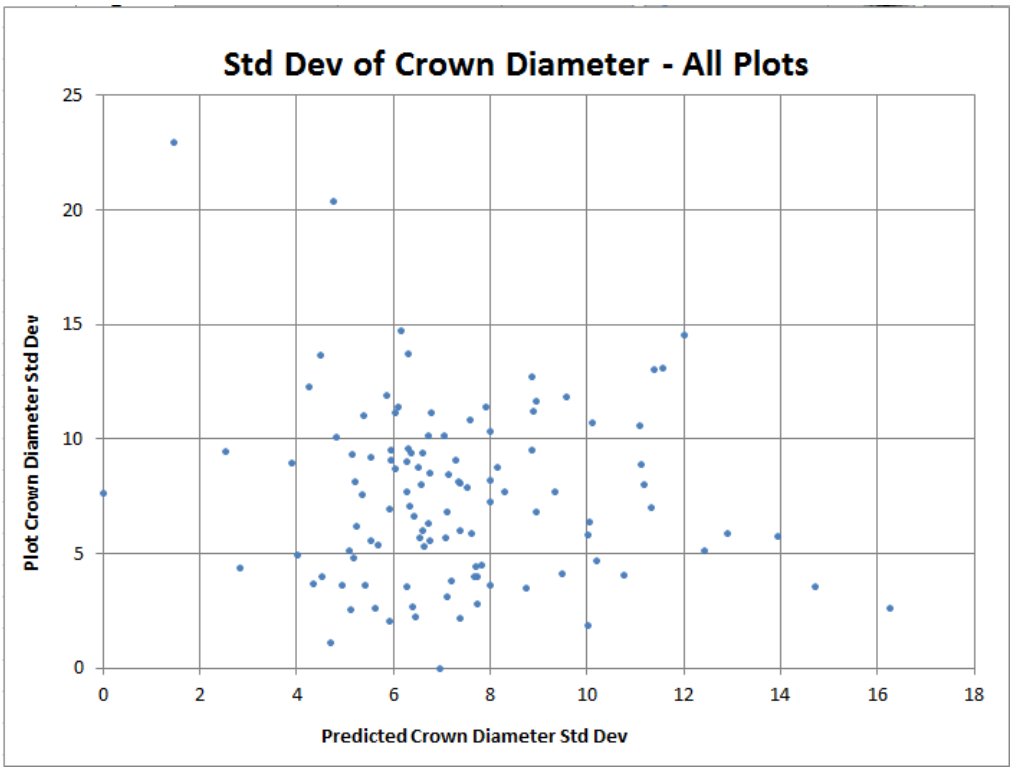

Figure 23. Scatterplot of predicted vs. observed crown diameter standard deviation.

4.2.3 Limiting Factors

Illumination angles, sensor viewing angles, species, stand density, and image quality can all affect the feasibility of identifying individual tree canopies for both automated and manual methods. Imagery must be of a high enough resolution for individual crowns to be visible; this usually means multiple pixels need to be able to capture a tree crown. Ideally, if a crown is 3 feet in diameter, a pixel of 1-foot (but preferably even higher to accommodate the mixed pixel issue) is needed, providing at least 9 pixels covering the crown. This is an ideal example where pixel mixing is not an issue. Differing image quality over an area can cause results to vary across a study site.

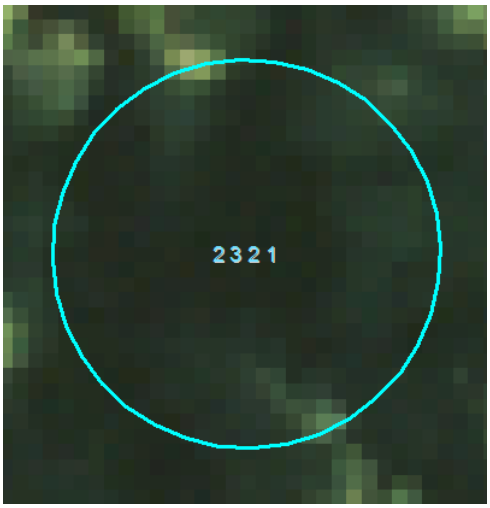

Figure 24. Plot showing no trees detected due to poor illumination and crown shadowing.

There are specific factors that can influence the TDA, by the nature in which it functions. One of the most significant is how the tree basins [i.e. gaps in the canopy] are calculated. Much of this hinges on a brightness value, which means that shade can heavily influence the accuracy in choosing between trees and basins. The most extreme occurrence of this was plot 2321, in which the algorithm detected no trees.

Field data indicates that plot #2321 has 11 living tally trees and a fairly open canopy. But because there is so much shade present in the image, trees are not represented by pixel brightness, and therefore no trees were recognized by the algorithm. This could be a specific issue when trying to identify late successional forest types, however, sometimes texture inherent in the imagery due to these shadows is utilized for successional forest class identification (Moskal & Franklin, 2002).

The TDA underestimates the number of trees in a plot by an average error of 9 trees per plot. This occurs because many trees in the image are masked by the crowns of others. Furthermore, 1-meter resolution is too course (not detailed enough) to capture some of the younger, smaller (less than 1 m crowns) trees within the inner plot, even if they were not covered by larger growth. Therefore, it might be necessary to adjust the variables of the algorithm depending on the age and structure of relative tree stands.

Some of these results do not depend strictly on tree size, however. A few plots that were dominated by Pacific Silver Firs showed poor results of tree crown delineation, compared to a landscape mostly dominated by Douglas Firs and Western Hemlocks. Because of this, the threshold pixel values within the algorithm might also be adjusted by tree species in order to bolster estimation accuracy.

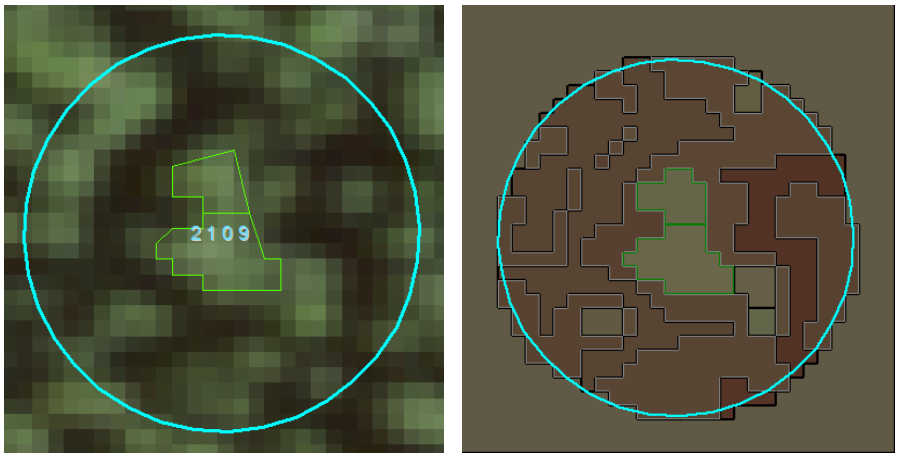

Figure 25. Pacific Silver Fir plot 2109.

Field data collection for plots 2109 and 2104: Landscape is dominated by irregularly spaced Pacific Silver Firs and blueberry bushes. The firs are a range of sizes (2in-12in) and are sometimes found in very tight groupings. Almost exclusively Pacific Silver Firs. Fairly large gap in the canopy, most trees have a relatively narrow crown and many are not within the size threshold.

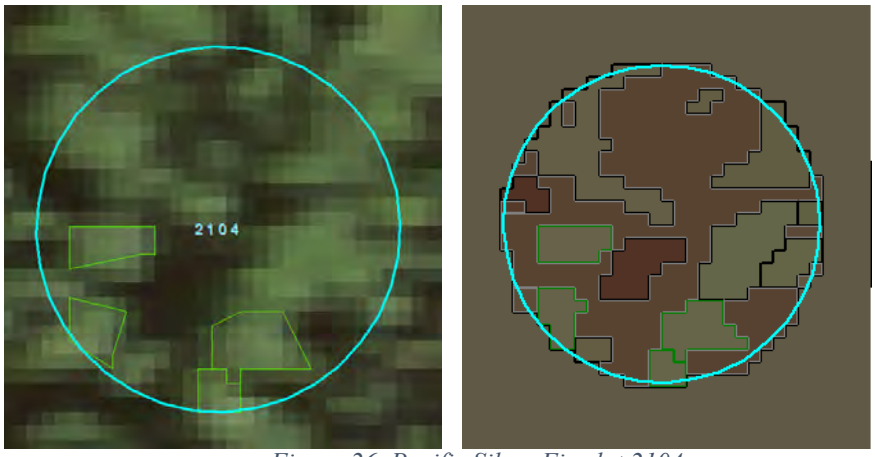

Figure 26. Pacific Silver Fir plot 2104.

Moreover, understory is often overshadowed or covered with the dominant canopy and cannot be detected in optical or imaging remote sensing data and subsequent techniques.

4.3 Recommendations

- We found that NAIP imagery, available for all of Washington State, was usable for successful crown delineation, if no other remotely sensed data is available, for the majority of sample plots. However, issues still exist within the approach of the delineation algorithm which needs the ability to adapt to varying stand types, especially deciduous-dominant or highly diverse stands.
- Without a more dynamic TDA, we recommend the LiDAR methods which tend to outperform the imagery at this task, especially due to LiDAR other usefulness in describing tree crowns such as capturing height.

5. Snag Detection

5.1 LIDAR Method

The methods described here were also used for Conifer/Deciduous Classification and Large Woody Debris.

The field crew collecting plot data recorded whether each tree measured was alive or dead, allowing for plot level counts of snags. There were plots with no snags present, creating a non-normal distribution of counts shown in Figure 27 below.

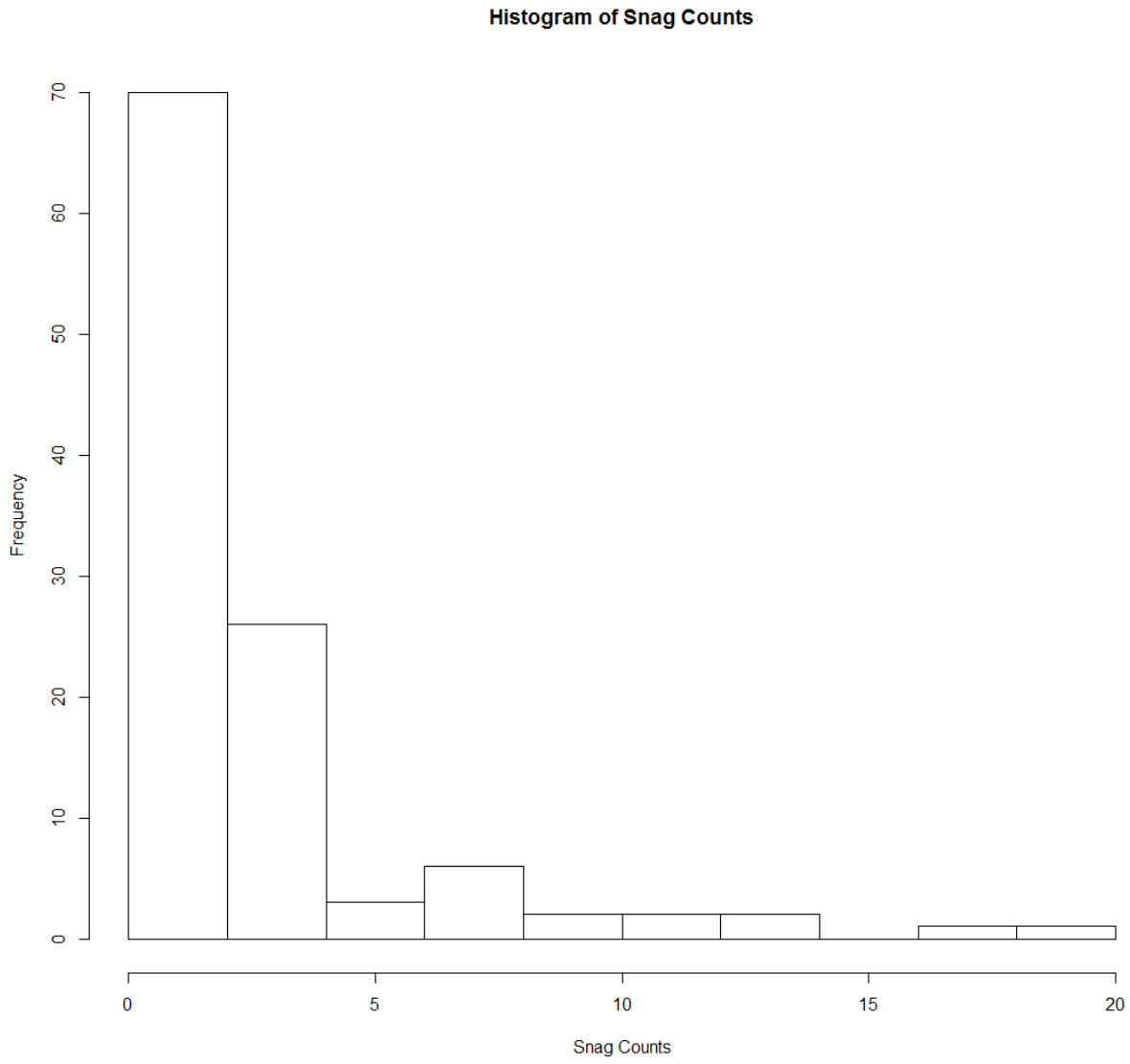

Figure 27. Histogram of snag abundance at field plots.

The variable should be transformed, but the square root transformation does not solve the issue, and zero cannot be log transformed (the log of zero is negative infinity). These plots cannot be removed, because they are legitimately zero, and models should be able to predict an absence of snags.

One method to deal with this, called a log-plus-one transformation, was not used, because an overrepresentation of plots without snags may result in too few plots across the range of the model, which would cause poor model performance.

The approach taken, is to use two models in combination. The first model is a logistic regression model to estimate the probability of snags being present or absent in a plot. The second model is a linear regression model used to estimate the abundance (number) of snags in a plot, and was developed using only plots with snags present. These two models are multiplied together to form the final model.

5.1.1 Logistic Regression Model

Using all plots, and the comprehensive modeling approach described in Section 3.1 LIDAR Method: Comprehensive Model Selection, models were built and ranked by their McFadden pseudo-R^2 values. However, unlike the methodology in Section 3.1.2 Intensity, L Moment, and Count metrics were not excluded from the comprehensive model selection process. Review of the models with the highest R^2 values resulted in selecting the model below.

Table 10. Snag Detection Logistic Model.

Metric	Model	McFadden pseudo-R^2
Snags Presence/Absence	SnagsPresenceAbsence = 168.87152 + (-7.81701 * A) + (-35.66202 * log(B)) + (-5.66108 * C) + (1.69955 * A * log(B)) + (0.20528 * A * C) + (1.16737 * log(B) * C) + (-0.04295 * A * log(B) * C)	0.60

Table 11. Snag Detection Logistic Model Variables.

Model Variable	Fusion CloudMetrics Variable	Variable Explanation
A	Elev.stddev	standard deviation of the heights, all returns
B	Int.P99	99th percentile of intensity values, all returns
C	(All returns above mean) / (Total first returns) * 100	percent cover; number of all returns above mean height / total number of first returns

5.1.2 Linear Regression Model

Using only plots with at least one snag, and the comprehensive modeling approach described in Section 3.1 LIDAR Method: Comprehensive Model Selection, models were built and ranked by their back-transformed R^2 values. However, unlike the methodology in Section 3.1, Intensity, L Moment, and Count metrics were not excluded from the comprehensive model selection process. Further review of the models with the highest R^2 values resulted in selecting the model below.

Table 12. Snag Detection Linear Model.

Metric	Model	R^2
Snags Abundance	log(snagsAbundance) = 0.82868 + (0.44633 * A) + (-0.01402 * B) + (-0.14325 * A * B)	0.43

Table 13. Table 12. Snag Detection Linear Model Variables.

Model Variable	Fusion CloudMetrics Variable	Variable Explanation
A	Elev.skewness	measure of lack of symmetry of the distribution of heights, all returns (McGaughey, 2016)
B	number of individual tree objects identified in the 6 ft. canopy height model	see Appendix D

5.1.3 Final Model

The logistic regression model for presence/absence and the linear regression model for abundance were multiplied together and regressed against the field measured snag counts.

This model had an R^2 of 0.47 and an RMSE of 2.53, shown in Figure 28.

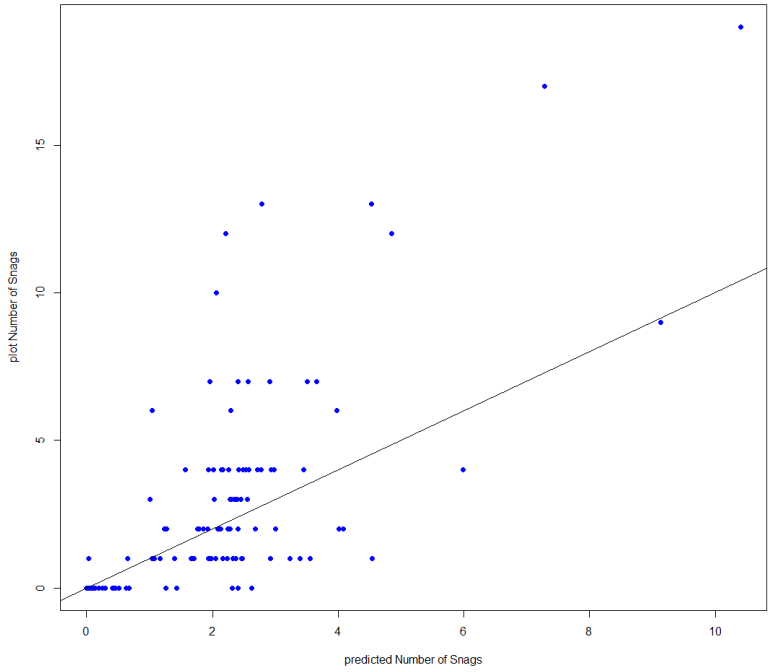

Figure 28. Predicted vs. plot snag counts with the line of equality.

5.1.4 Random Forest

The literature review performed before this pilot project identified a method that used Random Forest classification on LIDAR metrics to predict the presence of snags in various size classes (Martinuzzi, et al., 2009). This method was attempted to see how results compared to the presence/absence logistic regression model used above, with the results presented in Table 14 and Table 15.

The size classes identified by the researchers in that paper were tested, but only two of those classes are reported here, the ≥ 6" class (15cm) and the ≥ 10" class (25cm). The ≥ 6" class, is similar to the 5" minimum diameter cutoff used in our model. The ≥ 10" class is reported because it has approximately equal numbers of plots with and without snags. For small size classes, nearly all plots had snags, while for large size classes, almost no plots had snags, making the presence/absence classes unbalanced. Random Forest tends to work better with balanced presence/absence classes. It is expected that a model predicting all absence or all presence, would be very accurate, but have limited utility, in that it only provides information that is already known. The ≥ 10" class provides the most realistic and useful model results.

Table 14. Random Forest presence/absence classification results for ≥ 6" class.

		Actual data						
	Class	Present	Absent	Sum	Producer's accuracy	User's accuracy	Ommission error	Commission error
Predicted data	Present	76	7	83	90%	92%	0.10	0.08
	Absent	8	22	30	76%	73%	0.24	0.27
	Sum	84	29	113				

Table 15. Random Forest presence/absence classification results for ≥ 10" class.

		Actual data						
	Class	Present	Absent	Sum	Producer's accuracy	User's accuracy	Ommission error	Commission error
Predicted data	Present	37	17	54	70%	69%	0.30	0.31
	Absent	16	43	59	72%	73%	0.28	0.27
	Sum	53	60	113				

Although not examined in the referenced paper, Random Forest was also used to estimate snag abundance for the ≥ 6" and ≥ 10" classes. The resulting predictions were regressed against the plot counts of trees in these size classes, with the following results.

Table 16. Random Forest snag abundance model results.

Size Class	R^2	RMSE
≥ 6"	0.24	2.65
≥ 10"	0.26	1.46

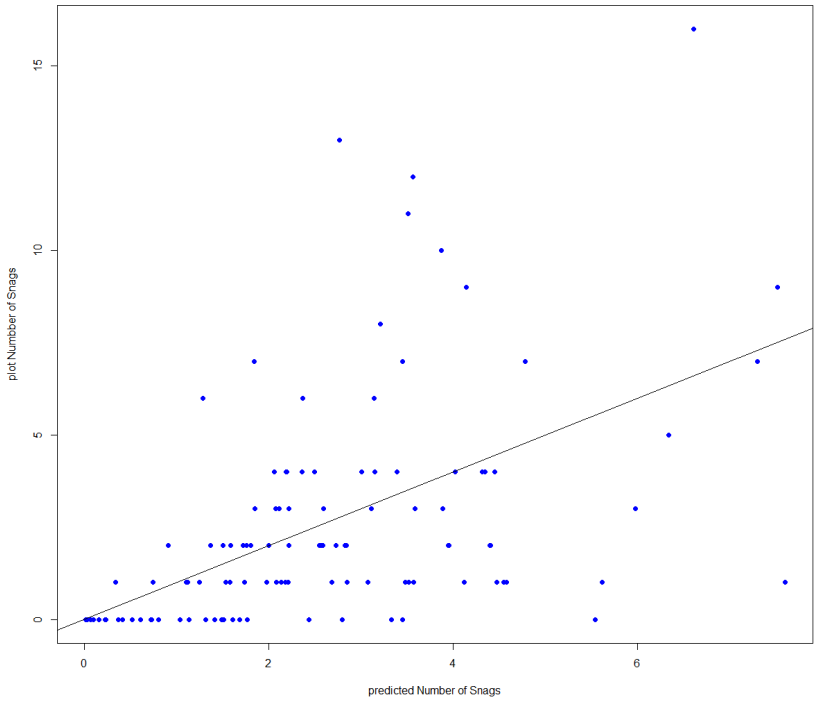

Figure 29. Random Forest ≥ 6" class, predicted vs. plot snag counts with the line of equality.

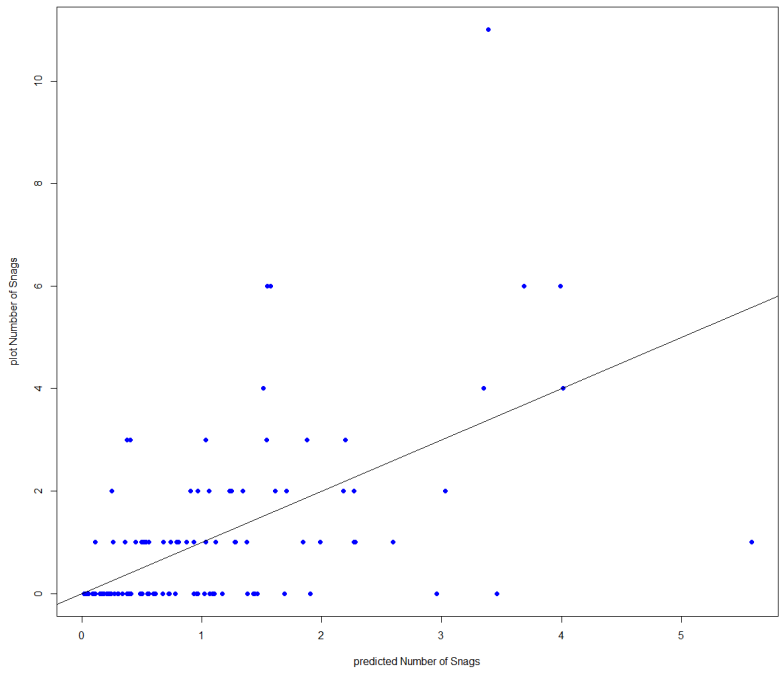

Figure 30. Random Forest ≥ 10" class, predicted vs. plot snag counts with the line of equality.

The results of the Random Forest methodology are in line with those described by the paper's authors, but are not better than those provided by the combined logistic regression / linear regression methodology used above.

5.4 Recommendations

- Snag detection is feasible with LiDAR approaches using multiple models, although the results are promising, these results would provide a 'rough' discernment of the snag properties on the landscape and should be supplemented with field observations. This is still a very active area of research with LiDAR and additional scientific developments should be monitored and tested to see if results can be improved.

6. Canopy Percent Cover

6.1 LIDAR Method

Canopy percent cover suitable for LiDAR assessment was not measured by the field crew as the cost and time to collect such data were deemed to be prohibitive. Moreover, canopy percent cover from LiDAR has already been established as a metric that is strongly related with LiDAR data in the literature, as documented in our previous pilot literature review (Moskal & Cooke 2015). Hemispherical photos were taken from plot center, but these photos were not processed to estimate cover. Although denisometer data was collected in the field the collection of such data is user subjective, and does not capture the structural three dimensional component of the canopy, thus, it is rarely used for comparisons to such high precision, three dimensional data as LiDAR. The densitometer is more suitable to understanding canopy closure.

LIDAR can be processed to estimate canopy percent cover. The Fusion program CloudMetrics (McGaughey, 2016) calculates several different cover metrics, all of which are different ratios of crown to non-crown LIDAR returns. The theory behind these metrics is that the denser the canopy, the less the laser will penetrate below the canopy, resulting in fewer non-crown returns. The available cover metrics from CloudMetrics are:

- Percentage of first returns above a specified height
- Percentage of first returns above the mean height
- Percentage of first returns above the mode height
- Percentage of all returns above a specified height
- Percentage of all returns above the mean height
- Percentage of all returns above the mode height
- Number of returns above a specified height / total first returns * 100
- Number of returns above the mean height / total first returns * 100
- Number of returns above the mode height / total first returns * 100

Typically, we consider the first metric, Percentage of first returns above a specified height, to be canopy percent cover. For this project, that was Percentage of first returns above two meters (6.56 ft.). First returns are more likely reflect off of the canopy than subsequent returns. Therefore, locations where first returns are reflecting off of objects below the two-meter height threshold likely have open canopy. The two-meter height threshold was chosen to separate trees from shorter shrubs.

6.1.1 Limiting Factors

There are different ways to estimate canopy closure or canopy cover (which are not the same) in the field, but they can be time consuming and the estimates they produce don't necessarily agree with one another or with LIDAR. None of these methods can be said to represent the precise field condition, thus while some are considered by researchers to have greater or lesser accuracy none can really serve as a check on the performance of the others.

6.1.2 Accuracy Assessment

A canopy percent cover model was not build for this project, so it is not possible to perform an accuracy assessment. Again, we avoided building this model so as not to under represent the utility of LiDAR data by comparing it to unsuitable field data. Previous work has shown that LiDAR outperforms imagery in canopy percent cover estimates as documented in our past literature review pilot (Moskal & Cooke 2015.)

6.2 Imagery Method

Although a LiDAR model was not constructed, for reasons of imprecise accuracy comparison, a cruder estimate was created from imagery to show some capability that exists with this approach. Some field data was readily available to gauge accuracy, making a provisional analysis more feasible. Canopy percent cover was calculated by summarizing the surface area of all individual tree crown objects, computing the ratio of this over an entire plot, and comparing that against field-crew estimations of canopy cover. Although we did not explore the relationships between densitometer and LiDAR, we did explore the optical data and field data relationships as this is commonly done in remote sensing research.

6.2.1 Accuracy Assessment

Estimated Canopy Percent Cover was within ± 25% of field estimated canopy cover for 63 of the 113 plots [56% of all plots]. This outcome is similar to imagery predictions of crown diameter, which are strongly dependent on how individual trees are identified from imagery. As the TDA is configured to fit the majority of plot compositions [Douglas Firs and Western Hemlocks] there are outliers that warrant a more dynamic approach. The field estimates of the canopy cover were estimated using a spherical densiometer. While this estimate is lacking some objective rigor that is associated with other metrics, it still provides an insight as to how well imagery algorithms are classifying tree canopy area per plot. Imagery predictions were generally underestimating the canopy percent cover when compared to field data. This follows in suit with crown diameter estimations, which were also underestimated more often than overestimated.

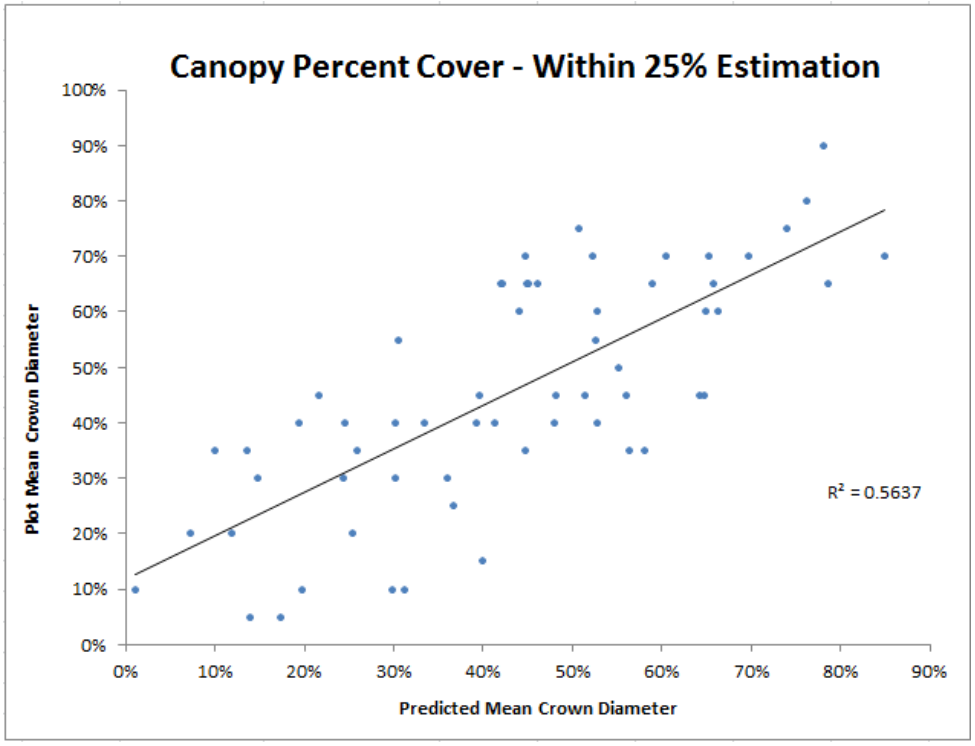

Figure 31. Imagery based percent canopy cover scatter plot.

6.2.2 Limiting Factors

Illumination angles, sensor viewing angles, species, stand density, and image quality can all affect the feasibility of identifying individual tree canopies for both automated and manual methods. Imagery

must be of a high enough resolution for individual crowns to be visible. Differing image quality over an area can cause results to vary across a study site.

Field estimations of percent canopy cover may have subjective biases because of the methodology used. Moreover, it may be possible to only estimate upper levels of tree canopy coverage using aerial/satellite imagery because of its inability to offer some of the vertical information capable in LiDAR.

6.3 Recommendations

- Remote sensing, either optical or LiDAR stands a good chance to find relationships between canopy cover, canopy closure, canopy %, however, defining which relationships are of particular interest are necessary before further analysis should be undertaken.
    - Processing of hemispherical plot photos could be used to assess the accuracy in some of these estimates.
    - A second pilot might include more rigorous and objective field collection tasks for obtaining canopy characteristics. For example, canopy cover (portion of ground covered) or canopy closure (portion of sky hemisphere obscured as viewed from single point; densitometer) could be investigated and compared to LiDAR and imagery data. This would help to determine the relative value of LiDAR vs. imagery for predicting riparian canopy shading.
- Provisional imagery analysis data could be used to reinforce the initial imagery segmentation algorithms by determining which imagery band and variable statistics influence canopy cover estimations.

7. Stand Density

7.1 LIDAR Method

Three methods were used to build stand density models from LIDAR. The first approach built a linear regression model based on individual tree objects (ITOs) from a segmented canopy height model. The second approach built a linear regression model using the method described in further detail in Section 3.1, the LIDAR Method for Canopy Height. The third method included the stratified bin of each plot, which indicates information about the height and cover values of each plot.

7.1.1 Crown Segmentation

An attempt to estimate density using ITOs developed using the crown segmentation methodology described in Appendix D was undertaken. All three resolutions of canopy height model, 3 ft., 6 ft., and 15 ft., were tested, with the 6 ft. model performing best. Individual tree objects identified through this method were counted to estimate stand density, but these counts were a poor predictor of stand density and were less effective than the linear regression model described in the next section. Development of the canopy height models and ITOs was very time consuming.

Table 17. Stand Density Model.

Metric	Model	R^2	RMSE
Density	sqrt(density) = 1.979 + 4.0048*sqrt(A)	0.34	76.55

Table 18: Model Variable.

Model Variable	Fusion CloudMetrics Variable	Variable Explanation
A	number of individual tree objects (ITOs) identified in the 6ft canopy height model	see Appendix D

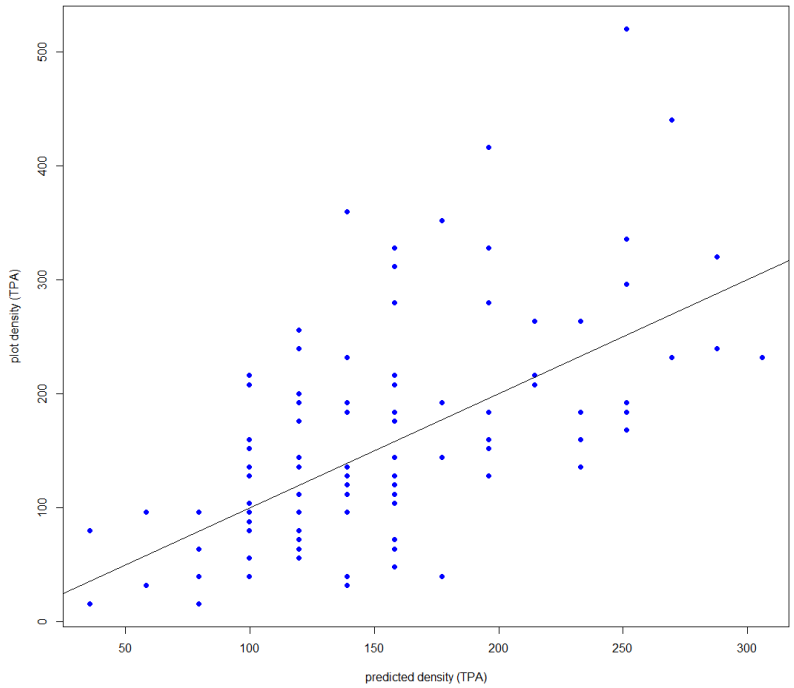

Figure 32. Predicted vs. plot density with the line of equality; 6 ft. Canopy Height Model individual tree objects (ITOs).

7.1.2 Standard Linear Regression Model Approach

The second model is a linear regression model developed using the comprehensive modeling approach described in Section 3.1 LIDAR Method: Comprehensive Model Selection. Models were built and ranked by their back-transformed R^2 values.

Table 19. Stand Density Linear Regression Model.

Metric	Model	R^2	RMSE
Density	sqrt(density) = -1.9701 + (2.1654*log(A)) + (16.4874*log(B)) + (0.3057*sqrt(C)) + (-5.8437*log(A)*log(B)) + (1.5078*log(B)*sqrt(C))	0.46	68.96

Table 20. Stand Density Linear Regression Model Variables.

Model Variable	Fusion CloudMetrics Variable	Variable Explanation
A	Elev.maximum	maximum height, all returns
B	Elev.kurtosis	measure of whether distribution of heights are heavy-tailed or light-tailed relative to a normal distribution, all returns (McGaughey, 2016)
C	Percentage.all.returns.above.6.56	percent cover; number of all returns above 2m / number of all returns

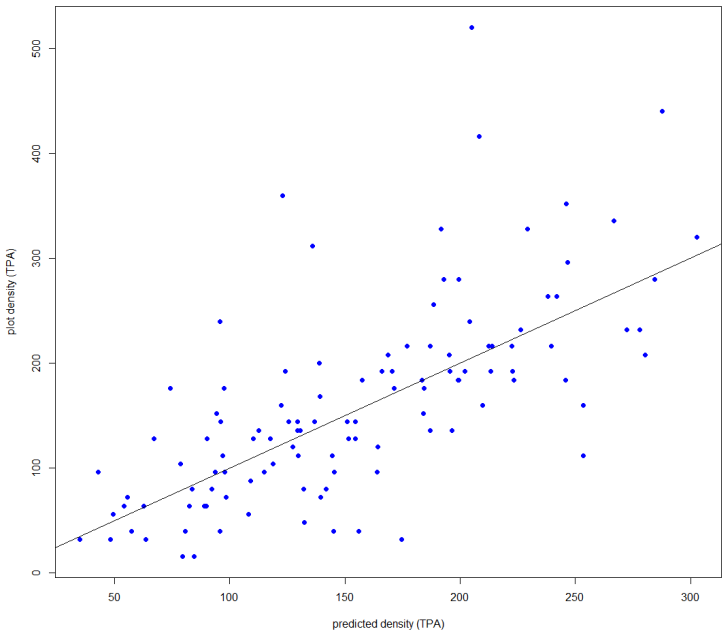

Figure 33. Predicted vs. plot density with the line of equality; standard linear regression approach.

7.1.3 Model with BIN

An alternative model was also developed using each plot's bin from the stratification process described in Appendix A. Using the 80th percentile height and percent cover values calculated in CloudMetrics, each plot was classified into its true bin. A linear regression model using the bin value as a factor was built. Adding this information slightly improved the model performance over the standard linear regression approach.

Because there are 12 bins and 12 interaction terms in this model, an equation with all 24 of the coefficients is not written here. However, it's simplified form and performance metrics are presented below.

Table 21. Stand Density Linear Regression Model with Bin.

Metric	Model	R^2	RMSE
Density	sqrt(density) ~ A + sqrt(B)	0.49	67.12

Table 22: Model variables.

Model Variable	Fusion CloudMetrics Variable	Variable Explanation
A	the bin of each plot as a factor	see Appendix B

B	number of individual tree objects (ITOs) identified in the 6ft canopy height model	see Appendix D

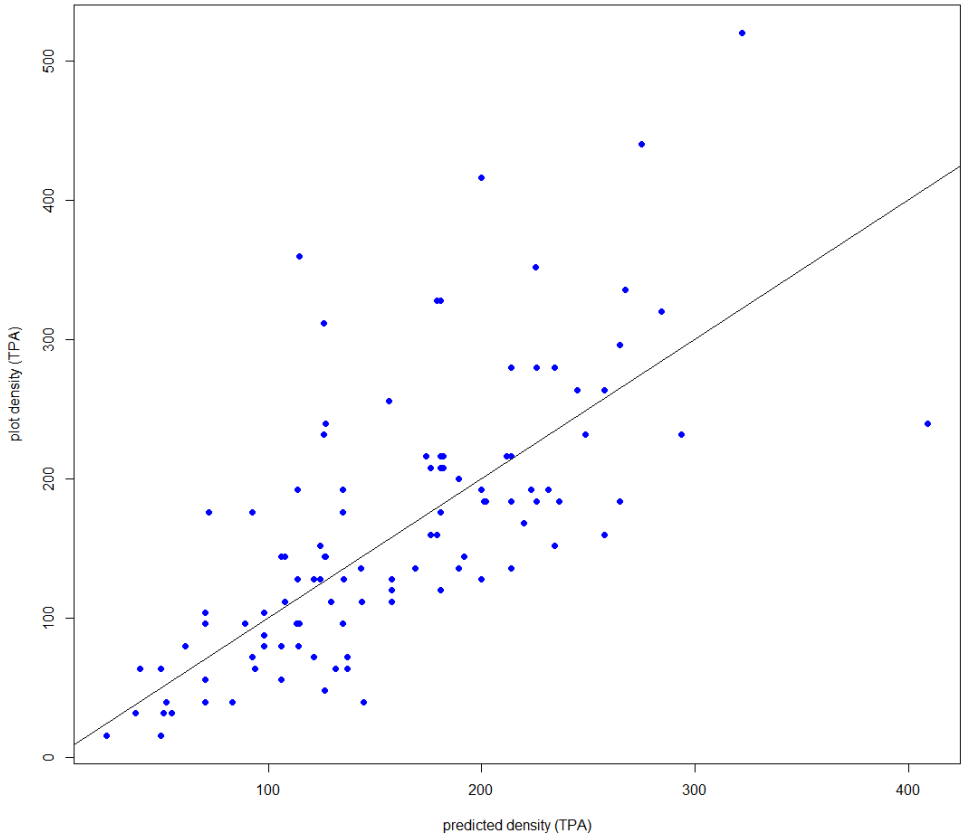

Figure 34. Predicted vs. plot density with the line of equality; model including bin.

7.2 Imagery Method

Like many of the other metrics, stand density is dependent on the existence of ITOs. Because of varying tree composition throughout the project area, one single TDA does not have the flexibility to address disparate scenarios. Ideally, the algorithm would first evaluate the area of interest, attempt a preliminary classification of composition types, and then execute the respective delineation function that best accommodates the spectral and spatial composition of that type. Types would vary according to presence of conifer/deciduous trees and maybe even species. However, the single TDA is still showing promising results for the majority of sample plots within the project area.

7.2.1 Accuracy Assessment

In 40% of plots, tree stand density predictions are within ± 5 trees of actual plot counts. In almost 75% of plots, predictions are within ± 10 trees. Following the error in estimation of the other metrics, the tree delineation tends to underestimate the number of trees per acre.

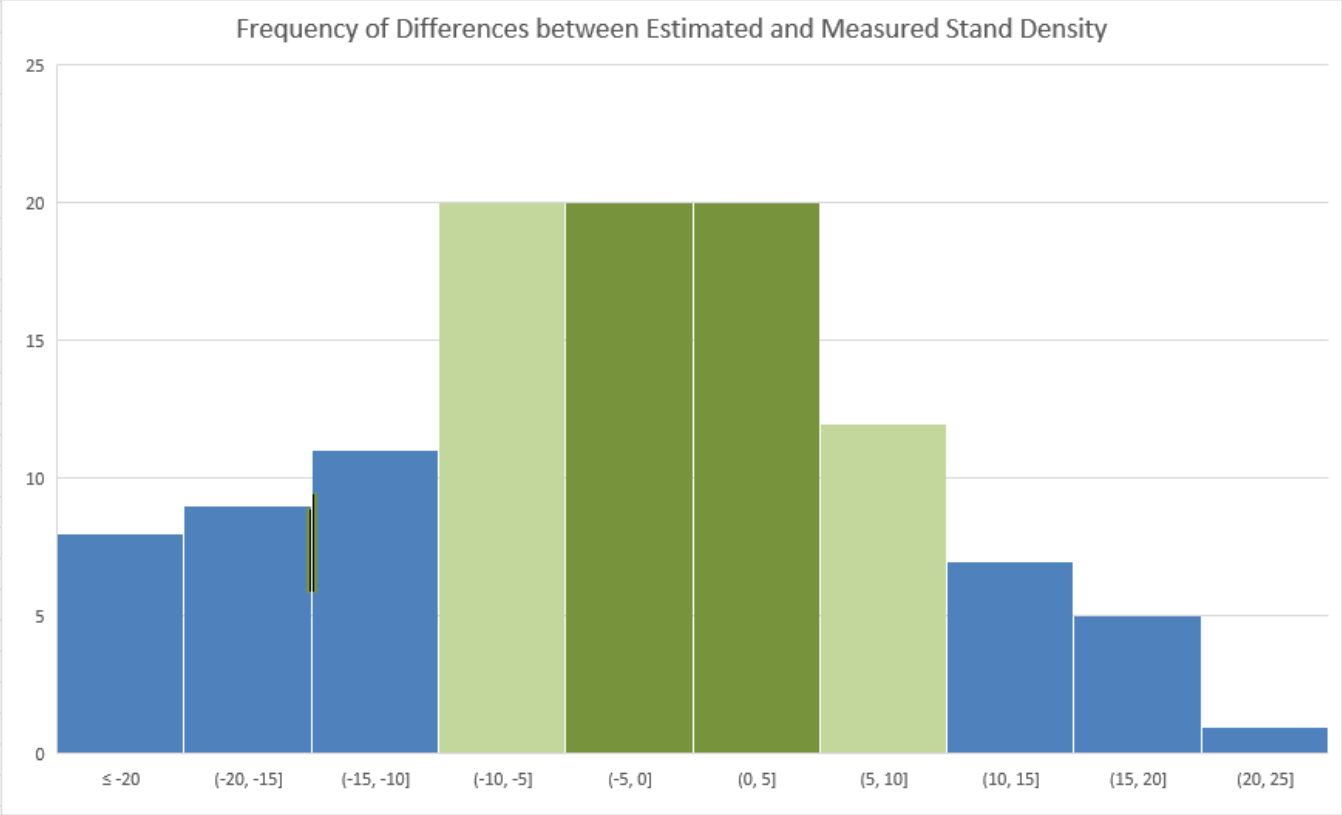

Figure 35. Frequency difference between estimated and measured stand density.

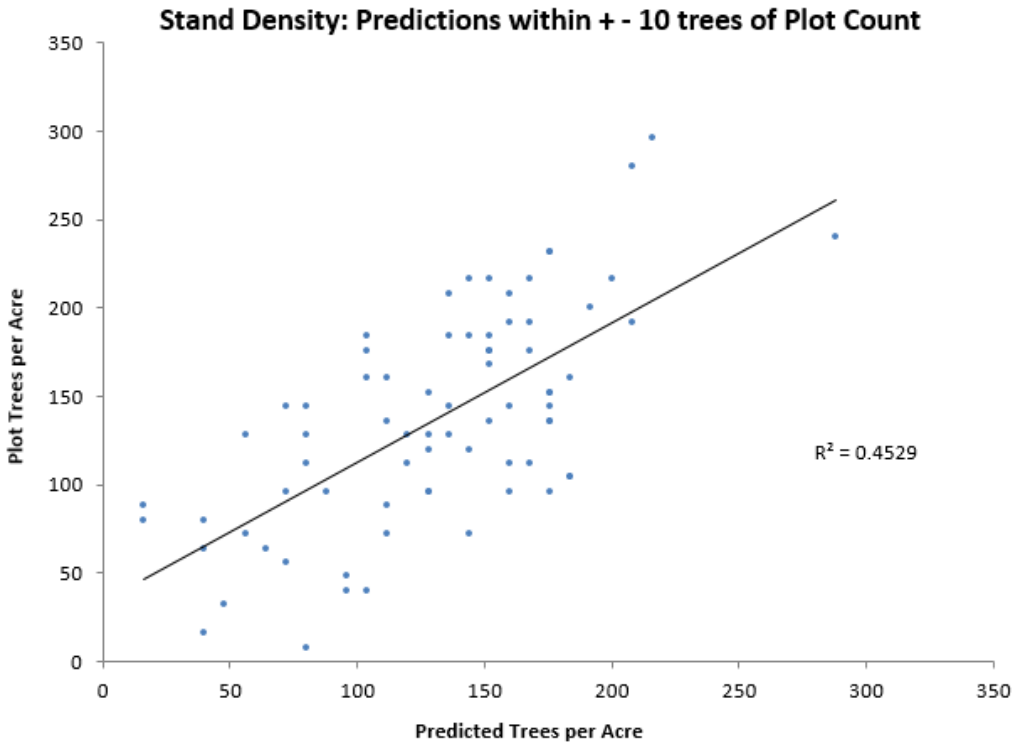

Figure 36. Stand density scatterplot +/- 10 trees

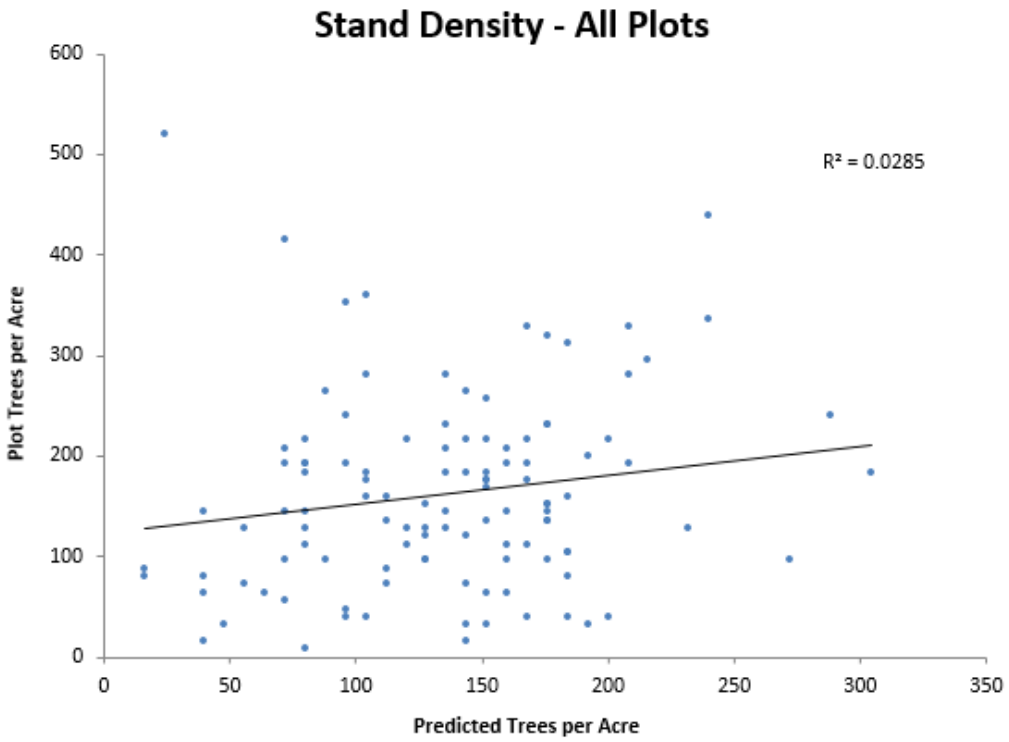

Figure 37. Stand density - all plots

7.2.2 Limiting Factors

Evaluating all plots together does reveal the need for model adjustment, else existing outliers cannot be accurately estimated. The highest margin of error was 62 in plot 2123, which was previously discussed under the Limiting Factors of the Crown Diameter section. Examining the results of all plots, our model's predictive capability decreases substantially.

7.3 Recommendations

- Stand density is achievable almost equally well with LiDAR and imagery based models, although, we suspect, in multilayer stands the LIDAR models might perform slightly better but we were not able to test this assumption

8. Conifer/Deciduous Classification

8.1 LIDAR Method

LIDAR was used to estimate the number of deciduous trees, following methods similar to the one described in Section 5.1 Snag Detection, LIDAR Method.

8.1.1 Logistic Regression Model

Using all plots, and the comprehensive modeling approach described in Section 3.1 LIDAR Method: Comprehensive Model Selection, models were built and ranked by their McFadden pseudo-R^2 values. However, unlike the methodology in Section 3.1.2 Intensity, L Moment, and Count metrics were not excluded from the comprehensive model selection process. Further review of the models with the highest R^2 values resulted in selecting the model below.

Table 23. Logistic Regression Model for Conifer/Deciduous Classification.

Metric	Model	McFadden pseudo-R^2
Deciduous Presence/Absence	deciduousPresenceAbsence = 8.53536 + (-1.94052 * log(A)) + (-0.09364 * B) + (0.07666 * C)	0.29

Table 24. Logistic Regression Model for Conifer/Deciduous Classification Variables.

Model Variable	Fusion CloudMetrics Variable	Variable Explanation
A	Elev.P20	20th percentile of the heights, all returns
B	Int.mean	mean intensity, all returns
C	(All returns above mean) / (Total first returns) * 100	percent cover; number of all returns above mean height / total number of first returns

8.1.2 Linear Regression Model

Using only plots with at least one hardwood tree, and the comprehensive modeling approach described in Section 3.1 LIDAR Method: Comprehensive Model Selection. Models were built and ranked by their back-transformed R^2 values. However, unlike the methodology in Section 3.1.2, Intensity, L Moment, and Count metrics were not excluded from the comprehensive model selection process. Further review of the models with the highest R^2 values resulted in selecting the model below.

Table 25. Linear Regression Model for Conifer/Deciduous Classification.

Metric	Model	R^2
Deciduous Abundance	log(deciduousAbundance) = 0.568310 + (-0.179342 * sqrt(A)) + (0.038097 * B) + (0.431291 * sqrt(C)) + (-0.008131 * sqrt(A) * B)	0.61

Table 26. Linear Regression Model for Conifer/Deciduous Classification Variables.

Model Variable	Fusion CloudMetrics Variable	Variable Explanation
A	Int.P30	30th percentile of intensity values, all returns
B	Percentage.first.returns.above.mean	percent cover; number of first returns above mean height / total number of first returns
C	number of ITOs identified in the 6 ft. canopy height model	see Appendix D

8.1.3 Final Model

The logistic regression model for presence/absence and the linear regression model for abundance were multiplied together and regressed against the field measured deciduous counts.

This model had an R^2 of 0.67 and an RMSE of 2.80.

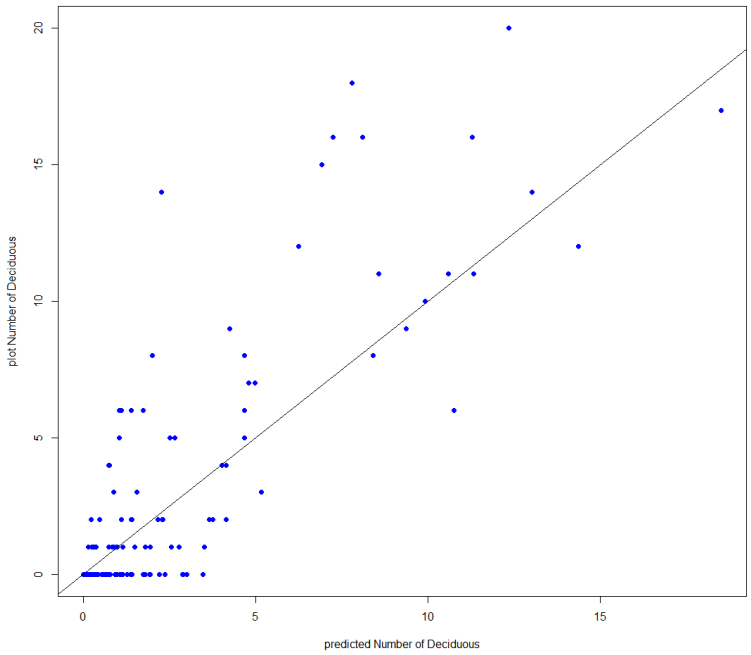

Figure 38. Predicted vs. plot deciduous counts with the line of equality.

8.1.1 Limiting Factors

Developing the canopy height model and ITOs used in the abundance model is very time consuming, taking several weeks for the Mashel watershed. The methods used to develop these datasets are described in Appendix D - Individual Tree Segmentation.

8.2 Imagery Method

Conifer/Deciduous classification, Species classification, and Basal Area are all predictors that, with imagery interpretation, rely much more on the statistical analysis of pixel content of individual trees. While previous metric predictions are still influenced by spectral analysis within the TDA, estimating more granular qualities of the tree, like species, requires further investigation of color compositions.

8.2.1 Provisional Spectral Analysis

Six plots were selected as training sites to develop a base for deciduous vs. conifer signatures. The plots were based on two factors. First, the number of trees in the sample plot are relatively well-predicted by the TDA, which provides a more stable base for individual comparison. Second, the tree composition is either conifer or deciduous-dominant. These sample plots provided a basis on how to construct the modelling approach.

Several rudimentary parameters from ITOs were evaluated in order to determine systematic differences between conifer and deciduous compositions. These include:

- Mean NDVI, Red, Green, Blue, and NIR spectral values
- The standard deviation of NDVI, Red, Green, Blue, and NIR
- Intensity, Hue, Brightness

Many of these variables show no statistical significance between conifer and deciduous data sets, or demonstrate collinearity within regression analyses. The predictors that do show promise are the Red, Green, and Intensity variables. Deciduous trees show a far greater variation within the Red and Greed spectral values [Appendix E].

To explore this, the standard deviations of these bands were used as broad thresholds to classify respective tree objects as conifer or deciduous. The following figures serve as visual comparisons. The table shows the tree object counts for respective standard deviation values.

Table 27. Red Band Imagery Standard Deviation Comparison.

Std Dev Values	Mixed Deciduous	Alder Dominant	Alder Dominant 2	Mixed Conifer	Mixed Conifer 2	DF and WH
1	0	0	0	0	0	0
2	0	0	0	0	1	0
3	0	1	0	3	0	0
4	0	0	0	2	2	1
5	0	2	1	5	0	1
6	0	0	2	3	0	2
7	0	0	1	3	4	4
8	0	2	0	2	0	3
9	1	2	0	0	3	2
10	3	0	0	0	5	0
11	0	4	3	0	2	1

12	1	1	1	0	2	1
13	1	2	0	0	0	0
14	1	0	5	0	0	0
15	0	0	3	0	0	0
16	2	1	3	0	0	0
17	0	0	0	0	0	0
18	1	0	0	0	0	0
19	0	0	0	0	0	0
20	1	0	0	0	0	0

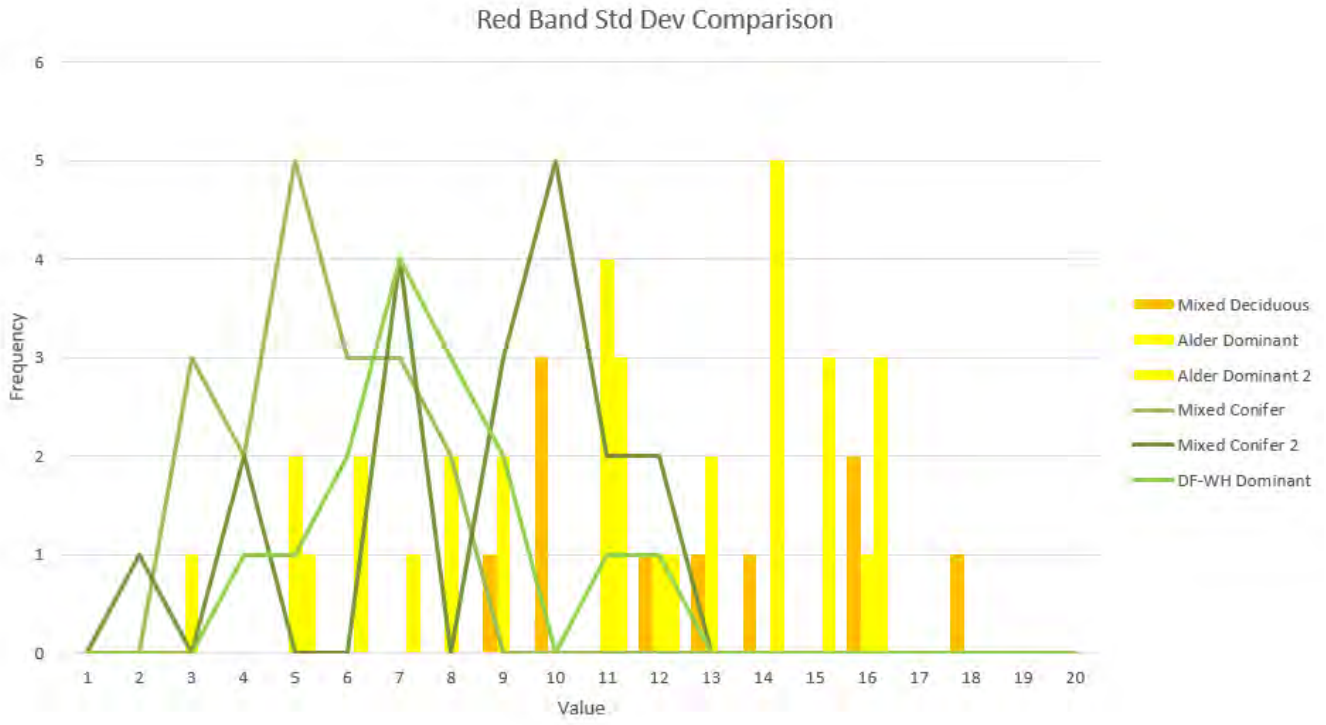

Figure 39. Red band standard deviation comparison.

Using only the mean Red and Green values for each ITO as explicit thresholds, the basic extension of the TDA shows general success with many sample plots, but fails to account for variability in others. For 46 of the sample plots [~41% of all plots] this approach predicted within +- 5 of the conifer tree count and was within +-10 trees for 70 sample plots [~62% of all plots].

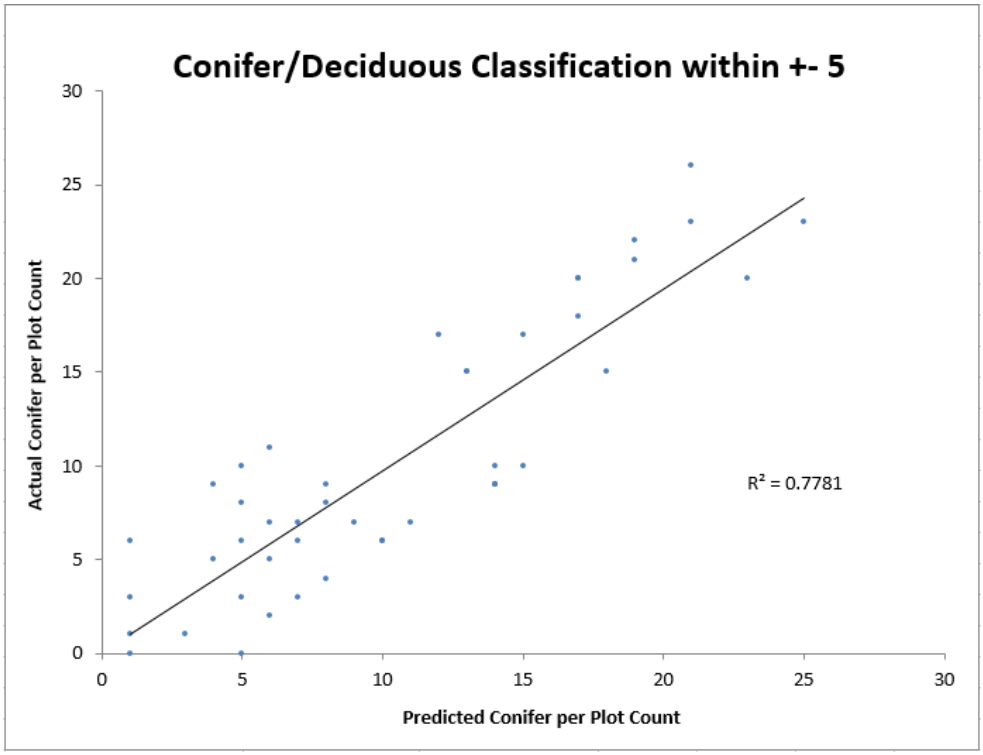

Figure 40. Coniferous/Deciduous classification: 41% of all plots

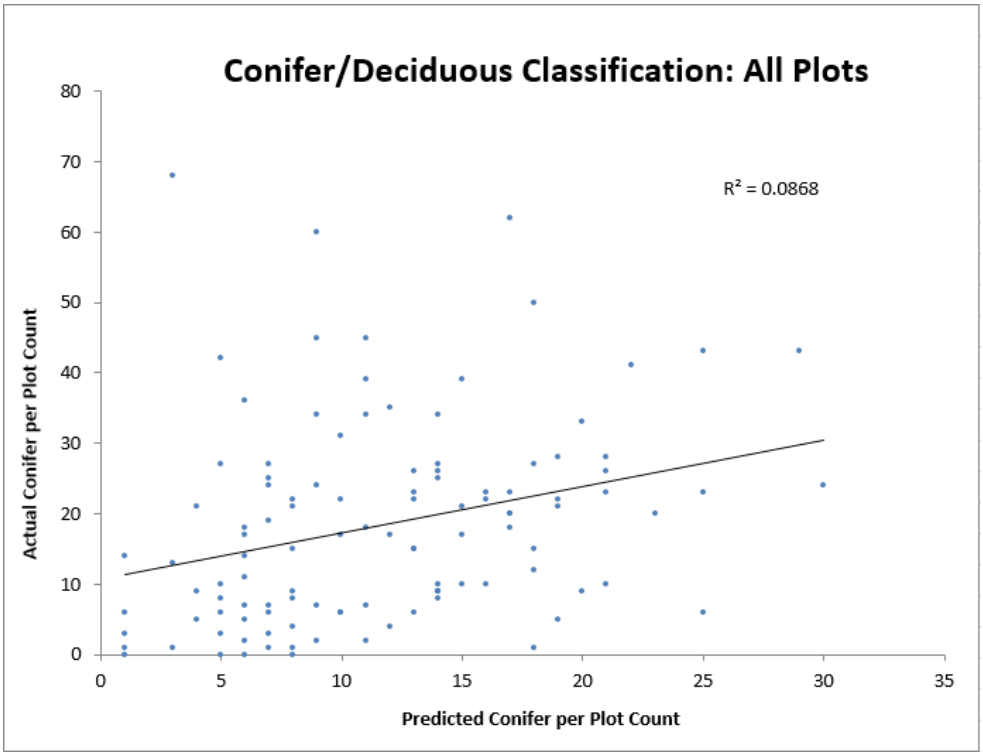

Figure 41. Coniferous/Deciduous classification scatterplot: all plots.

8.2.2 Linear Regression Model

A regression model was constructed as another approach, using the Red and Green band variables as its base. Forty remaining spectral and spatial variables were tested in several permutations and progressively narrowed down to the most significant coefficients. The dependent variable was the ratio of conifer trees to all trees for each plot. Field data was modified by adding a binary coding of 1=conifer 0=deciduous. This was based on the species of the tree. This value was then summed for each plot and divided by the plot's total tree count.

Table 28. Coniferous/Decisions Classification Linear Regression Model.

Metric	Model	R^2
Conifer Abundance	Plot.ConiferRatio = 2.81841 + A(0.02716) + B(0.13621) + C(0.409775) + D(-45.04506) + E(-0.05550)	0.29

Table 29. Coniferous/Decisions Classification Linear Regression Model Variables.

Model Variable	eCognition IndividualTreeObject.Variable
A	Mean Red
B	Mean Green
C	Standard Deviation of GLCM Entropy
D	Mean Intensity
E	Standard Deviation of Predicted Crown Diameter

The Gray Level Co-Occurrence Matrix (GLCM) method is a way of extracting second order statistical texture features by considering the relationship between groups of two (usually neighboring) pixels in the original image. The GLCM is a tabulation of how often different combinations of pixel grey levels occur, in a given direction, in an image object. The grey-level co-occurrence matrix can reveal certain attributes pertaining to the spatial distribution of the grey levels in an image object. Homogeneous scenes, like many of the conifer-dominant stands, will exhibit higher GLCM /entropy values, in both mean and variance.

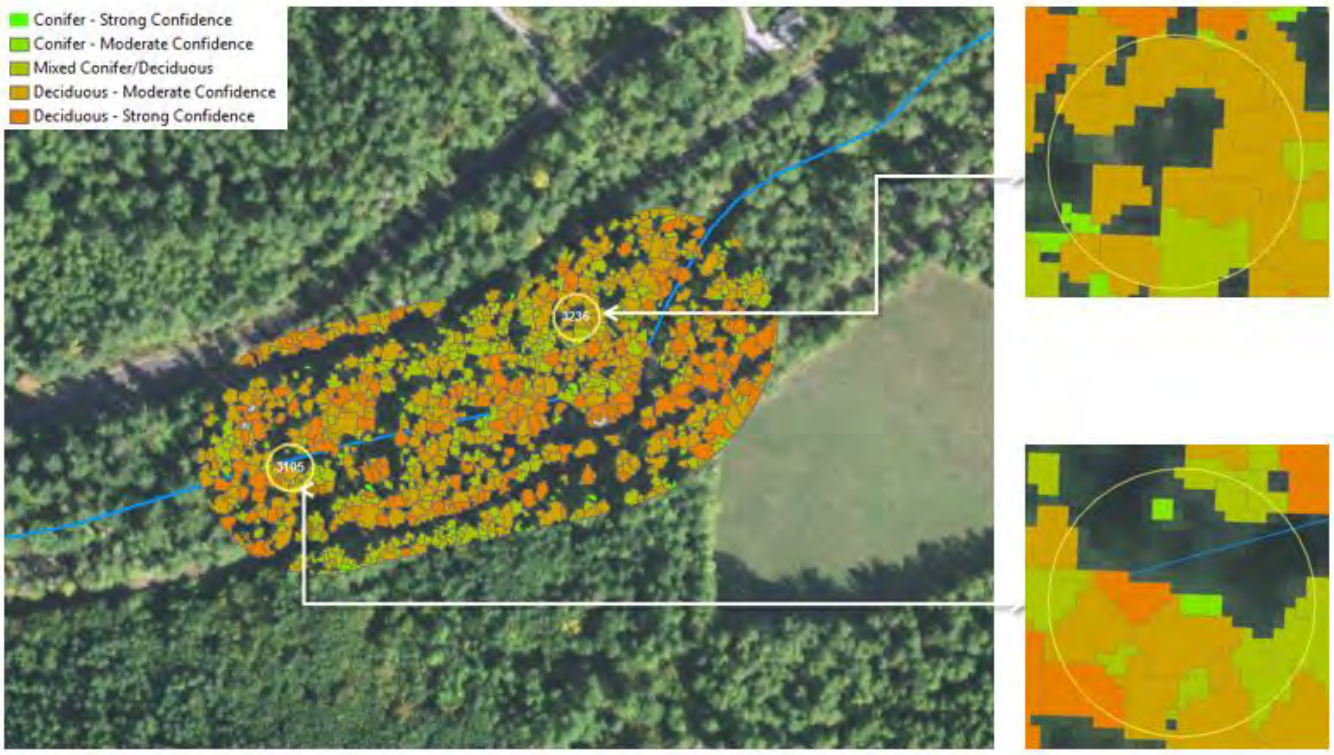

Figure 42. Example of imagery based coniferous/deciduous crown classification along a stream reach.

8.2.3 Limiting Factors

The major limiting factor in this prediction again resides within the initial TDA. The majority of tree species collected from the field are Western Hemlocks and Douglas Firs, which contribute to much of the TDA's accuracy. Deciduous trees are not captured within individual tree crown objects as accurately since their overall disproportion in number influenced the design of the algorithm much less. Still, this technique was chosen because it builds much of the provisional work for calculating tree species.

A different approach that would circumvent the dependence on the TDA is to perform a similar spectral analyses but on the entire plot-level image instead of ITOs. This might inherit more complexities with grass, shrubs, and open ground, but these features could also be suppressed. Even in a rudimentary analysis the general proportions of deciduous and conifer presence might be detected fairly accurately, as current results suggest.

8.3 Recommendations

- Our findings indicate that the spectral information from imagery is adding ability to separate the two, further research should be devoted into fusing LiDAR and imagery for this purpose but it is beyond the scope of this study and could be investigated in a separate project.
- There are other approaches with imagery that have proven to be effective but were not employed in this study. One alternative is to evaluate the spectral composition at plot-level instead of individual tree-level. This circumvents any error associated with the TDA, but might also introduce bias from non-tree vegetation within the plot. Still, research has shown this approach to be effective at determining coniferous and deciduous composition.

- Stem maps could have provided additional support to the TDA creation by allowing specific geo-spatial comparisons of coniferous and deciduous tree existence.

9. Vegetation Class (Seral Stage)

9.1 LIDAR Method

Vegetation class is a description of how a stand is progressing through a development process and how the individual trees are interacting with each other and their specific, local environment.

There are many different schemes used for classifying vegetation into development stages, with possibly one, Oliver and Larson (Oliver & Larson, 1990), establishing the most commonly used terminology. As time has passed, schemes for classifying vegetation seem to have become more complicated, increasing the number of classes from the four described in Oliver and Larson, to as many as six or eight.

LIDAR is a tool that can help describe stand structure. Any method to estimate vegetation class from LIDAR must use the structure as a proxy for development progress. To this end, only classes that can be distinguished from one another structurally can be identified using LIDAR. This argues for a simple classification scheme.

We chose a four class scheme based on Oliver and Larson, but because the names of vegetation classes reflect stages of a biological process, and because LIDAR can only tell you structural characteristics, we propose a different naming scheme for these vegetation classes.

Table 30. Proposed Vegetation Classes.

Oliver and Larson Class	Proposed LIDAR Class
Stand Initiation	Initiation/Establishment
Stem Exclusion	Exclusion/Closure
Understory Re-Initiation	Maturation
Old-Growth	Diversification

Vegetation class was not measured by the field crew and would be a highly subjective measurement had it been done. It is therefore not possible to test the accuracy of any model, but we can propose an approach to assigning vegetation class that is similar to the binning process used to determine field plot locations, described in Appendix A - Plot Location Selection.

LIDAR measures height and cover extremely well, and is also capable of describing the distribution of the heights. A wide distribution of heights indicates a more open and variable canopy structure, while a narrow distribution of heights indicates a closed and consistent canopy. The combination of these three metrics, height, cover, and distribution of heights, could be used to identify several different structural classes.

For this project, a metric called surface area ratio, or rumple, will be used to describe the distribution of the heights. It compares, as the name implies, the surface area of the canopy height model, to the surface area of the ground model. For the 75 ft. cells used for this project, the ground model cells have an area of 5625 ft. A completely flat canopy height model would also have a surface area of 5625 ft., producing a surface area ratio of one. As the canopy height model becomes increasingly rough (a wider

distribution of heights), the surface area increases, causing the surface area ratio to increase. Rumple values for the Mashel watershed are less than one along edges and areas with no data, otherwise, they range from 1 to just over 8.

Oliver and Larson define a class, understory re-initiation, which is a non-useful class with regards to LIDAR. Very few LIDAR returns will penetrate the primary forest canopy in a closed stand, making it very difficult to determine much about understory vegetation. It would be misleading to call this class understory re-initiation.

9.2 Vegetation Class Descriptions

1. Initiation/Establishment: open with short vegetation. The 20 ft. maximum height is the approximate height at which trees would be clear to grow.
2. Exclusion/Closure: increasing canopy closure, and height. When a stand reaches 80% cover, it would commonly be considered closed canopy. The 60 ft. maximum height is the approximate height at which trees would reach stem exclusion.
3. Maturation: closed canopy with tall trees.
4. Diversification: Canopy breakup and release of understory.

The heights described here are based on expert opinion from discussions within RSAG. They are approximations and represent general guidelines, not hard class boundaries. Stand definitions would traditionally be based on tree diameters (Johnson & O'Neil, 2001). Height is used here because LIDAR is suited to accurate height measurements.

9.2.1 Hierarchical Classification Scheme

A hierarchical classification scheme can be used to assign areas on the landscape to vegetation classes, based on their values in the different LIDAR metrics. When an area is assigned to a class in one rule, it may no longer be assigned to another class, using another rule. The following rules are applied in order.

1. Initiation/Establishment: cover less than 30% or height less than 20 ft.
2. Exclusion/Closure: cover 30% to 80% and height 20 ft. to 60 ft.
3. Diversification: cover 75% to 100%, height 80 ft. or taller, and Rumple 2 or more.
4. Maturation: Everything else.

Figure 43 demonstrates how these hierarchical classification scheme boundaries subdivided the LIDAR-derived cover and height. These boundaries are unrealistic and arbitrary and do not represent realistic forest conditions well. A plot with an 80^{th} percentile height of 100 ft. and a percent cover of 29.9% would be in a different class than a plot with the same height but a percent cover of 30%. As a response, to these limitations, we propose a probability based classification scheme in the next section.

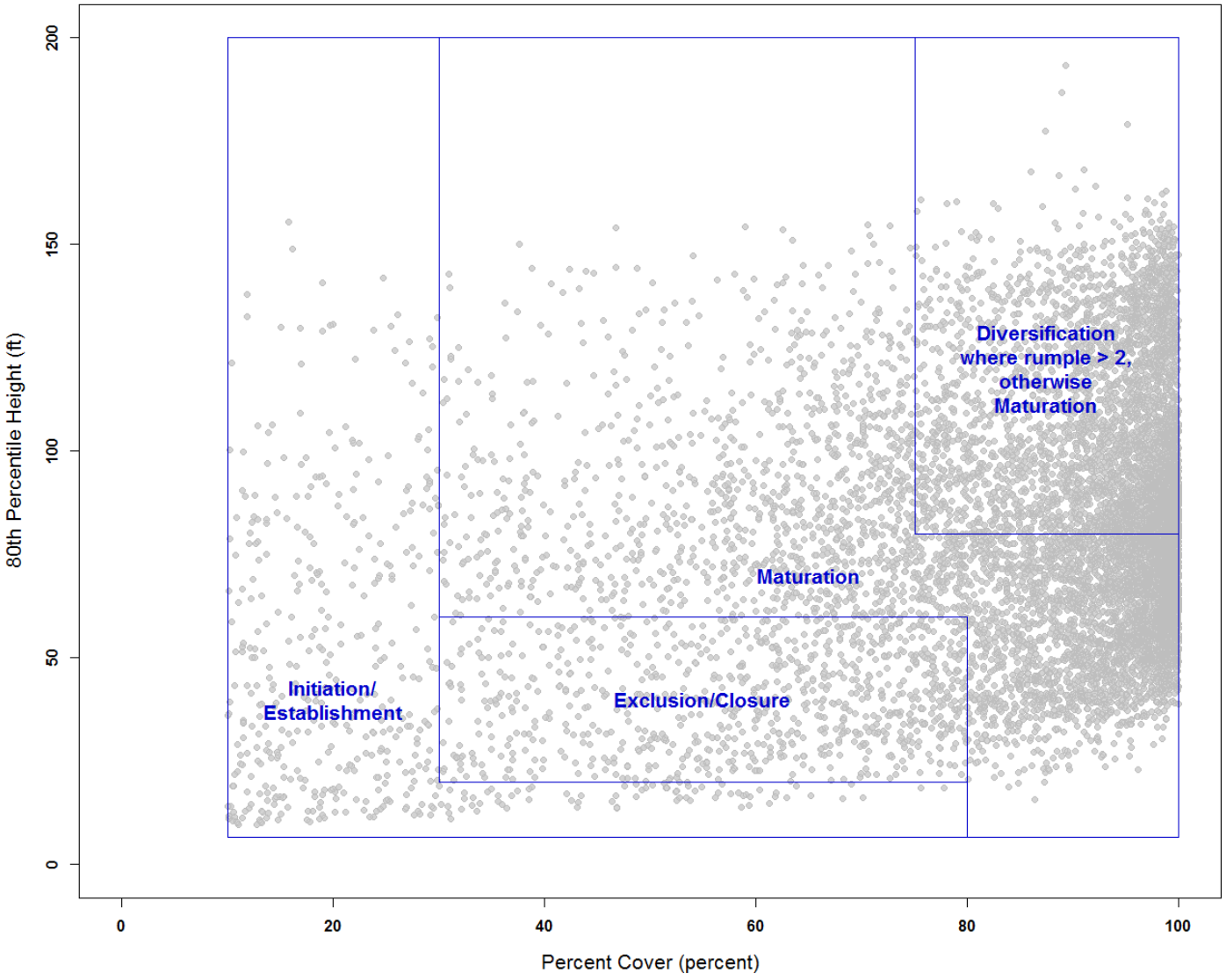

Figure 43. Vegetation Classes on LIDAR metrics plot.

9.2.2 Probability Classification Scheme

Another approach to dividing areas into vegetation classes is to develop probability curves and combine them using weighted averages. The combined probability value can be classified into separate classes. This removes the need to set hard boundaries, as was done in the hierarchical classification scheme, and allows height, cover, and rumple to interact in determining the class.

Height and Cover probability functions were developed using Chapman-Richard's equations, loosely following growth and yield curves.

Two probability functions were developed for rumple, which were averaged. The first is a logistic regression function dividing rumple values for smooth canopies from those for rough canopies. The

second probability function is a Poisson function used to indicate at what range of cover values a stand in the diversification class would occur. Old, diversified stands, will have canopy openings.

These probability curves can be combined using a weighted average, into a single probability value across the ranges of the three metrics.

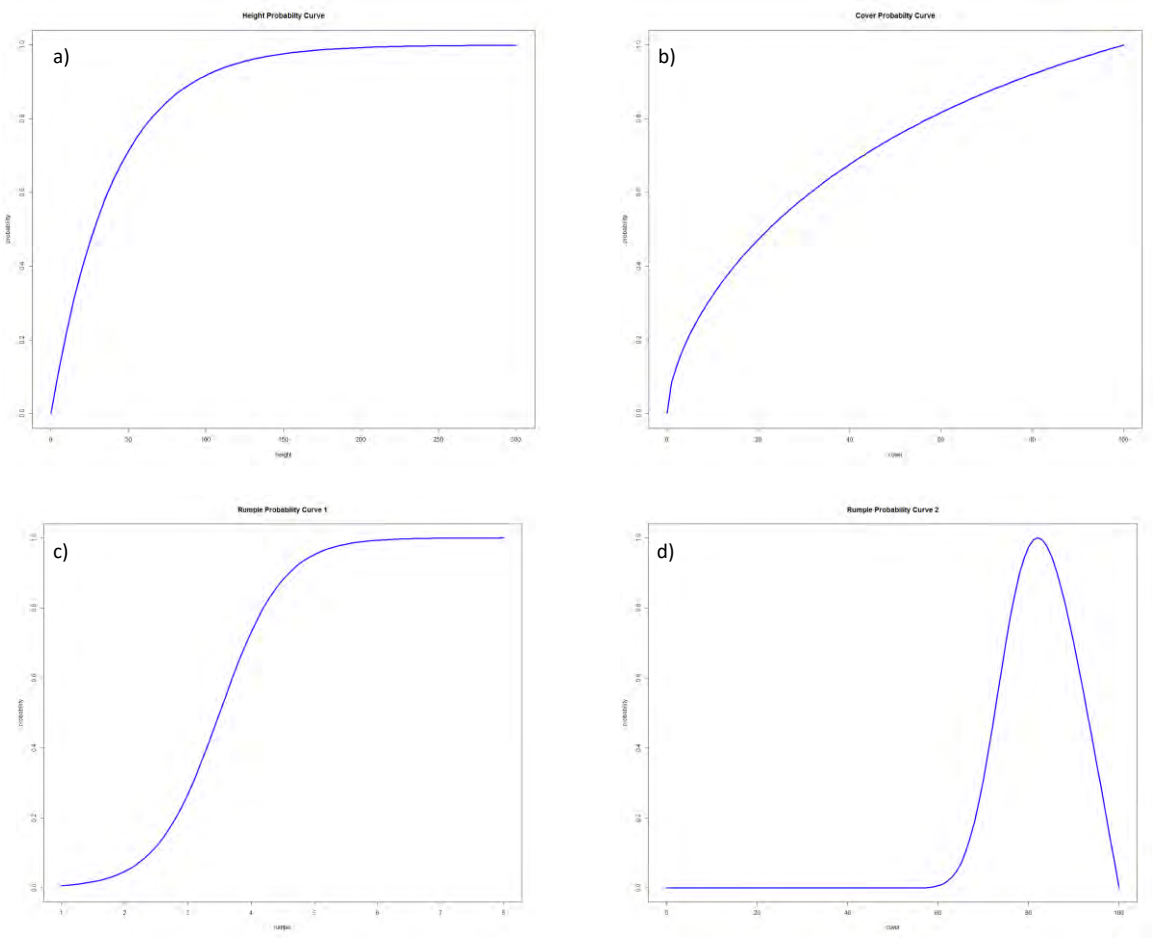

Figure 44. a) Height probability curve; b) Cover probability curve; c) Logistic regression probability curve for rumple d) Poisson probability curve for rumple. Stands in the diversification class should have cover in the range of approximately 75% to 95%.

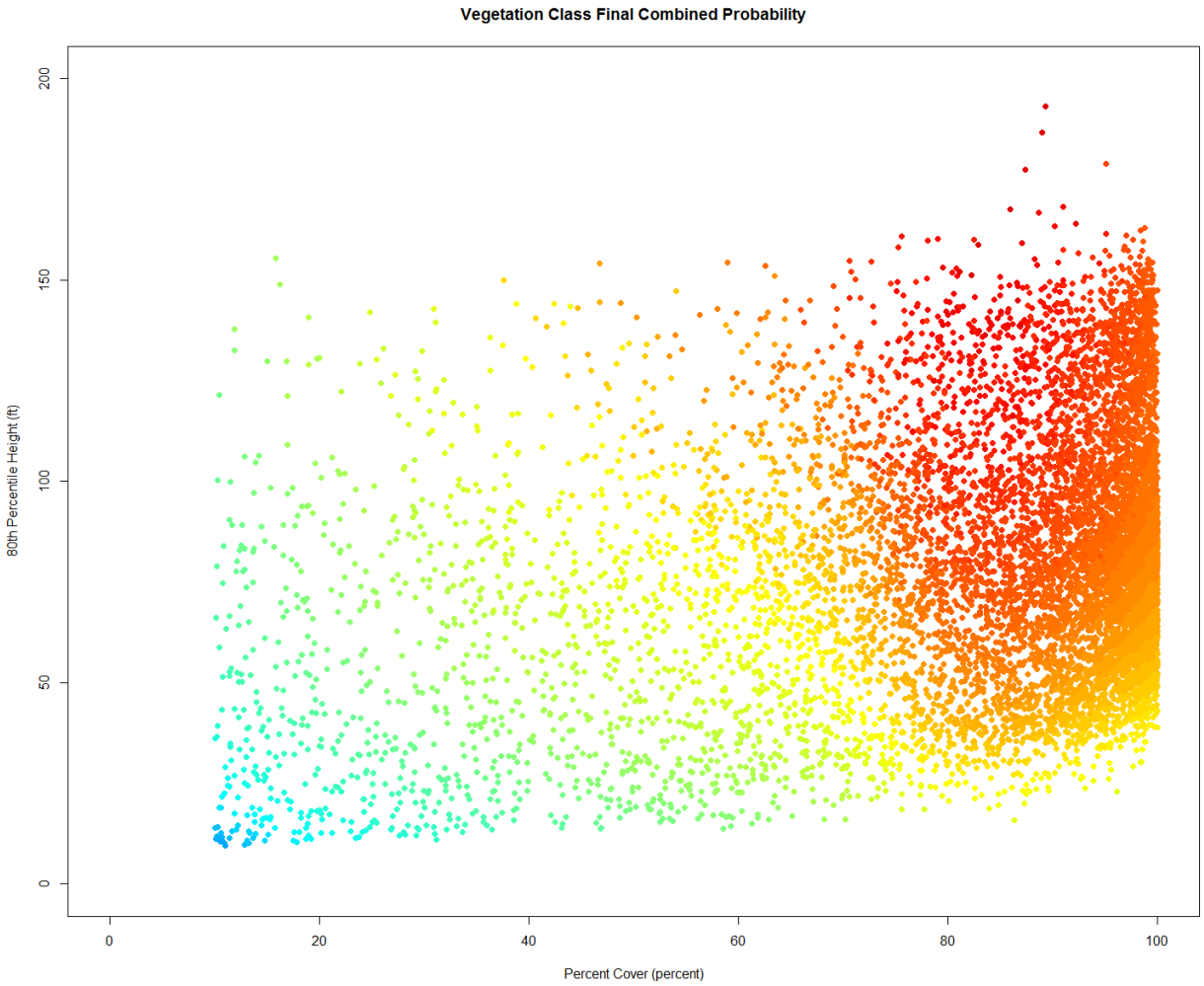

Figure 45. Combined probability values plotted against cover and height.

The combined probability value can be classified into vegetation classes. As can be seen in the plot below, class boundaries now curve across height and cover. Additionally, the maturation and diversification classes overlap with one another depending on rumple values.

The methodology presented here is a demonstration of how this process could be used. The shapes of the probability curves and the classification of the final combined probability values are theoretical and have not been tested thoroughly. Further work needs to be done to define these factors.

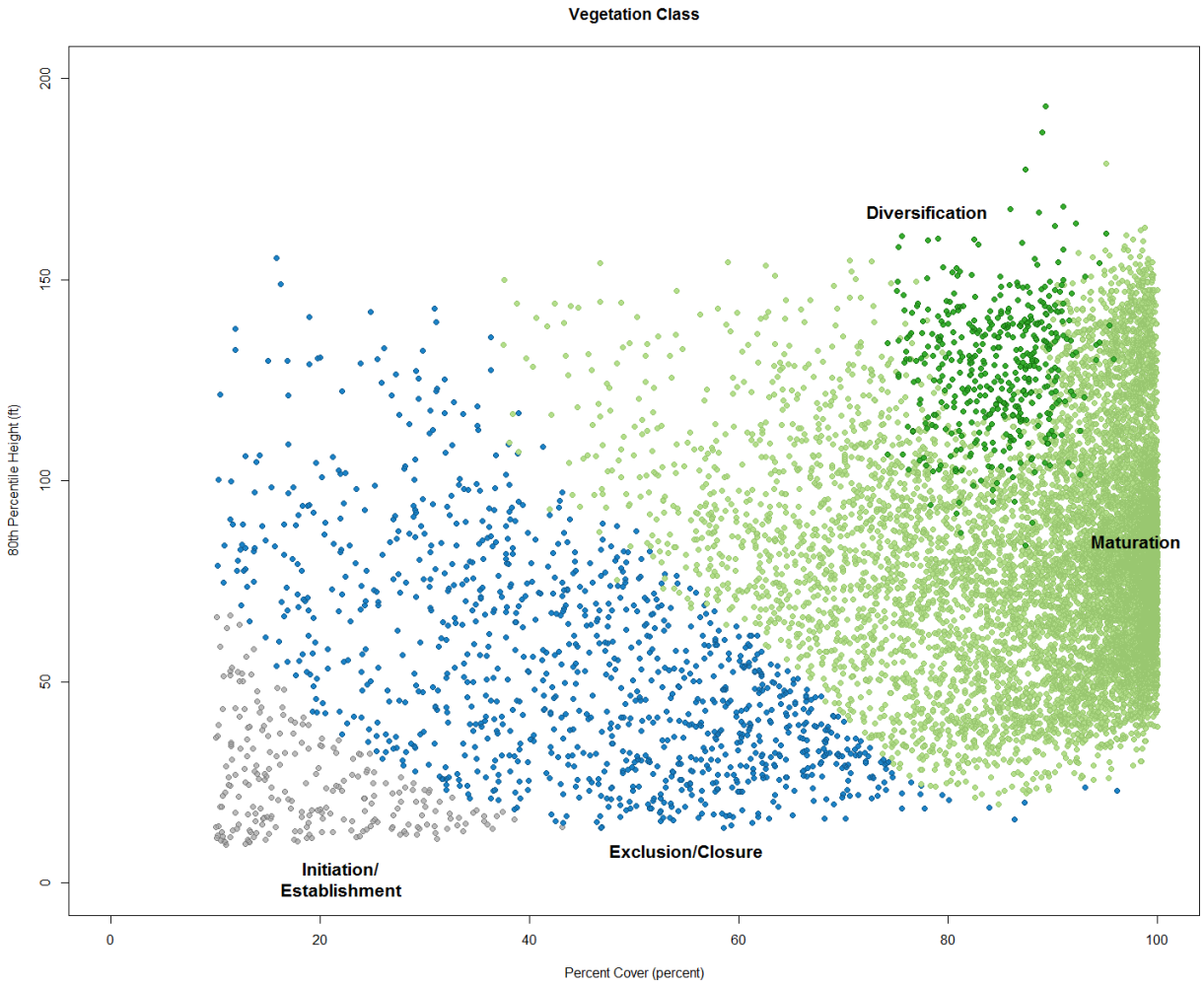

Figure 46. Vegetation classes based on combined probability values, plotted against cover and height.

9.2 Satellite/Aerial Imagery Method

Optical imagery has been used to detect stand layering and vegetation classes when other data such as LiDAR are not available (Moskal & Franklin, 2002). However, riparian stands are much more complex to work with due to the topography and structure challenges of these landscapes, and both of these components are inhibited by shadows present in optical imagery. Thus, because structure is a critical component to seral stage assessment and not a suitable characteristic shown to be reliably and consistently extracted from optical imagery in varying landscape types, this was not attempted with the imagery data.

9.3 Recommendations

- There is some promise in separating structural characteristics of vegetation with LiDAR that are likely to be related to seral stages, but much more work would need to be done to support this. **Additionally, more work is needed to understand how these stages support riparian forest functions**.

10. Species Identification

10.1 LIDAR Method

Currently there are no known large scale, high accuracy methods for identifying species from LIDAR.

10.1.1 Limiting Factors

LIDAR describes the physical arrangement and crown densities of a stand, and also provides limited near-infrared intensity information. In order to identify the species of trees in a stand, they would have to be unique in terms of physical shape or intensity, which is not the case here. Furthermore, in order to describe the shape or examine the intensity values for a tree, the laser reflection from it alone need to be separated from the reflections off of neighboring trees in the point cloud. This is not possible in dense stands, or stands with complicated crown structures.

10.2 Imagery Method

It is possible to use pixel-based statistics for each ITO in order to identify tree species. Known trees and corresponding ITCs can be used as training sites which will form the unique signatures for each tree species that a classification algorithm will use. The input for each ITC consists of a single multispectral vector, containing signatures for:

- Mean intensity value
- The Standard Deviation of this mean
- Mean-lit value [ave. of all pixels in an ITO that have a pixel value above the mean intensity of all pixels in the object]
- Tree top value, which is the brightest pixel in the ITO

10.2.1 Accuracy Assessment

Because stem mapping was not implemented in the project's data collection component, there are no explicit trees that can be used as training objects for accuracy assessment. There were enough stands that were deciduous-dominant and coniferous-dominant to create a prediction that can gauge the two compositions, but without the exact position of any particular tree species it might not be possible to predict this level of granularity.

10.2.2 Limiting Factors

Exact, known locations of individual trees. Overlapping of tree crowns [which we found on several occasions, large alder trees with smaller red cedar or Douglas firs growing underneath.] Illumination angles, sensor viewing angles, species, stand density, and image quality can all affect the feasibility of identifying individual tree canopies for both automated and manual methods. Imagery must be of a high enough resolution for individual crowns to be visible. Differing image quality over an area can cause results to vary across a study site.

10.3 Recommendations

- Timely and cost effective remote sensing techniques are weak at establishing large scale species mapping. A program that supplements the remotely sense assessments would be needed, potentially based on ground survey.
- Hyperspectral remote sensing pilot investigation can be undertaken to assess the feasibility of such approach for species assessment in the State of Washington, but with lack of wall-to-wall hyperspectral coverage, data costs, data calibration issues and often the need to fuse the data with other remotely sensed data such as LiDAR the timing of such project is not immediate

11. Basal Area

11.1 LIDAR Method

The method used to build this linear regression model is described in further detail in Section 3.1, the LIDAR Method for Canopy Height.

11.1.2 Accuracy Assessment

R^2 values are back-transformed where necessary.

Table 31. Basal Area Model.

Metric	Model	R^2	RMSE
Basal Area	sqrt(basalArea) = 4.63914 + (-0.39478*A) + (-5.63122*B) + (0.11590*C) + (1.25605*A*B)	0.73	62.11

Table 32. Basal Area Model Variables.

Model Variable	Fusion CloudMetrics Variable	Variable Explanation
A	Elev.MAD.median	Median of the absolute deviations from the overall median height, all returns
B	Canopy.relief.ratio	(mean height - minimum height) / (maximum height - minimum height), all returns
C	Percentage.all.returns.above.6.56	percent cover; number of all returns above 2m / number of all returns

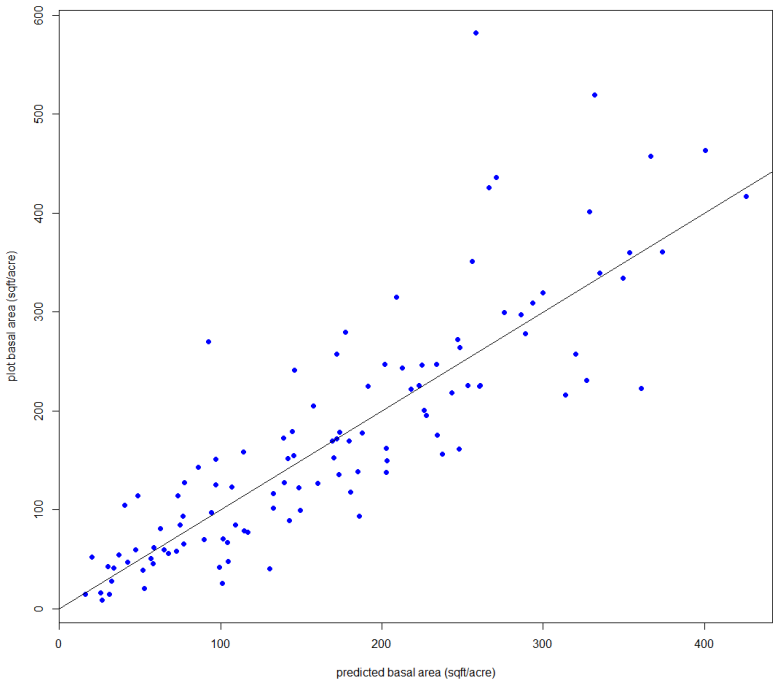

Figure 47. Predicted vs. plot basal area with the line of equality.

11.2 Imagery Method

Basal Area predictions were based on a linear regression model, with all independent variables being respective signatures of ITOs. The literature review for this project informed which larger set of variables to be used within the initial model. Then, this model was gradually narrowed down to only the most influential components show below.

Table 33. Imagery Basal Area Model.

Metric	Model	R^2
Basal Area	Plot-level Basal Area = 297.6084 + A(-2091.1627) + B(-1468.3947) + C(1089.6580) + D(-0.08564)	0.27

Table 34. Imagery Basal Area Model Variables.

Model Variable	eCognition IndividualTreeObject.Variable
A	Standard Deviation of Hue
B	Standard Deviation of NDVI
C	Mean GLCM Homogeneity
D	Sum of Crown Coverage

Additional regressions statistics found in Appendix E.

11.2.2 Limiting Factors

Illumination angles, sensor viewing angles, species, stand density, and image quality can all affect the feasibility of identifying individual tree canopies for both automated and manual methods. Imagery must be of a high enough resolution for individual crowns to be visible. Differing image quality over an area can cause results to vary across a study site.

11.3 Recommendations

- LiDAR outshines optical remote sensing and provides reasonably accurate results, however, more specific understanding of how these models perform at different stand types and if these should be modeled uniformly or separately (per stand type) on the landscape needs to be understood through further research. Moreover, the performance of the models cannot be judged just on the accuracy as the costs of developing additional models should also be considered.

12. Large Woody Debris

12.1 LIDAR Method

LIDAR was used to estimate the volume of large woody debris following the methods described in Section 4.1, Snag Detection, LIDAR Method.

12.1.1 Logistic Regression Model

Using all plots, and the comprehensive modeling approach described in Section 3.1 LIDAR Method: Comprehensive Model Selection, models were built and ranked by their McFadden pseudo-R^2 values. However, unlike the methodology in Section 3.1.2, Intensity, L Moment, and Count metrics were not excluded from the comprehensive model selection process. Further review of the models with the highest R^2 values resulted in selecting the model below.

Table 35. LWD Lidar Logistic Model.

Metric	Model	McFadden pseudo-R^2
LWD Presence/Absence	LWDPresenceAbsence = -9.2428 + (2.6817*log(A)) + (3.9671 * B)	0.22

Table 36. LWD Lidar Logistic Model Variables.

Model Variable	Fusion CloudMetrics Variable	Variable Explanation
A	Elev.P80	80th percentile of the heights, all returns
B	Int.P01	1st percentile of intensity values, all returns

12.1.2 Linear Regression Model

Using only plots with at least one piece of large woody debris, and the comprehensive modeling approach described in Section 3.1 LIDAR Method: Comprehensive Model Selection, models were built and ranked by their back-transformed R^2 values. However, unlike the methodology in Section 3.1.2, Intensity, and L-Moment metrics were not excluded from the comprehensive model selection process. Further review of the models with the highest R^2 values resulted in selecting the model below.

Table 37. LWD LiDAR Linear Regression Model.

Metric	Model	R^2
LWD Abundance	LWDAbundance = 34935.70 + (-9914.09 * sqrt(A)) + (-10272.33 * sqrt(B)) + (-170.85 * C) + (3215.37 * sqrt(A) * sqrt(B)) + (54.99 * sqrt(A) * C) + (72.14 * sqrt(B) * C) + (-22.11 * sqrt(A) * sqrt(B) * C)	0.21

Table 38. LWD LiDAR Linear Regression Model Variables.

Model Variable	Fusion CloudMetrics Variable	Variable Explanation
A	Elev.MAD.mode	Median of the absolute deviations from the overall mode height, all returns
B	Elev.P20	20th percentile of the heights, all returns
C	(All returns above 2m) / (Total first returns) * 100	percent cover; number of all returns above 2m height / total number of first returns

12.1.2 Final Model

The logistic regression model for presence/absence and the linear regression model for abundance were multiplied together and regressed against the field measured downed woody debris volumes.

This model had an R^2 of 0.19 and an RMSE of 6223.04.

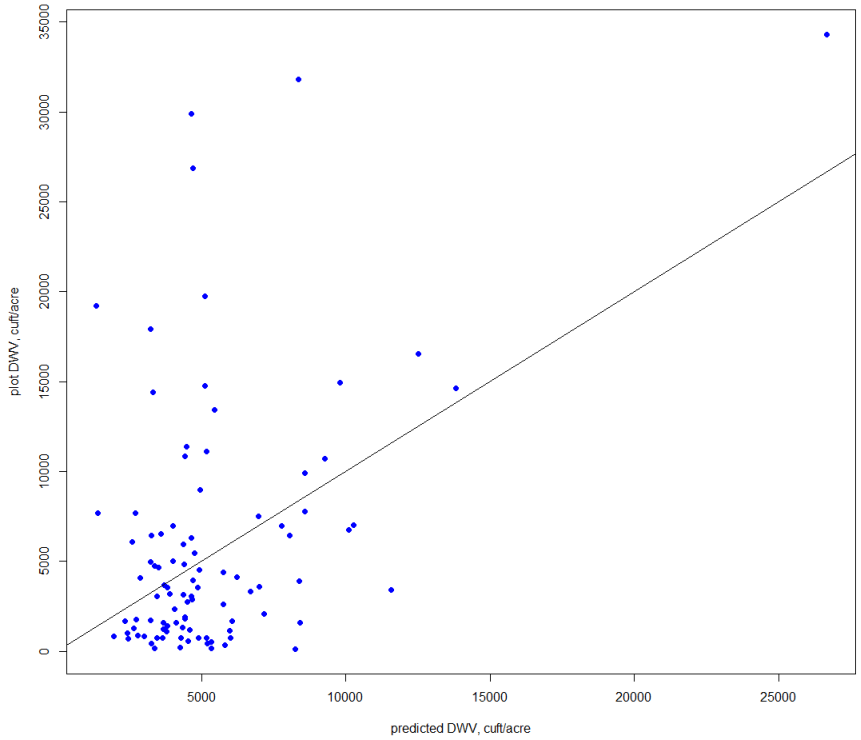

Figure 48. Predicted vs. plot large woody debris volumes with the line of equality.

12.3 Recommendations

- LWD estimates from LiDAR are cursory at best, likely many errors of omission.

13. Age

Age was not measured during the fieldwork. It was not practical to measure in terms of time, and many landowners would not have allowed their trees to be cored.

13.1 LIDAR Method

This was not studied for this project. LIDAR describes the physical arrangement and crown densities of a stand, and also provides limited near-infrared intensity information. It is only possible to measure age if it can be estimated from structural or intensity information.

13.1.1 Limiting Factors

Under very specific circumstances, such as a managed stand, where species and site index are known, and factors such as stand density are controlled, height-age models could be used to estimate age. In unmanaged forests, where species is not known, and stand dynamics are very complex, this becomes impossible.

13.1.2 Accuracy Assessment

An age model was not build for this project, so it is not possible to perform an accuracy assessment.

13.2 Recommendations

Explore other methods such as historical aerial photos or landowner records to determine stand establishment. Explore structural metrics out of LIDAR for stands with established known stands.

14. Diameter at Breast Height - DBH

14.1 LIDAR Method

The method used to build this linear regression model are described in further detail in Section 3.1, the LIDAR Method for Canopy Height.

Table 39. DBH LiDAR Model.

Metric	Model	R^2	RMSE
Quadratic Mean Diameter	sqrt(diameter) = 0.605765 + (-0.025342 * A) + (0.774230 * log(B)) + (0.323547 * sqrt(C)) + (0.022183 * A * log(B)) + (-0.106525 * log(B) * sqrt(C))	0.70	2.77

Table 40. DBH LiDAR Variables.

Model Variable	Fusion CloudMetrics Variable	Variable Explanation
A	Elev.MAD.median	Median of the absolute deviations from the overall median height, all returns
B	Elev.P20	20th percentile of the heights, all returns
C	Percentage.all.returns.above.mode	percent cover; number of all returns above mode height / number of all returns

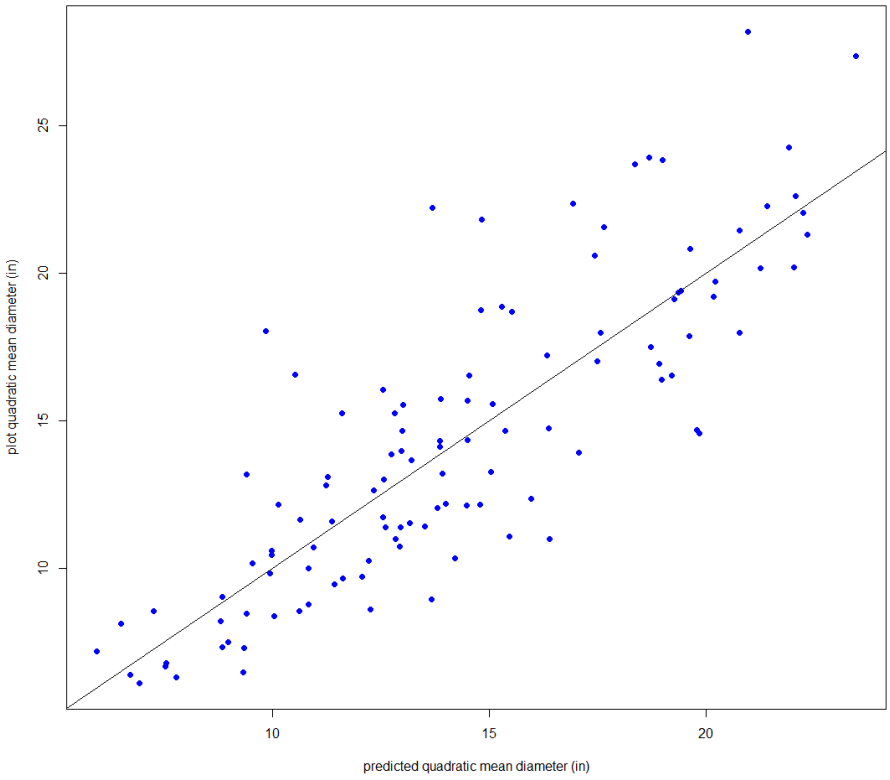

Table 41. Predicted vs. plot quadratic mean diameter with the line of equality.

14.2 Recommendations

- Lidar provides quite suitable DBH estimated.

15. Example of Future Technologies

This section is co-authored with Dr. David Shean, Applied Physics Laboratory, University of Washington.

Photogrammetry is a well-established technique used to make measurements from remotely sensed imagery, these measurements can be performed in three dimensions if the data is acquired in stereo, or with some overlap. Newer processing techniques have recently become available and applied to many types of stereo date, including imagery from aerial acquisitions such as NAIP and satellite imagery such as World View. Once of these techniques, Structure from Motion (SfM) is a photogrammetric range imaging technique for estimating three-dimensional structures from two-dimensional image sequences that may be coupled with local motion signals. It is studied in the fields of computer vision and visual perception. The technique works with two and more imagers and produces point clouds similar to LiDAR point clouds which can be further processed to surface models. In this section we demonstrate how such a technique can perform at estimating canopy height in the Mashel watershed. These methods are further described by (Shean, 2016). In general, the technique uses two World view scenes and produces a surface height model, we then apply the already existing LiDAR ground model to derive a canopy height model shown in Figure 49. The data is gridded to a coarser model to allow for a better derivation of height values form the satellite data. Height values were calculated from a raster analysis using the difference map relative to LiDAR DTM. Raster value statistics were first calculated for each plot. Then, the mean and maximum raster values for each plot were averaged and compared against the field measured data. We derive at a height model with an R2 value of a 0.51 (Figure 50). Again, this is still a very preliminary method, but worth considering, as the technology is improving and this type of approach could facilitate the temporal monitoring of forest height and structure change once a LiDAR data set is available State wide. The LiDAR is only needed once for the ground model. Similar approach could be applied and tested on NAIP imagery.

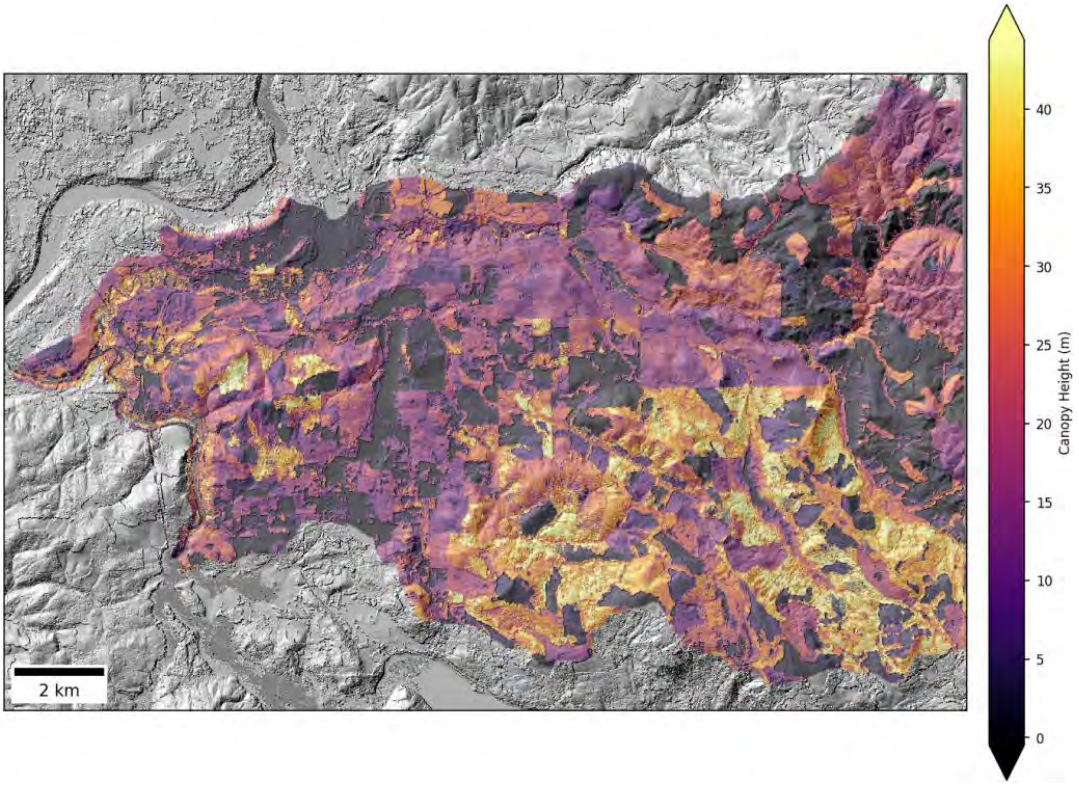

Figure 49. World View based Canopy height model gridded to 8m.

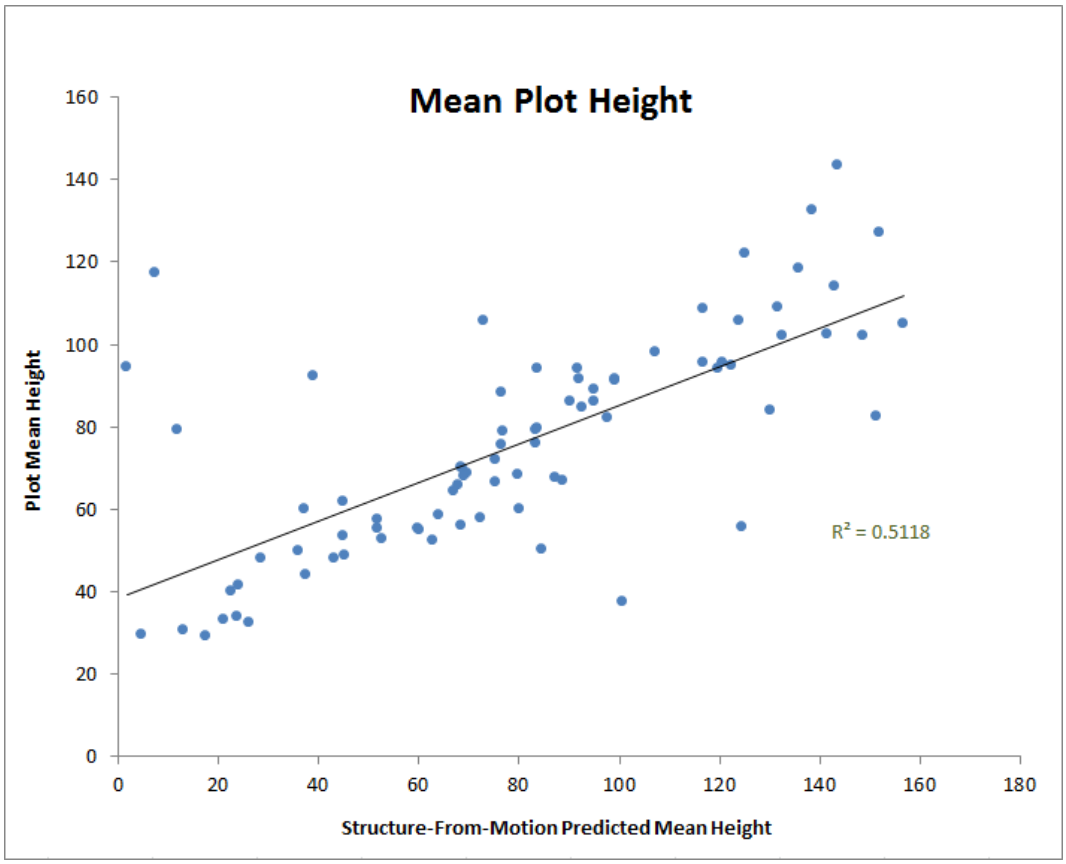

Figure 50. Results for SfM estimated height.

16. Estimated Costs

The 'cheapness' or price in this assessments assume that LiDAR will be available state wide and that the optical imagery (such as NAIP) will also be available, these data costs are set at 0 as other funding sources would be covering the costs of these data. This is not the actual cost of these data, moreover, if satellite imagery would be used as the optical data the cost of these data can be very high and vary by sensor as well as volume of data requested. It should be noted that the software used for processing the LiDAR data (FUSION) is free, as opposed to the image analysis software, which in not (eCognition).

In some cases, the accuracy is a relative accuracy as estimated by visual interpretation of the remotely sensed-based models by the analyst as no appropriate data were available to measure the accuracy, when a relative accuracy is used a fill gradient shades the triangles in the figures below.

The 'fastness' refers to estimates model development and processing time, this is dependent on the computing power, same computing resources are assumed for both approaches. Equipment costs are not estimated here as these change quickly. Estimates are provided only for the riparian metrics analyzed; empty graphs indicate the analysis was not undertaken for the particular data type. The processing time for the imagery tends to be higher as the Object Based Image Analysis (OBIA) methods necessary are quite analyst and computer time intensive.

Other consideration for either approach is the data storage, backup and redundancy needs. Both would be necessary costs to be assessed regardless of which remote sensing technology is utilized, especially as the monitoring phases are implicated. This consideration should include the ability to reference original raw data, such as original LiDAR point clouds. This type of task is often necessary as new algorithms and tools become available are needed to make the temporal dataset comparable over periods of time.

The analysis uses a triangle with the legend described in Figure 41. In Figure 52, it can be observed that LiDAR, when considering the three metrics outperforms optical imagery, this was part of the considerations, not just the accuracy and performance of the models, when making our recommendation in the above sections.

Figure 51. Cost Analysis legend.

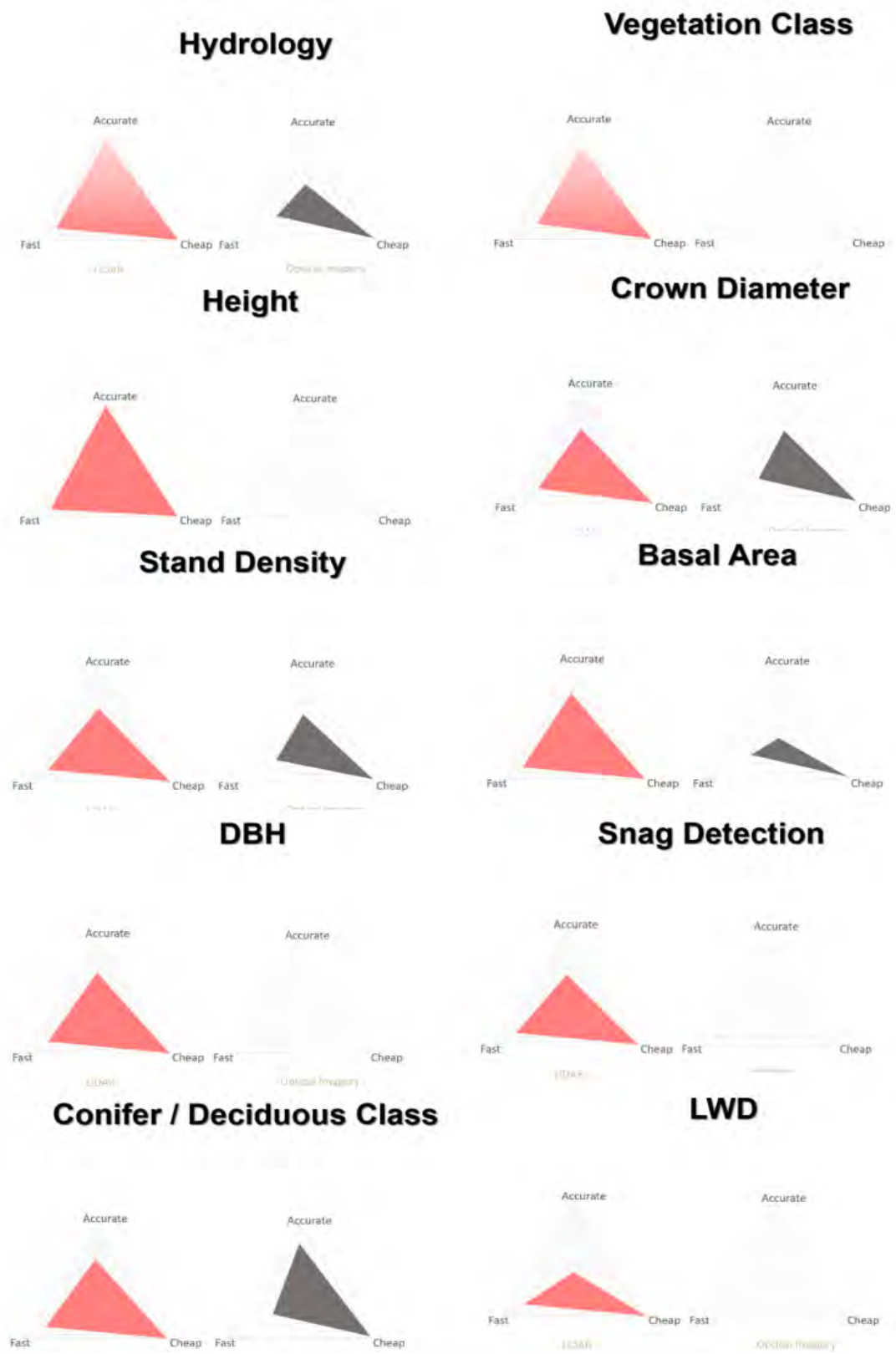

Figure 52. Estimated costs versus processing time versus accuracy (LiDAR on left and optical imagery on right).

17. Discussion

The pilot project summarized in this report found that based on the performance and accuracy of the riparian metric models tested, as well as the costs (data and software) and processing time, ***LiDAR is the most appropriate remote sensing technology for establishing a baseline assessment of riparian forest stand conditions that will allow for long term monitoring and sustainable management of these forest types.*** Although optical imagery shows some promise, especially in the areas of separating conifers and deciduous vegetation, the ability of LiDAR to capture the structural complexity of theses stands and the ground component of the landscape critical for understanding hydrology is what outperforms the optical imagery. New technologies build on the foundation of photogrammetry, could prove to be useful for future monitoring efforts once the baseline conditions are established and we conclude that these technologies should continue to be assessed and tested, but the challenge of combining remote sensing technologies in monitoring programs should also be kept in mind.

Next steps for State level monitoring:

- Regardless of which remote sensing technology is implement a field sampling menthols would need to be devised and conducted to capture the range of forest types in the State. Our protocol can be used to guide the field campaign, but the capture and cost of capture of additional variables should be assessed.
    - Establish field plots at state level.

- Models developed by this pilot are location and data sensitive, and although these could be applied at other locations we do not truly understand the limitation and performance of these models at the state level. It is likely that models would need to be developed for a variety of forest types in the State, but we do not know how many of these type of models would be needed.
    - Models will need to be developed for other forest types and potentially other LiDAR data characteristics in the state.
    - Find out what is the minimum number of models needed for the state.
    - Find out if the models are reusable, at what time point do the models hold up, 5 years, 10 years?

The next phase of a pilot should address the practicability of the application of remote sensing at the state level and the above set of tasks would allow those questions to be addressed. Moreover, the next phase pilot should address the scale at which the metrics describe characteristics that correlate with ecological function of riparian forests.

17.1 Limitations

- Remotely sensed data such as LiDAR is not available for the whole state of Washington, and optical data, such as NAIP, although available for the State, is not flown on a yearly basis.
- We were not able to test some of the algorithm performance, such as segmentation of the imagery in eCognition and segmentation of the LiDAR data. Stem mapping could have allowed us to do this and improved this project, a future approach should collect a subset of plots that are stem mapped.
- As new remote sensing technologies become available, combining those into existing monitoring programs can become a challenge, this, a monitoring program needs to be designed with these issues in mind.

References

Conrad, R. H., Fransen, B., Duke, S., Liermann, M., & Needham, S. (2003). *The Development and Assessment of the Preliminary Model for Identifying Fish Habitat in Western Washington.* Cooperative Monitoring Evaluation & Research. Olympia, WA: Washington State Department of Natural Resources.

Costa-Cabral, M. C., & Burges, S. J. (1994). Digital Elevation Model Networks (DEMON): A model of flow over hillslopes for computation of contributing and dispersal areas. *Water Resources Research, 30*(6), 1681–1692. doi:10.1029/93WR03512

Fransen, B. R., Duke, S. D., McWethy, L. G., Walter, J. K., & Bilby, R. E. (2006). A Logistic Regression Model for Predicting the Upstream Extent of Fish Occurrence Based on Geographical Information Systems Data. *North American Journal of Fisheries Management, 26*(4), 960-975. doi:10.1577/M04-187.1

Gobakken, T., Korhonen, L., & Næsset, E. (2013). Laser-assisted selection of field plots for an area-based. *Silva Fennica, 47*(5). doi:10.14214/sf.943

Hawbaker, T. J., Keuler, N. S., Lesak, A. A., Gobakken, T., Contrucci, K., & Radeloff, V. C. (2009). Improved estimates of forest vegetation structure and biomass with a LiDAR-optimized sampling design. *Journal of Geophysical Research, 114*(G2). doi:10.1029/2008JG000870

Johnson, D. H., & O'Neil, T. A. (2001). *Wildlife-Habitat Relationships in Oregon and Washington.* Corvallis: Oregon State University Press.

Maltamo, M., Bollandsås, O. M., Næsset, E., Gobakken, T., & Packalén, P. (2010). Different plot selection strategies for field training data in ALS-assisted forest inventory. *Forestry, 84*(1), 23-31. doi:10.1093/forestry/cpq039

Martinuzzi, S., Vierling, L. A., Gould, W. A., Falkowski, M. J., Evans, J. S., Hudak, A. T., & Vierling, K. T. (2009). Mapping snags and understory shrubs for a LiDAR-based assessment of wildlife habitat suitability. *Remote Sensing of Environment, 113*(12), 2533-2546. doi:10.1016/j.rse.2009.07.002

McGaughey, R. J. (2016). *FUSION/LDV: Software for LIDAR Data Analysis and Visualization.* Seattle, WA: United States Department of Agriculture Forest Service Pacific Northwest Research Station. Retrieved from http://forsys.cfr.washington.edu/fusion.html

Moskal, L. M. and A. Cooke, 2015. Feasibility of applying remote sensing to a riparian stand conditions assessment, Agreement No. IAA 15-118 (Revised 1/1/2015); Prepared for Washington Department of Natural Resources.

Moskal, L. M. (2016). *The Riparian Assessment Field Guide 2016. Extensive Riparian Vegetation Monitoring – Remote Sensing Pilot Study.* Seattle, WA: Precision Forestry Cooperative, University of Washington. Retrieved from https://drive.google.com/file/d/0BxHwRx7YcFmSakR2RVpRUjlKUDA/view?usp=sharing

Moskal, L. M., & Franklin, S. E. (2002). Multistory forest stand discrimination with multiscale texture from high spatial detail airborne imagery,. *Geocarto International*, 7(4); 53-66.

Oliver, C. D., & Larson, B. C. (1990). *Forest Stand Dynamics.* New York: McGraw-Hill.

Poppenga, S. K., Worstell, B. B., Stoker, J. M., & Greenlee, S. K. (2010). *Using selective drainage methods to extract continuous surface flow from 1-meter lidar-derived digital elevation data.* Reston, Virginia: U.S. Geological Survey Scientific Investigations Report 2010–5059.

Shean, D. E. (2016). An automated, open-source pipeline for mass production of digital elevation models (DEMs) from very high-resolution commercial stereo satellite imagery. *ISPRS J. Photogramm. Remote Sens*, 101-117.

Appendix A - Hydrology Processing

Stream channel locations were created using a combination of ESRI ArcGIS geoprocessing tools, Saga GIS (http://saga-gis.sourceforge.net/en/) raster processing hydrology tools, and Safe Software's Feature Manipulation Engine (FME).

The source digital elevation model (DEM) data were created by the LIDAR vendor, Quantum Spatial (Watershed Sciences at the time of the data acquisition), as individual, approximately 32 square mile, tiles with the following specifications:

- Cellsize: 3 foot x 3 foot
- Projection: EPSG 2927; NAD 1983 HARN Washington State Plane South US Feet (FIPS 4602)

Nine tiles covered some portion of the Mashel Watershed Administrative Unit (WAU). These nine tiles were mosaicked into a single DEM, which was then clipped to the spatial extent of the WAU with a buffer of 500 feet. All processing was performed on the mosaicked, clipped DEM.

Digital Culvert

The exact locations of streams, roads, and culverts are not known with any useful accuracy, and even if precise positions were known for a single location or landowner, high accuracy information is not widely available. It is obvious that roads have an important impact on the surface flow of water and must be taken into account if an accurate DEM-derived stream layer is to be developed.

One possible method to deal with this problem is described in a 2010 U.S. Geological Survey Scientific Investigations Report (Poppenga, et al. 2010). This method involves identifying large sinks, and burning paths into the DEM to route flow out of these large sinks through digital culverts. This method only requires the source DEM.

Processing Steps

The following steps describe the process of building stream channels from the source DEM.

1. In Saga GIS, the source DEM was processed using a sink filling algorithm developed by (Wang and Liu 2006), with a minimum slope (Degree) of 0.1.
2. The source DEM and the sink-filled DEM from step one were used as inputs in a python script-based ArcGIS tool modeled on the USGS SIR, and developed by NRSIG. The tool takes four inputs, set as follows:

- Minimum Sink Depth: 1
- Minimum Sink Volume: 1000
- Maximum Sink Volume: 1,000,000
- Low Point Search Distance Outside of Sink: 50

3. The tool produces a new burned DEM with elevations lowered along sink exit paths, and several other ancillary GIS datasets.
4. In Saga GIS, the new burned DEM from step two was processed using the same sink filling algorithm (Wang and Liu 2006) as step one, with a minimum slope (Degree) of 0.1.
5. In Saga GIS, the burned, sink-filled DEM from step three was processed using the DEMON flow accumulation algorithm (Costa-Cabral and Burges 1994) to produce a flow accumulation raster, using the following settings:
    - Executing tool: Flow Accumulation (Flow Tracing)
    - Flow Accumulation Unit: cell area
    - Method: DEMON
    - DEMON - Min. DQV: 0.000000
    - Flow Correction: no
6. In Saga GIS, the flow accumulation raster from step four was converted into a stream line vector dataset. Flow accumulation values needed to be greater than or equal to 1.5 hectares of contributing area, to be considered a stream.

Additional Attributes

Strahler Order

In FME, a workbench was created to take the stream lines from step five above and turn them into a network dataset with nodes at segment junctions, and a calculated topology. This network was used within the workbench to calculate the Strahler Order (in FME) for each segment. Additionally, the network was used to determine flow accumulation, as described below.

Segment End Flow Accumulation

The flow accumulation value at the downstream end of each stream segment was extracted from the DEMON flow accumulation raster, one cell upstream from each network node.

Width Class

For purposes of symbolizing the stream layer on a map, a width class attribute was calculated based on each stream segment's flow accumulation value, using the following function:

$$widthClass = round(0.144 * flowAccumulation^{0.163})$$

Unique Channel ID

A python script was developed to assign a unique ID to each channel (stream) by traversing up the channel network segment by segment from the exit point of the watershed. At each branch in the network, the segment with highest flow accumulation value maintains the parent's channel ID, while the other branches are assigned new IDs.

Appendix B - Plot Location Selection

Introduction

The Mashel watershed in southeastern Pierce County, Washington, is over 57,000 acres with 530 miles of streams in the official Department of Natural Resources (DNR) hydrology GIS dataset. It was important to locate the 130 field plots in locations that represent the full range of riparian forest types in the watershed.

Using a technique based on the literature (Hawbaker, et al., 2009), (Maltamo, Bollandsås, Næsset, Gobakken, & Packalén, 2010), (Gobakken, Korhonen, & Næsset, 2013), and on previous projects for the USDA Forest Service (USFS) and USDI Bureau of Land Management (BLM), the watershed was pre-stratified into bins, and eight to 14 plot locations were randomly chosen for each bin from potential areas of the watershed in that bin. Certain bins made up a higher proportion of the watershed, so these bins were assigned more plots.

LIDAR metrics were used to pre-stratify the watershed. The LIDAR processing software, Fusion (McGaughey, 2016), was used to create metrics for the watershed at a resolution of 75 feet (approximately $1/8^{th}$ acre). These metrics describe many attributes of the forest structure. By locating plots across the range of forest structures in the watershed, it is believed that plots will better capture the range of forest types, than if they were randomly located without stratifying.

Identifying the Study Area

Land Use

The ownership in the Mashel WAU is predominantly three types of landowners, the University of Washington, the DNR, and private timber industry (Corporate). The remaining areas are Tribal, municipal and state agencies (non-DNR), conservation groups, private utilities, and other private ownership including small forest landowners.

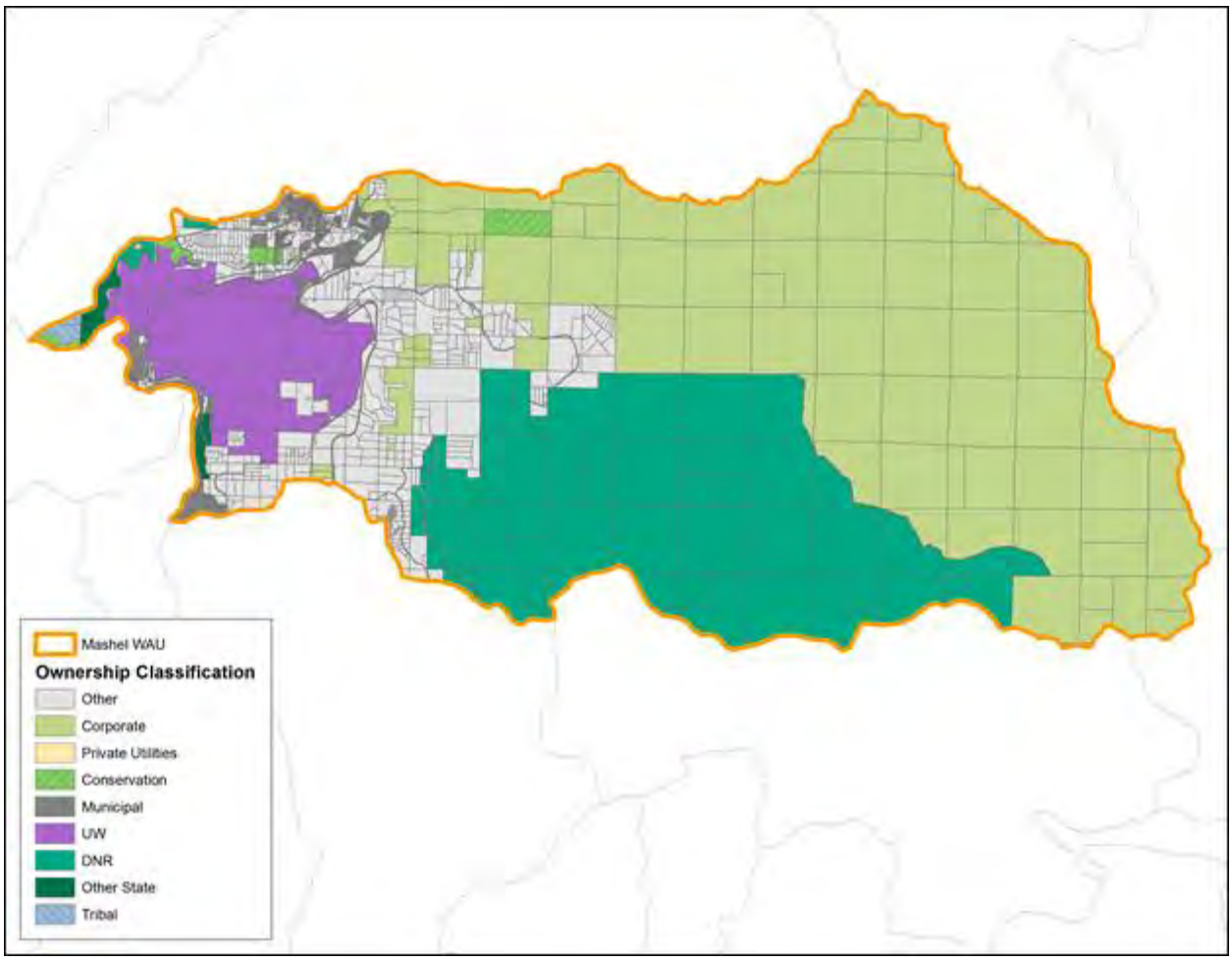

Figure *53*: Land owners of the Mashel watershed.

The purpose of this project is to describe the status of riparian buffers on managed forest land in the watershed. Areas outside of buffers or on properties with non-forest land uses were removed from further consideration.

2015 parcel data for Pierce County was used to identify the property boundaries and assessed land uses of the properties in the watershed. Parcels without resource land, land use classification were removed. Resource lands are those in the Resource Production and Extraction land use category as defined in [WAC 458-53-030 Stratification of assessment rolls—Real property](http://apps.leg.wa.gov/wac/default.aspx?cite=458-53-030) (http://apps.leg.wa.gov/wac/default.aspx?cite=458-53-030).

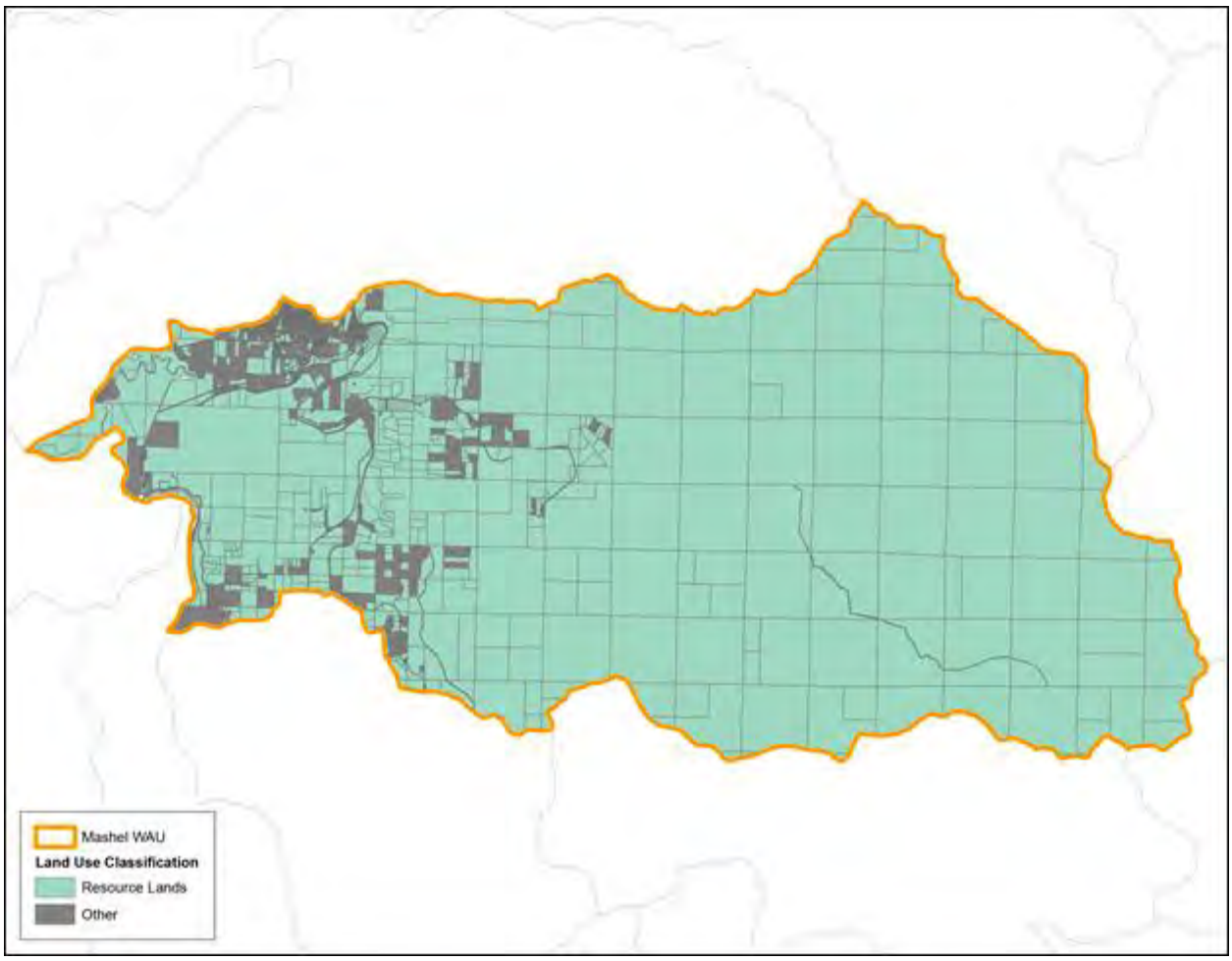

Figure 54: Resource lands in the Mashel watershed.

Non-Forested Areas

Non-Forested areas were removed as well, by looking at two calculated LIDAR metrics, the 80th percentile height and the percent cover. Areas meeting any of the following criteria were removed:

- metrics could not be calculated due to missing or inadequate LIDAR coverage
- the 80th percentile height was less than two meters
- the percent cover was less than 10 percent

Stream Buffers

Plots should be located inside of stream buffers, but the DNR Forest Practices stream buffering rules are very complicated, and the existing DNR hydrology dataset is known to be inaccurate, particularly in upper reaches. Following RSAG guidance, stream buffers for the purposes of this project were defined as follows:

- All type F and S streams were buffered 225 feet (three 75 ft. cells)
- All type N streams were buffered 75 feet (one 75 ft. cell) for the first 1500 feet upstream from a type F or S stream

Areas outside of these stream buffers were removed.

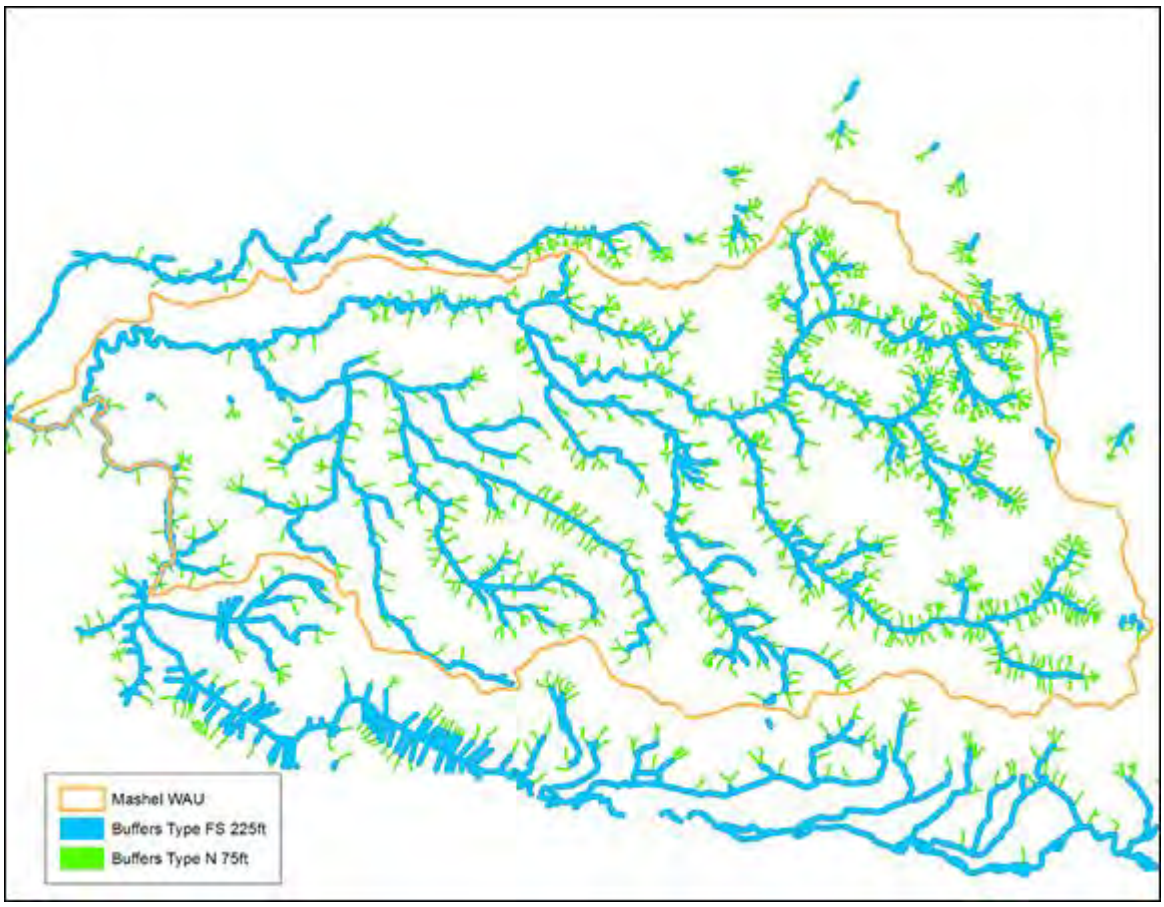

Figure 55: Stream buffers.

Combining

The valid areas in the previous maps were combined to create a final valid area to be used for the principal components analysis (PCA) sampling in the next step. Only LIDAR cells within this final valid area were sampled for the PCA.

Selecting LIDAR Metrics

Principal Components Analysis was performed to help narrow down the LIDAR metrics that will be used to stratify the landscape. Previous experience on similar projects, also guided these decisions. Ten thousand sample points, were selected randomly within the valid study area defined above, and 18 LIDAR metrics were measured at each point. These measurements were used in the PCA.

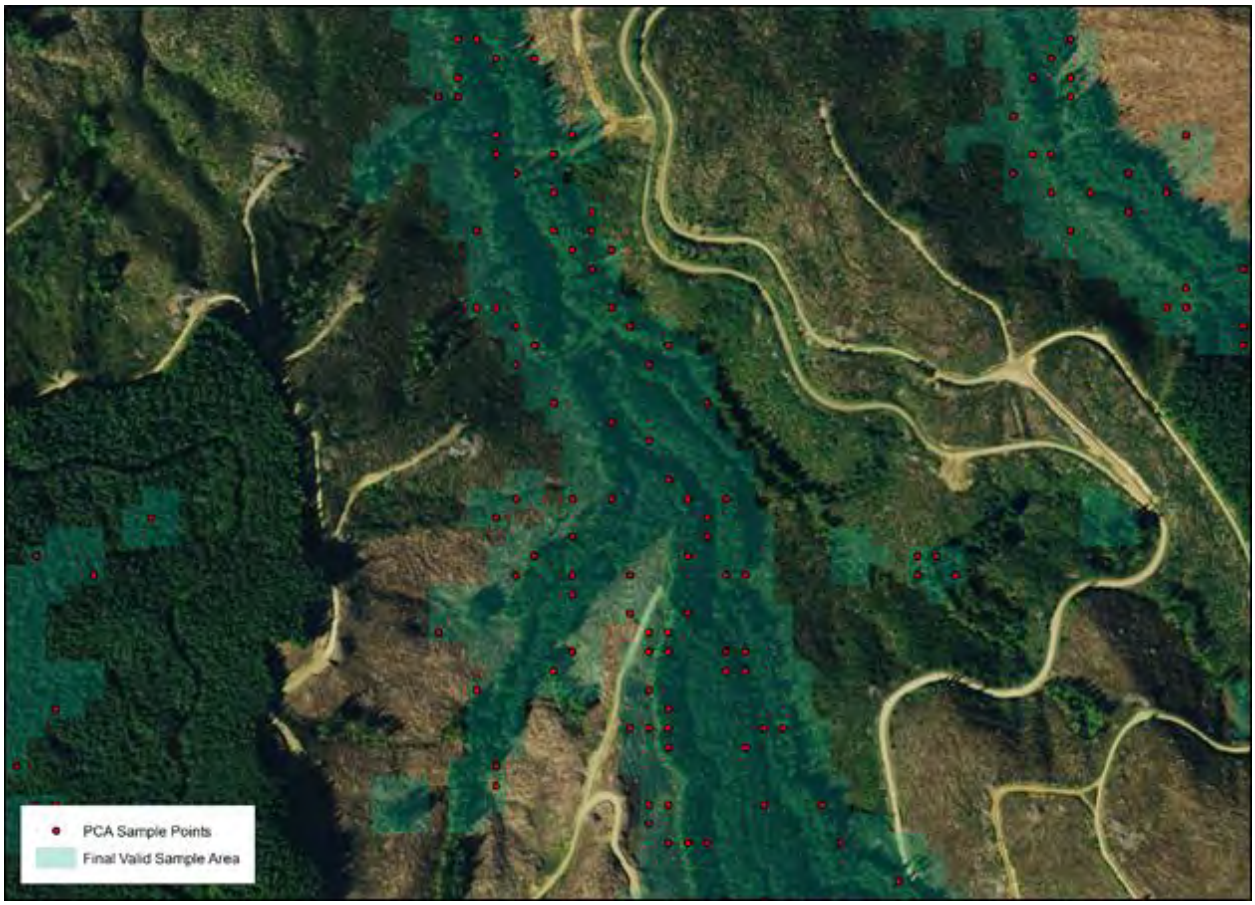

Figure 56: Example sample points.

The first three components explain nearly all of the variability on the landscape.

Table 42: PCA Importance of Components.

Importance of Components:			
	Comp.1	Comp.2	Comp.3
Standard deviation	3.42	1.99	1.26
Proportion of Variance	0.65	0.22	0.09
Cumulative Proportion	0.65	0.87	0.96

Experience has shown that while using more metrics to stratify the landscape increases the cumulative proportion in the PCA, using more than two metrics makes fieldwork much less practical. Increasing the number of metrics used, increases the number of bins, and in order to guarantee enough plots in each bin, there have to be more plots. This is expensive and takes time, with each additional metric compounding the problem. Two metrics seems to be an ideal compromise between explanatory ability and practicality.

Height drives the first principal component, with various metrics having similar importance, while the second principal component is driven by cover.

Table 43: Principal components analysis results.

	Comp.1	Comp.2	Comp.3
1st_cover_above6p5616	0.13	0.41	0.28
all_1st_cover_above6p5616	0.18	0.32	0.32
all_cover_above6p5616	0.13	0.41	0.24
elev_ave_6p5616plus	0.29	-0.01	-0.14
elev_cubic_mean	0.29	-0.08	-0.05
elev_CV_6p5616plus	-0.09	-0.35	0.44
elev_P10_6p5616plus	0.22	0.17	-0.39
elev_P25_6p5616plus	0.26	0.09	-0.29
elev_P50_6p5616plus	0.28	-0.01	-0.13
elev_P75_6p5616plus	0.29	-0.08	-0.03
elev_P80_6p5616plus	0.29	-0.10	-0.01
elev_P95_6p5616plus	0.28	-0.14	0.06
elev_P99_6p5616plus	0.27	-0.14	0.09
elev_quadratic_mean	0.29	-0.05	-0.08
elev_stddev_6p5616plus	0.21	-0.28	0.31
elev_variance_6p5616plus	0.16	-0.27	0.31
FIRST_RETURNS_1st_cover_above6p5616	0.13	0.41	0.28
FIRST_RETURNS_elev_P90_6p5616plus	0.28	-0.12	0.05

Because the metrics chosen are being used to stratify the landscape for field crews, it is helpful to choose metrics that make sense to people at a plot. 80th percentile height is similar to what a field crew would see as plot or stand height. LIDAR measurements of cover are not the same as canopy closure, but low cover occurs in a more open plot, and a high cover occurs in a more closed plot, which a field crew can see. So choosing a height and cover metric to stratify the landscape makes sense from a statistical and practical standpoint. While several height metrics perform similarly in the first principal

component, elev_P80_6p5616plus, the 80th percentile height (P80), was selected. From the second principal component, 1st_cover_above6p5616, the percent cover (PC) was selected.

Defining Bins

The range and distribution of the P80 and PC values from the 10 thousand sample points were used to define the bins.

PC was divided into four classes. The top class ranged from 90% to 100%, and the bottom three classes were equal width subdivisions of the range from 10% to 90%, approximately 27% wide each. The distribution of PC values skews heavily to high cover.

Within each PC class the P80 values were subdivided into three classes. The middle P80 class is centered on the mean value and is a one standard deviation wide (a ½ standard deviation above and below the mean). The top P80 class is everything taller than the middle class, and the bottom P80 class is everything shorter. The bin definitions are presented below in Figure 57 and

Table 44.

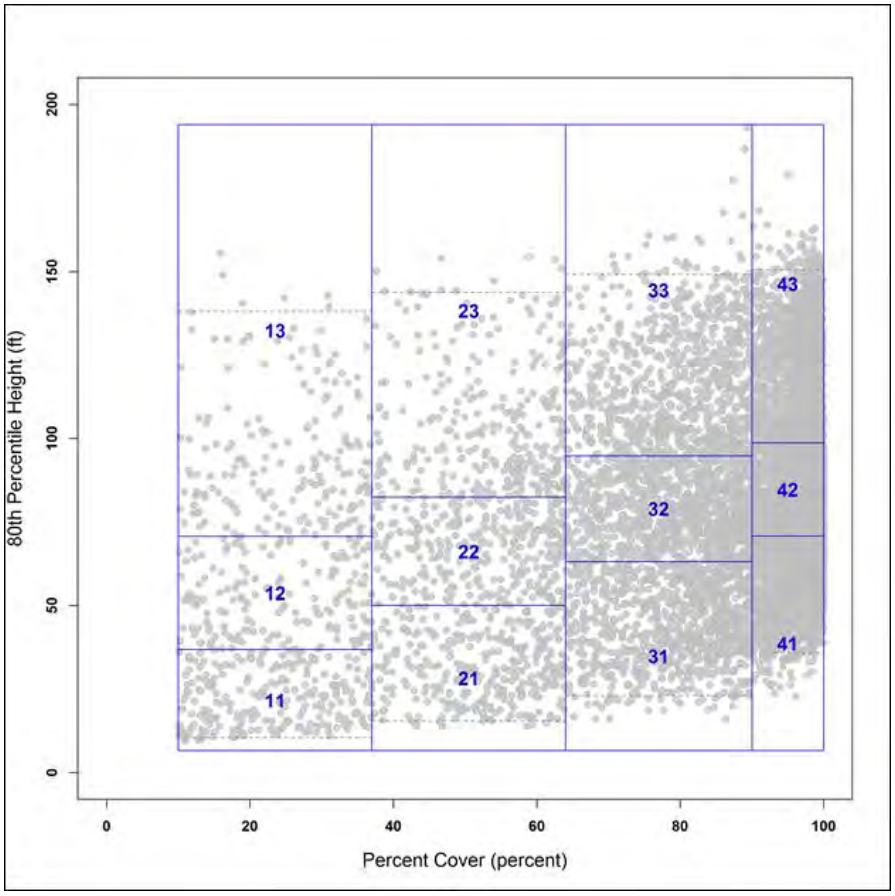

Figure 57: Bin boundaries with the 10k sample points.

Table 44: Bin boundary values.

Bin	PC Min	PC Max	P80 Min	P80 Max	Percent
11	10	37	6.6	36.9	2%
12	10	37	36.9	70.8	2%
13	10	37	70.8	max	2%
21	37	64	6.6	50.1	3%
22	37	64	50.1	82.5	3%
23	37	64	82.5	max	3%
31	64	90	6.6	63.2	10%
32	64	90	63.2	94.9	10%
33	64	90	94.9	max	9%
41	90	100	6.6	70.9	19%
42	90	100	70.9	98.7	22%
43	90	100	98.7	max	15%

Sampling for Locations

Every 75 ft. cell in the valid study area, had its bin calculated using the P80 and PC LIDAR datasets and the bin ranges defined above in

Table 44. Plot locations were then randomly selected using these bin values. The field crew was tasked with measuring 130 plots total, with 8 to 14 in each bin. 50 extra plots were selected for each bin to account for issues that might arise.

Pre-Fieldwork Review

The LIDAR data was flown in 2011 and the plots were measured in 2016, a five-year gap, and the DNR hydrology dataset is known to have inaccurate locations for stream channels. It was therefore very likely that management activity or disturbances could have occurred at plot locations, or that plots were located next to non-existent streams. To prevent wasted time for the field crew, all plots were compared to 2015 imagery, before the field work, to make sure that plots seemed to have the appropriate trees for their bin, and that they were actually in a riparian buffer. Any plots with issues were removed, and the first available alternate plot location was used in its place.

Appendix C – Field Data Collection

Planning

Project details, context, and input/resources from all team members was synthesized to create a field guide detailing the many elements of data collection [supplement]. This document follows FIA guidelines and was also reviewed by all team members prior to implementation. It contains information explaining both the nuances within the information to be collected and the methodologies and administrative considerations in doing so.

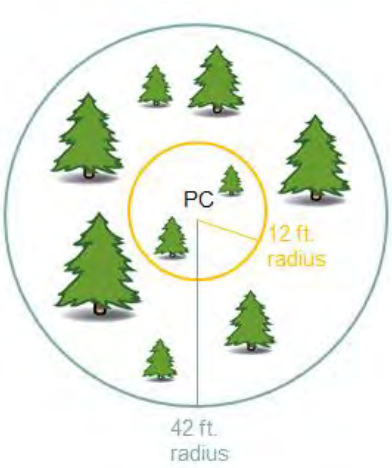

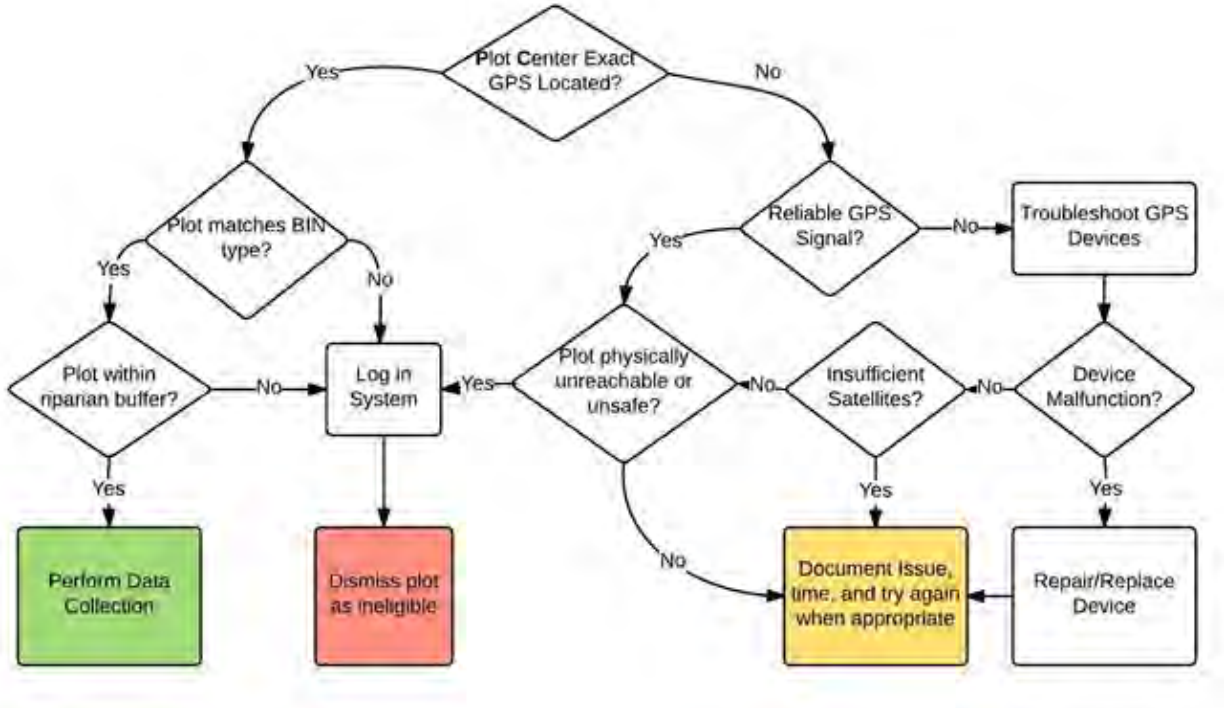

Execution

Field Collection efforts transpired 6/1/2016 - 9/17/2016. Two crew members operated throughout the duration of the period, based primarily in Pack Forest. A total of 113 plots were sampled. The following is a summary table of final plot results.

	BINS												
Status	**11**	**12**	**13**	**21**	**22**	**23**	**31**	**32**	**33**	**41**	**42**	**43**	**Total**
Available	19	5	7	35	26	15	29	25	37	39	39	46	322
Sampled	9	8	7	8	9	9	10	9	11	10	11	12	113
Ineligible		2	1		1				1		1		6
Unreachable	1	5				3	2	10	1				22
Total	**29**	**20**	**15**	**43**	**36**	**27**	**41**	**44**	**50**	**49**	**51**	**58**	**463**

Available = pre-determined/unsampled field plots.
Sampled = completed/successful data collection
Ineligible = plot ruled out on site by field crew
Unreachable = plot access not approved or unobtainable from private landowners

A total of 2,879 trees were sampled, 2,546 of which were alive and 333 dead. Of the living trees, about 90% [2,285] were large trees [DBH greater than 5 in.] and the remaining 264 were small, living trees. Summary metrics by tree species can be found in the next section.

Data Collection Review - Metrics by Plot

The following are several graphical and tabular displays of field collection data. Information is grouped both at the plot level, and then granulated further by tree species. Logistical field collection data, tree data, coarse woody debris data, and summarized plot data are all available in the field database supplement.

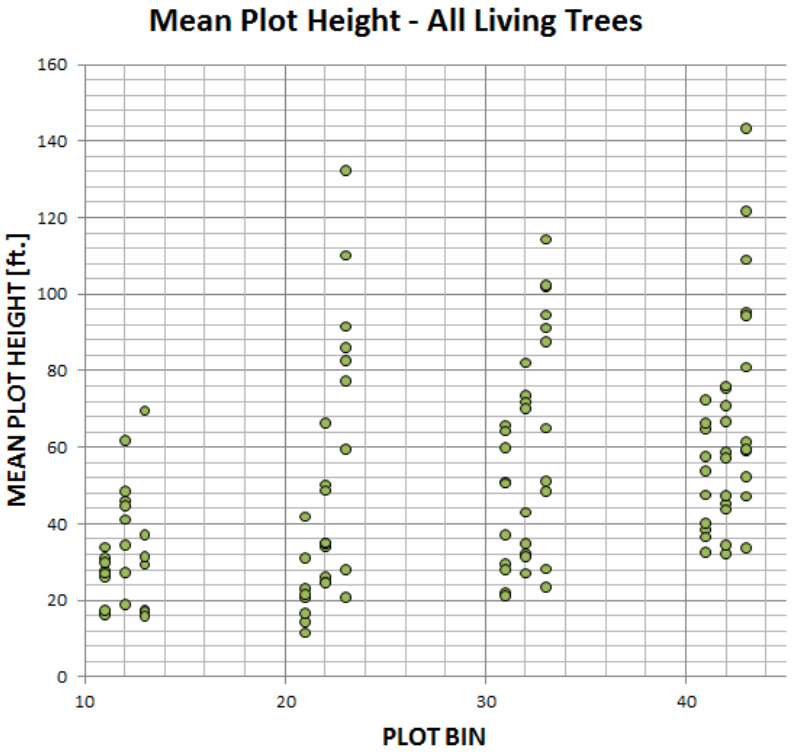

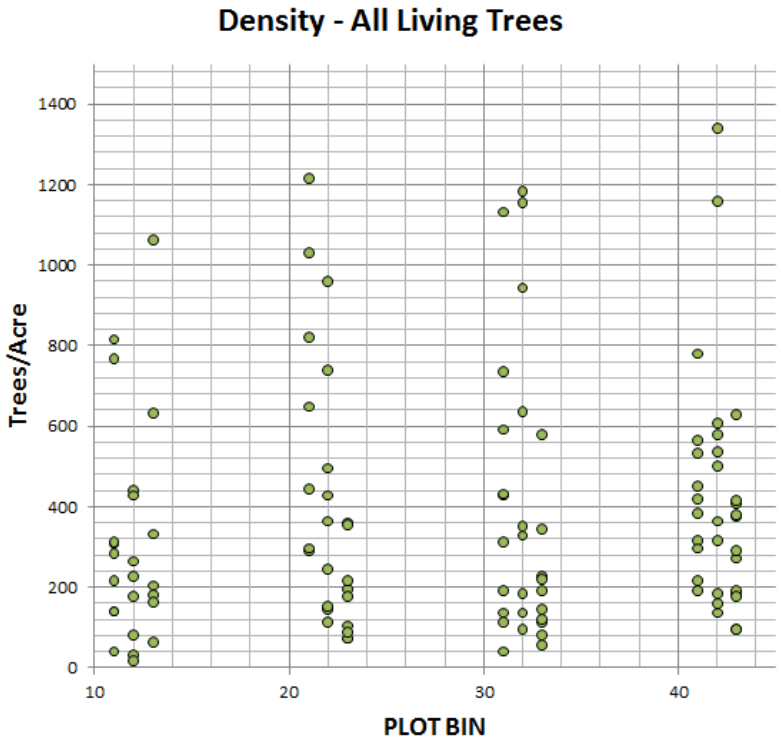

Data Collection Review - Tree Metrics by Species

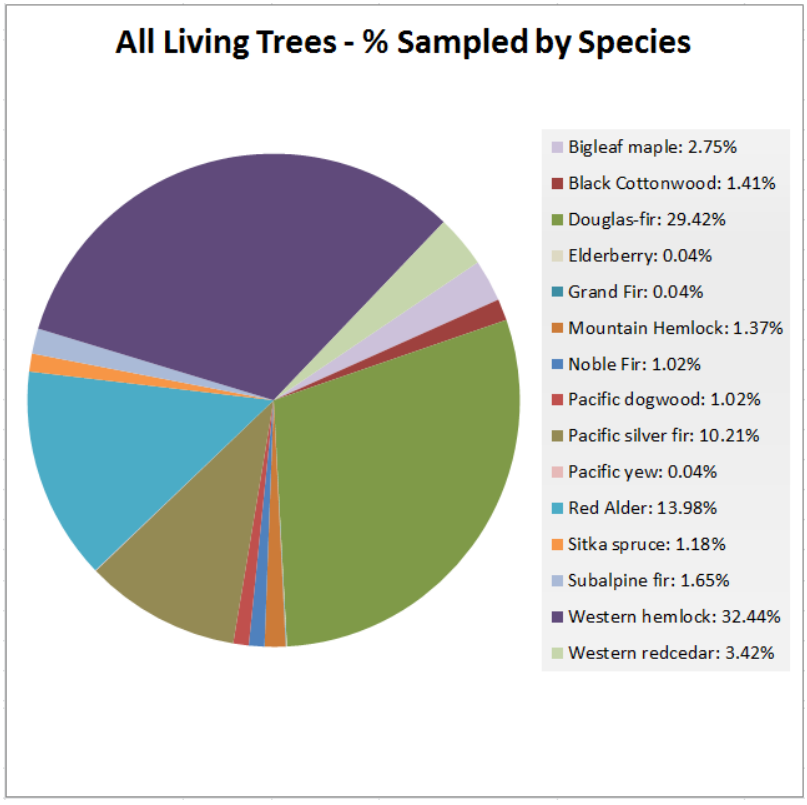

Status	Alive
Tree Type	All Trees

Tree Species	Count	Min DBH (in)	Max DBH	Mean DBH	Min Height (ft)	Max Height	Mean Height	Min Crown Diameter (ft)	Max Crown Diameter	Mean Crown Diameter	Mean Crown Height (ft)
bigleaf maple	70	1	31.2	4.0	7.5	112	27	4	60	15.34	12.65
black cottonwood	36	1.3	35.5	13.1	14	163.9	74	7	50	21.97	36.96
Douglas-fir	749	1.1	151	13.8	3	195	78	1	85	22.12	38.59
elderberry	1	1.1	1.1	1.1	11.1	11.1	11	6	6	6.00	4.00
grand fir	1	20	20	20.0	72.9	72.9	73	26	26	26.00	14.10
mountain hemlock	35	1.2	22.3	7.4	7	116.9	34	1	44	12.57	10.19
noble fir	26	1.1	10.1	6.2	7	50	30	3	17	10.68	4.36
Pacific dogwood	26	1	5.3	2.4	9	32	22	6	33	17.27	9.90
Pacific silver fir	260	1	22.8	8.2	7	130	40	2.5	28	13.17	8.10
Pacific yew	1	11.4	11.4	11.4	32.6	32.6	33	23	23	23.00	8.70
red alder	356	1	64.3	11.2	7	148	64	2	50	21.03	37.44
Sitka spruce	30	4.7	79.7	19.2	11.2	150.9	76	14	65.1	28.94	36.80
subalpine fir	42	2.4	13.9	9.9	14	75.6	56	5	24	16.90	17.50
Western hemlock	826	1	97.2	10.5	7	174	64	2	66.8	19.53	29.15
western redcedar	87	2.5	66.2	16.3	8	128.4	60	8	55	23.98	16.34
Summary Values	**2546**	**1**	**151**	**11.3**	**3**	**195**	**63**	**1**	**85**	**19.78**	**29.33**

Status	Alive
Tree Type	Large Trees

Tree Species	Count	Min DBH (in)	Max DBH	Mean DBH	Min Height (ft)	Max Height	Mean Height	Min Crown Diameter (ft)	Max Crown Diameter	Mean Crown Diameter	Mean Crown Height (ft)
bigleaf maple	17	5	31.2	11.3	23.5	112	57	15	60	33.94	21.43
black cottonwood	35	5.7	35.5	13.4	28.8	163.9	76	7	50	22.37	37.83
Douglas-fir	725	5	151	14.1	3	195	80	1	85	22.51	39.76
grand fir	1	20	20	20.0	72.9	72.9	73	26	26	26.00	14.10
mountain hemlock	28	5	22.3	8.5	18	116.9	40	5	44	14.00	11.82
noble fir	22	5	10.1	6.9	19.9	50	34	8	17	11.62	4.81
Pacific dogwood	2	5	5.3	5.2	22.4	28.7	26	21	31	26.00	5.00
Pacific silver fir	235	5	22.8	8.9	9	130	43	6	28	14.00	8.61
Pacific yew	1	11.4	11.4	11.4	32.6	32.6	33	23	23	23.00	8.70
red alder	331	5	64.3	11.9	10	148	68	2	50	21.98	39.65
Sitka spruce	29	5.4	79.7	19.7	11.2	150.9	78	14	65.1	29.42	38.03
subalpine fir	40	6	13.9	10.3	24.8	75.6	58	11	24	17.48	18.17
Western hemlock	730	5	97.2	11.5	8	174	70	5	66.8	20.80	32.08
western redcedar	86	5.2	66.2	16.5	20	128.4	61	8	55	24.17	16.46
Summary Values	**2282**	**5**	**151**	**12.3**	**3**	**195**	**69**	**1**	**85**	**20.95**	**31.91**

Status	Alive
Tree Type	Small Trees

Tree Species	Count	Min DBH (in)	Max DBH	Mean DBH	Min Height (ft)	Max Height	Mean Height	Min Crown Diameter (ft)	Max Crown Diameter	Mean Crown Diameter	Mean Crown Height (ft)
bigleaf maple	53	1	4.5	1.7	7.5	37	18	4	18	9.37	9.78
black cottonwood	1	1.3	1.3	1.3	14	14	14	8	8	8.00	6.50
Douglas-fir	24	1.1	4.9	3.0	10	28.4	19	4	18	10.31	3.29
elderberry	1	1.1	1.1	1.1	11.1	11.1	11	6	6	6.00	4.00
mountain hemlock	7	1.2	4.3	3.0	7	17.5	13	1	12	6.86	3.64
noble fir	4	1.1	4.1	2.4	7	16.6	12	3	8	5.75	2.00
Pacific dogwood	24	1	4.1	2.1	9	32	22	6	33	16.54	10.31
Pacific silver fir	25	1	4.1	2.3	7	27.5	13	2.5	10	5.42	3.32
red alder	25	1	4.8	2.0	7	43.8	17	2	19	8.44	7.02
Sitka spruce	1	4.7	4.7	4.7	11.5	11.5	12	15	15	15.00	1.00
subalpine fir	2	2.4	2.8	2.6	14	18	16	5	6	5.50	4.00
Western hemlock	96	1	4.9	2.5	7	38.9	17	2	28	9.94	7.02
western redcedar	1	2.5	2.5	2.5	8	8	8	8	8	8.00	6.00
Summary Values	**264**	**1**	**4.9**	**2.3**	**7**	**43.8**	**17**	**1**	**33**	**9.70**	**6.94**

Status	Dead
Tree Type	All Trees

Tree Species	Count	Min DBH (in)	Max DBH	Mean DBH	Min Height (ft)	Max Height	Mean Height
bigleaf maple	1	32.6	32.6	32.6	80.6	80.6	81
black cottonwood	6	1.2	11.4	5.5	10.3	36.4	19
Douglas-fir	109	2.2	27	10.0	6	112.6	43
Pacific silver fir	10	2.7	17.6	10.9	17	83.6	44
red alder	62	5	28	10.5	5	104.8	30
Sitka spruce	12	4.6	14.7	7.1	9	62.1	36
subalpine fir	2	6.1	7.3	6.7	30.1	32.5	31
Western hemlock	126	1.2	22.3	8.7	6.3	118.1	37
western redcedar	5	6.4	32.8	14.7	11.5	93.4	33
Summary Values	**333**	**1.2**	**32.8**	**9.6**	**5**	**118.1**	**38**

Appendix D - Individual Tree Segmentation

LIDAR

It was originally believed that individual trees might be identifiable to some extent in the LIDAR data, and that these individual trees might be useful for estimating stand density, estimating crown diameter, classifying trees as conifers or deciduous, and identifying snags. This work was done to test the ability to accurately identify individual trees in the LIDAR dataset used for this project.

The process for identifying individual trees involves creating a canopy height model (CHM) and segmenting that model using watershed segmentation. The primary user input into this process is the resolution (cell size) of the canopy height models. It was unknown if one resolution was more appropriate than another for identifying trees, so three resolutions were tested: 3 ft., 6 ft., and 15ft. These different resolutions may perform better for small or large trees.

Data Processing

CHMs are a top surface model from which the ground elevation has been subtracted, normalizing the surface to height above ground, rather than elevation. The CHMs were created using Fusion LIDAR processing software and ESRI ArcGIS.

Three different canopy height models with 3 ft., 6 ft., and 15 ft. cell sizes were built using the Fusion program CanopyModel.exe and vendor provided DEM ground models.

With the CHM representing heights above ground, areas of extreme height (areas with heights over 300 ft.) were removed in ArcGIS using Raster Calculator.

There are power lines in the southwest corner of the watershed travelling from Tacoma Public Utilities' Alder and La Grande dams on the Nisqually River. LIDAR returns off of the lines can be mistaken as trees in canopy height models, so the CHM heights along these power lines were set to zero manually in ArcGIS.

There are cells in the CHMs with no data. To fill in these holes, three median filter rasters were created for each of the three CHM resolutions. The Focal Statistics tool was used in Spatial Analyst in ArcGIS with 3 by 3, 5 by 5, and 7 by 7 square neighborhoods. This tool gives each cell the median value of its neighboring cells. This is a useful way to fill in missing areas, but has the effect of smoothing the surface. The 3 by 3 neighborhood fills in small holes, while the 5 by 5 and 7 by 7 neighborhoods fill in progressively larger holes, smoothing the surface more and more. Holes that are too large to be filled by the 7 be 7 neighborhood were considered to be truly no data, which usually occurs in areas of open water, where the laser does not reflect. Once the median filter rasters were created, the CHMs were filled in an iterative process. Areas of the CHMs with no data were replaced with the 3 by 3 median filter. After that was completed, areas of the CHMs that were still no data were replaced with the 5 by 5 median filter. And finally, after that, areas of the CHMs that were still no data were replaced by the 7 by 7 median filter. This filled in holes while minimizing the smoothing.

The Fusion program TreeSeg.exe (McGaughey, 2016) was used to perform tree segmentation on the canopy height models. It produces polygons representing individual tree crowns and points representing the highest point in each polygon using a watershed segmentation method. These objects are not actual trees, but rather mounds in the CHMs. These are referred to as individual tree objects (ITOs).

Tree polygons with their high points inside the field plot boundaries were identified, and the number of trees per plot were counted. The counts of individual trees were used as inputs in linear regression models for some metrics, and were used to test the effects of CHM resolution on tree counts as described below.

CHM Resolution Performance

It was initially unknown how well the tree counts from the different resolutions of canopy height models matched the plots (Figure 58).

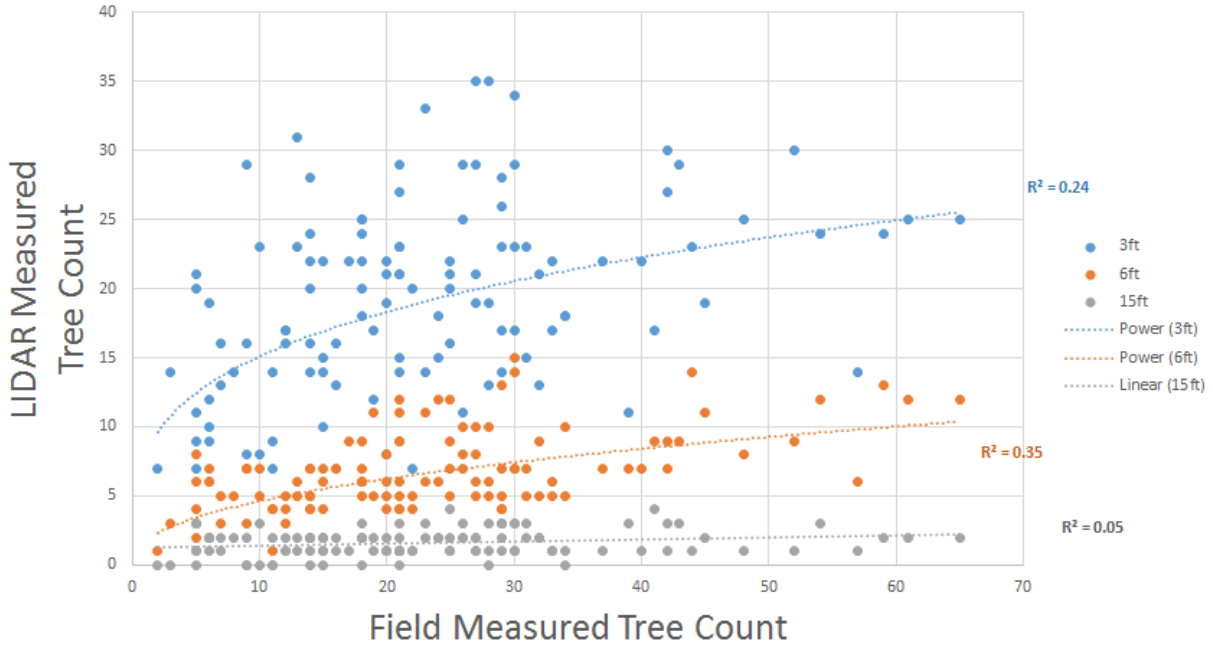

Figure 58: Field measured tree counts vs. ITO counts from three CHMs with 3 ft. (blue), 6 ft. (orange) and 15 ft. (grey) resolutions, with regression lines. R^2 values: 3 ft. = 0.24; 6 ft. = 0.35; 15 ft. = 0.05.

The number of trees counted in the field is almost universally higher than that measured in the LIDAR CHMs, at all three resolutions. The R^2 values are also all very low, ranging from 0.05 for the 15 ft. model to 0.35 for the 6 ft. model.

The field crew measured large trees down to a minimum 5" diameter. It is likely that many of these trees with small diameters are not detectable in the CHMs because they are below the primary canopy. To test this, a minimum diameter threshold was set and all trees with diameters smaller than the threshold were not counted. The threshold started at 5" and increased to 31" one inch at a time. Above 31" there were not enough plots with trees for the regression models to produce meaningful results. Back-transformed R^2 values for log-linear regression models were calculated for each CHM resolution at each diameter threshold (Figure 59).

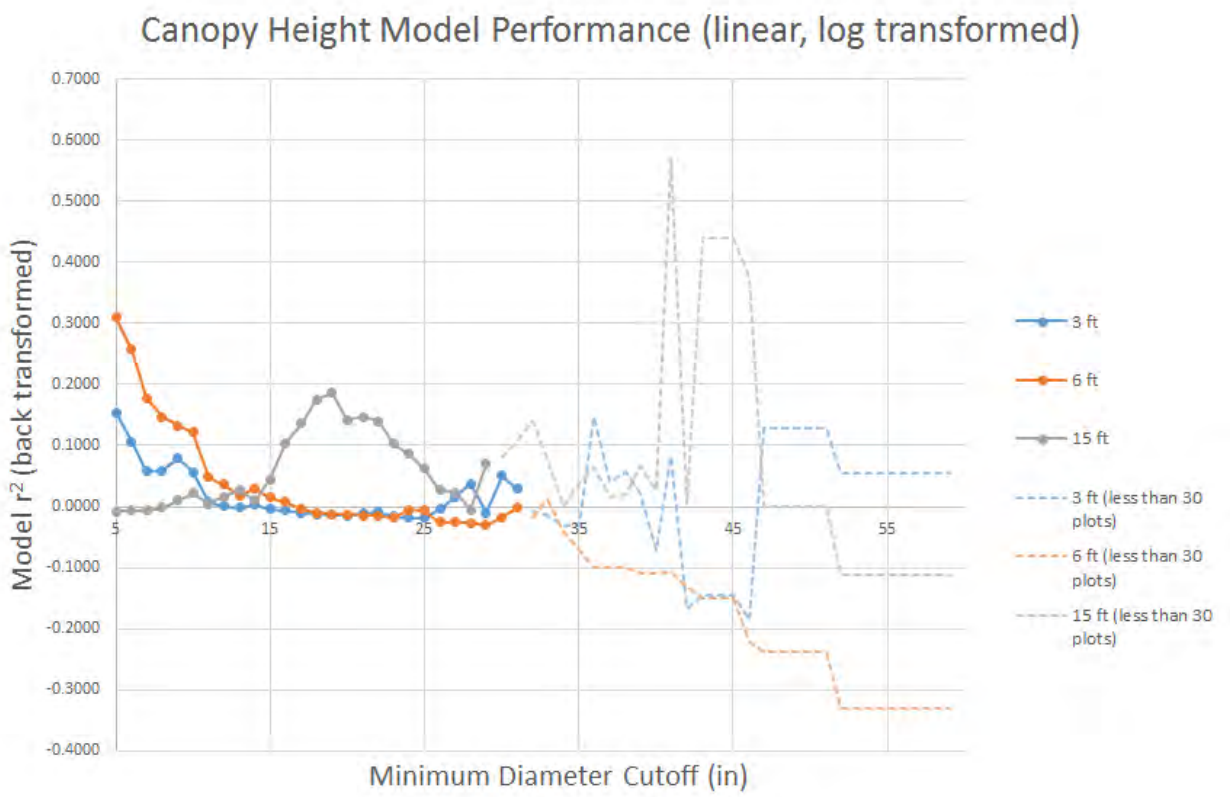

Figure 59: Regression model fit as trees below the minimum diameter threshold are removed from the field measured tree counts.

The best performing model was the 6 ft. canopy height model, keeping the 5" minimum diameter. This model had a back-transformed R^2 of 0.31 (Figure 60).

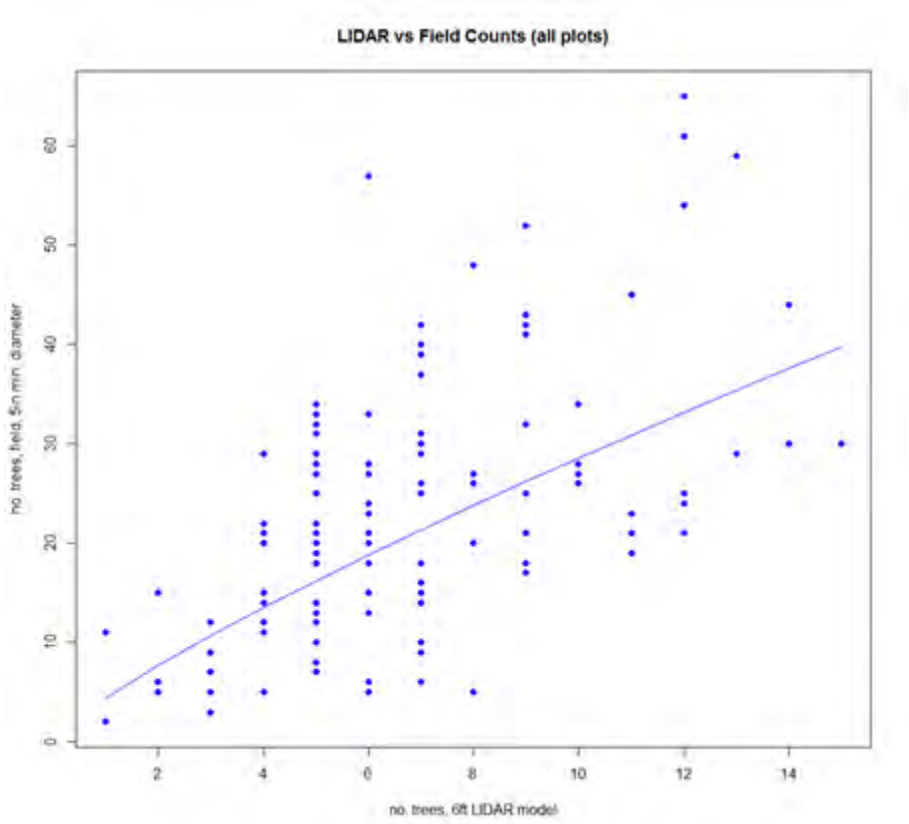

Figure 60: Tree counts from the 6 ft. CHM vs. field tree counts for trees with a 5" diameter or greater.

The inability to identify individual trees from the LIDAR makes it difficult to use the tree polygons for further analysis identifying snags, or classifying ITOs as conifer of deciduous.

Appendix E – Imagery Analyses: Supplemental Information

Aerial and Satellite Data Comparison

Initial Tree Delineation algorithms were compared between aerial [NAIP 1m resolution] and satellite imagery [WorldView-3 1.3m color resolution and 0.31cm panchromatic resolution]. The aerial imagery, being slightly higher resolution, showed better, initial results for identifying individual trees. This was also evident upon visual inspection of the images over several of the sample plots. The WorldView-3 imagery was obtained without cost for this project, making a comparison to NAIP imagery feasible. Isolation and analysis of the panchromatic imagery in conjunction with NAIP may have provided better explanatory power within the models, but this approach was outside the scope of the pilot and pushed time constraints needed to complete it.

Tree Delineation Algorithm [TDA] – Processing Time and Resources

The entire algorithm takes approximately 45 minutes to process all plot samples, using the following system specifications:

- Imagery: NAIP @ 1m resolution
- Operating System: Enterprise Server
- Processor: Xeon CPU E5-2699 v4 @ 2.20GHz, 2200 Mhz, 22 Cores, 44 Logical Processors
- Physical Memory: 256 GB

The export process takes anywhere from 5-10 minutes. Note that these figures are evaluating only the imagery found within sample plot boundaries and not the entire Mashel project area

Conifer/Deciduous Analysis

Comparing Red and Green Band Values Between Conifer and Deciduous-dominant Plots

t-Test: Two-Sample Assuming Unequal Variances $\alpha=0.05$

	Red StdDev Deciduous	*Red StdDev Conifers*
Mean	11.20080383	8.026076348
Variance	14.45132712	13.25574072
Observations	45	71
Hypothesized Mean Difference	0	
df	91	
t Stat	4.454946528	
P(T<=t) one-tail	1.19109E-05	
t Critical one-tail	1.661771155	
P(T<=t) two-tail	2.38218E-05	
t Critical two-tail	1.986377154	

Regression Output for Estimating Conifer Abundance

Regression Statistics	
Multiple R	0.532911652
R Square	0.283994829
Standard Error	0.268197855
Observations	113

	df	*SS*	*MS*	*F*	*Significance F*
Regression	5	3.05273181	0.610546	8.488052301	8.5442E-07
Residual	107	7.696519581	0.07193		
Total	112	10.74925139			

	Coefficients	*Standard Error*	*t Stat*	*P-value*
Intercept	2.818408388	0.468731742	6.012839	2.57318E-08
Mean Red	0.027157447	0.008617472	3.15144	0.0021076
Mean Green	0.136210745	0.070553322	1.930607	0.05617826
Mean Intensity	-45.04054571	18.25347895	-2.4675	0.015191035
StdDev of Crown Diameter	-0.055496041	0.017973598	-3.08764	0.00256982
StdDev of GLCM Entropy	0.409775106	0.270072828	1.517276	0.132145953

Basal Area Analysis

Regression Statistics	
Multiple R	0.519681591
R Square	0.270068956
Standard Error	118.8102384
Observations	113

	df	*SS*	*MS*	*F*	*Significance F*
Regression	4	564058.7	141014.7	9.989795	6.45E-07
Residual	108	1524514	14115.87		
Total	112	2088573			

	Coefficients	*Standard Error*	*t Stat*	*P-value*
Intercept	297.6084368	37.46583617	7.943462	2.01324E-12
StdDev of Hue	-2091.162663	1412.001827	-1.48099	0.141520442
StdDev of NDVI	-1468.394664	1077.068661	-1.36333	0.175615423
Mean GLCM Homogeneity	1089.657983	576.5766948	1.889875	0.061455794
Sum of Crown Coverage	-0.085638098	0.03866449	-2.2149	0.028866442

Appendix F – Fusion LIDAR Metric Descriptions

Below is a description of the individual metrics calculated by the Fusion LIDAR processing software for each plot. These are calculated using the CloudMetrics executable. The description is taken from the manual provided with Fusion (McGaughey, 2016).

CloudMetrics computes the following statistics using elevation and intensity values for each LIDAR sample:

- Total number of returns
- Count of returns by return number (support for up to 9 discrete returns)
- Minimum
- Maximum
- Mean
- Median (output as 50th percentile)
- Mode
- Standard deviation
- Variance
- Coefficient of variation
- Interquartile distance
- Skewness
- Kurtosis
- AAD (Average Absolute Deviation)
- MADMedian (Median of the absolute deviations from the overall median)
- MADMode (Median of the absolute deviations from the overall mode)
- L-moments (L1, L2, L3, L4)
- L-moment skewness
- L-moment kurtosis
- Percentile values (1st, 5th, 10th , 20th, 25th, 30th, 40th, 50th, 60th, 70th, 75th, 80th, 90th, 95th, 99th percentiles)
- Canopy relief ratio ((mean - min) / (max – min))
- Generalized means for the 2nd and 3rd power (Elev quadratic mean and Elev cubic mean)

In addition to the above metrics, CloudMetrics also computes various ratios of returns above a height break when the /above:# switch is used:

- Percentage of first returns above a specified height (canopy cover estimate)
- Percentage of first returns above the mean height/elevation
- Percentage of first returns above the mode height/elevation
- Percentage of all returns above a specified height
- Percentage of all returns above the mean height/elevation
- Percentage of all returns above the mode height/elevation
- Number of returns above a specified height / total first returns * 100
- Number of returns above the mean height / total first returns * 100
- Number of returns above the mode height / total first returns * 100

GLOSSARY

InSAR stands for Interferometric Synthetic Aperture Radar - InSAR sometimes abbreviated IfSAR, is an approach in generating high-resolution digital data through the use of Digital Elevation Model (DEM) and an orthorectified radar image.

Lorey's Height - Lorey's mean height weights the contribution of trees to the stand height by their basal area. Thus Lorey's mean height is calculated by multiplying the tree height (h) by its basal area (g), and then dividing the sum of this calculation by the total stand basal area:

$$h_L = \frac{\sum g * h}{\sum g}$$

Lorey's mean height is more stable than an unweighted mean height because it is less affected by mortality and harvesting of the smaller trees.

National Agriculture Imagery Program (NAIP) acquires aerial imagery during the agricultural growing seasons in the continental United States. A primary goal of the NAIP program is to make digital ortho photography available to governmental agencies and the public within a year of acquisition. Projects are contracted each year based upon available funding and the imagery acquisition cycle. Beginning in 2003, NAIP was acquired on a 5-year cycle. 2008 was a transition year, and a three-year cycle began in 2009. Since the NAIP program began in 2003, vendors have been transitioning to digital sensors in imagery acquisition. Sinece 2009, most NAIP imagery has been acquired with digital sensors rather than film cameras.

Quadratic Mean Diameter is the diameter of the tree of average per tree basal area. This becomes a convenient in that we often have basal are per acre and trees per acre but not the diameters of all the trees.

Root Means Square Error (RMSE) estimates the deviation of the actual y-values from the regression line.

Structure from Motion (SfM) is a photogrammetric range imaging technique for estimating three-dimensional structures from two-dimensional image sequences that may be coupled with local motion signals. It is studied in the fields of computer vision and visual perception.